**University of Alberta**

# Flow and Filtration into HDD Wells in River Bottom Sediments for Potable Water

by

Sean Matthew Birch

A thesis submitted to the Faculty of Graduate Studies and Research in partial fulfillment of the requirements for the degree of Master of Science.

in

Geotechnical Engineering

Department of Civil and Environmental Engineering

Edmonton, Alberta

Spring 2003

National Library of Canada
Acquisitions and Bibliographic Services
395 Wellington Street
Ottawa ON K1A 0N4
Canada

Bibliothèque nationale du Canada
Acquisitions et services bibliographiques
395, rue Wellington
Ottawa ON K1A 0N4
Canada

*Your file Votre référence*

*Our file Notre référence*

The author has granted a non-exclusive licence allowing the National Library of Canada to reproduce, loan, distribute or sell copies of this thesis in microform, paper or electronic formats.

L'auteur a accordé une licence non exclusive permettant à la Bibliothèque nationale du Canada de reproduire, prêter, distribuer ou vendre des copies de cette thèse sous la forme de microfiche/film, de reproduction sur papier ou sur format électronique.

The author retains ownership of the copyright in this thesis. Neither the thesis nor substantial extracts from it may be printed or otherwise reproduced without the author's permission.

L'auteur conserve la propriété du droit d'auteur qui protège cette thèse. Ni la thèse ni des extraits substantiels de celle-ci ne doivent être imprimés ou autrement reproduits sans son autorisation.

0-612-82249-4

Canada

**University of Alberta**

**Library Release Form**

**Name of Author:** Sean Matthew Birch

**Title of Thesis:** Flow and Filtration into HDD Wells in River Bottom Sediments for Potable Water

**Degree:** Master of Science

**Year This Degree Granted:** 2003

Permission is hereby granted to the University of Alberta Library to reproduce single copies of this thesis and to lend or sell such copies for private, scholarly or scientific research purposes only.

The author reserves all other publication and other rights in association with the copyright in the thesis, and except as herein before provided, neither the thesis nor any substantial portion thereof may be printed or otherwise reproduced in any material form whatever without the author's prior written permission.

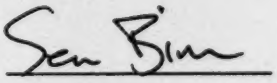

9467 – 66 Avenue
Edmonton, Alberta, Canada
T6E 0L9

April 4, 2003

**University of Alberta**

**Faculty of Graduate Studies and Research**

The undersigned certify that they have read, and recommend to the Faculty of Graduate Studies and Research for acceptance, a thesis entitled Flow and Filtration into HDD Wells in River Bottom Sediments for Potable Water submitted by Sean Matthew Birch in partial fulfillment of the requirements for the degree of Master of Science in Geotechnical Engineering.

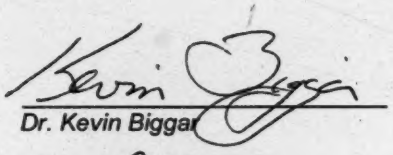

*Dr. Kevin Biggar*

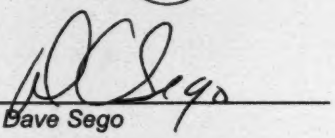

*Dr. Dave Sego*

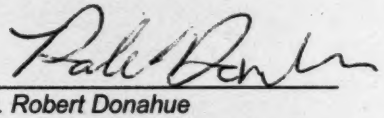

*Dr. Robert Donahue*

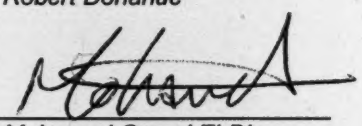

*Dr. Mohamed Gamal El-Din*

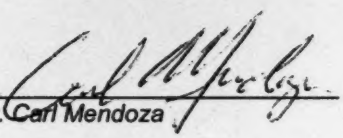

*Dr. Carl Mendoza*

April 4, 2003

## ABSTRACT

Horizontal Directional Drilling (HDD) may be used to pre-treat surface water for drinking water provision. Placed in the saturated sediments beneath rivers, they could serve as an alternative to the intake structures commonly used by water treatment plants, using the sediments as filters. Pilot-scale field tests were conducted in 2000 and 2001 to estimate the improvement in water quality achieved from such a system. These tests indicate that turbidity can routinely be reduced by 75%-85%, and particle counts by 80%-90%.

Finite-element models were then used to evaluate the flow rate of water produced by such horizontal wells. The model results were examined for their sensitivity to well length, diameter, depth, and the aquifer hydraulic conductivity. The effect of pipe hydraulics was included to examine well length optimization. Numerical model results generally agree well with published accounts of horizontal collector well and infiltration gallery performance.

## TABLE OF CONTENTS


| | | |
|---|---|---|
| Chapter 1 | Introduction | 1 |
| 1.1 | Background | 1 |
| 1.2 | Examples of Similar Work | 2 |
| 1.3 | Objectives | 2 |
| 1.4 | Methodology | 2 |
| 1.5 | Organization of Thesis | 3 |
| 1.6 | References | 4 |
| Chapter 2 | Horizontal Directional Drilling for Potable Water: Experimental Evaluation | 5 |
| 2.1 | Introduction | 5 |
| 2.1.1 | Research Objectives | 6 |
| 2.1.2 | Examples of Horizontal Wells Used for Potable Water Supply | 7 |
| 2.2 | Experimental Setup | 7 |
| 2.2.1 | Test Equipment | 7 |
| 2.2.2 | Test Box Operation | 9 |
| 2.2.3 | Turbidity and Particle Count Sampling and Testing Methods | 10 |
| 2.2.4 | Flow Rate Measurement | 11 |
| 2.3 | Experimental Results | 11 |
| 2.3.1 | Turbidity Removal | 11 |
| 2.3.2 | Particle Counts | 12 |
| 2.3.3 | Flow Rates | 12 |
| 2.3.4 | Decommissioning of Test Equipment | 13 |
| 2.3.5 | Laboratory Testing | 14 |
| 2.4 | Discussion of Results | 15 |
| 2.4.1 | Turbidity Removal | 15 |
| 2.4.2 | Particle Counts | 17 |
| 2.4.3 | Flow Rates | 17 |
| 2.4.4 | Applicability of Data | 19 |

2.5 Limitations of Test Method 20
2.5.1 Nature of Porous Medium 20
2.5.2 Test Duration 21
2.5.3 The Hyporheic Zone 22
2.6 Conclusions 23
2.7 Acknowledgements 24
2.8 References 25
Chapter 3 Horizontal Directional Drilling For Potable Water: Numerical Modelling 38
3.1 Introduction 38
3.1.1 Research Objectives 39
3.1.2 Examples of Horizontal Wells Used for Potable Water Supply 40
3.1.3 Analytical and Numerical Solutions of Flow into Horizontal Wells 40
3.2 Experimental Setup 42
3.2.1 Test Equipment 42
3.2.2 Experimental Procedure 43
3.3 Experimental Results and Discussion 43
3.3.1 Measured Flow Rates 43
3.3.2 Decommissioning of Test Equipment 44
3.3.3 Laboratory Testing 45
3.4 Numerical Model Setup 46
3.4.1 Software 46
3.4.2 Test Box Model Geometry 46
3.4.3 Riverbed Model Geometry 47
3.4.4 Test Box Model Boundary Conditions 47
3.4.5 Riverbed Model Boundary Conditions 47
3.4.6 Test Box Model Material Properties 48
3.4.7 Riverbed Model Material Properties 50
3.5 Numerical Model Results and Discussion 52

3.5.1 Test Box Model 52
3.5.2 Riverbed Model 54
3.6 Limitations of Testing and Numerical Modelling 57
3.6.1 The Hyporheic Zone 58
3.7 Conclusions 59
3.8 Acknowledgements 60
3.9 References 61
Chapter 4 Conclusions 81
4.1 Field Test Results 81
4.2 Numerical Model Results 82
4.3 Recommendations for Future Work 83
4.4 References 84
Appendix A Flow Rate Measurements 86
Appendix B Turbidity Measurements 92
Appendix C Particle Count Measurements 99
Appendix D Laboratory Test Procedures 110
D.1 Constant Head Permeability Tests 111
D.2 Dry Density Measurements for Test Boxes 112
D.3 Maximum and Minimum Index Density Tests 114
Appendix E Laboratory Measurements 115
E.1 Hydraulic Conductivity Measurements 116
E.2 Dry Density Measurements 124
E.3 Maximum and Minimum Index Density Measurements 125
Appendix F Numerical Modelling Procedures 126
F.1 Iterative Determination of Material Properties and Boundary Conditions 127
F.2 Determination of Accuracy Settings 130
Appendix G Text Input to FlexPDE 131
Appendix H Numerical Model Input Parameters And Results 139

Appendix I Numerical Model Graphical Output 144

Appendix J Photographs 160

## LIST OF TABLES


| | | |
|---|---|---|
| Table 2.1 | Wellscreen properties | 28 |
| Table 2.2 | Granular backfill characteristics | 28 |
| Table 2.3 | Particle count results (2001) | 28 |
| Table 2.4 | Mean measured flow rate for different backfill materials | 29 |
| Table 3.1 | Wellscreen properties | 64 |
| Table 3.2 | Granular backfill characteristics | 64 |
| Table 3.3 | Soil types and mean measured flow rates by testing season | 64 |
| Table 3.4 | Test box model input parameters | 65 |
| Table 3.5 | Riverbed model flow rate computations for select cases | 65 |
| Table 3.6 | Inflow rates from published studies and select numerical model results | 65 |
| Table A.1 | Flow Rate Measurements | 87 |
| Table B.1 | Turbidity Measurements | 93 |
| Table C.1 | Particle Count Results | 100 |
| Table E.1 | Sand Properties: Clean, Loose Sample | 116 |
| Table E.2 | Hydraulic Conductivity Measurements: Clean, Loose Sample | 116 |
| Table E.3 | Hydraulic Conductivity Calculations: Clean, Loose Sample | 117 |
| Table E.4 | Sand Properties: Clean, Dense Sample | 117 |
| Table E.5 | Hydraulic Conductivity Measurements: Clean, Dense Sample | 117 |
| Table E.6 | Hydraulic Conductivity Calculations: Clean, Dense Sample | 118 |
| Table E.7 | Sand Properties: Dirty, Loose Sample | 118 |
| Table E.8 | Hydraulic Conductivity Measurements: Dirty, Loose Sample | 119 |
| Table E.9 | Hydraulic Conductivity Calculations: Dirty, Loose Sample | 119 |
| Table E.10 | Sand Properties: Dirty, Dense Sample (A) | 120 |
| Table E.11 | Hydraulic Conductivity Measurements: Dirty, Dense Sample (A) | 120 |
| Table E.12 | Hydraulic Conductivity Calculations: Dirty, Dense Sample (A) | 121 |
| Table E.13 | Sand Properties: Dirty, Dense Sample (B) | 121 |
| Table E.14 | Hydraulic Conductivity Measurements: Dirty, Dense Sample (B) | 122 |

| | | |
|---|---|---|
| Table E.15 | Hydraulic Conductivity Calculations: Dirty, Dense Sample (B) | 123 |
| Table E.16 | Density measurements from test boxes | 124 |
| Table E.17 | Moisture content measurements | 125 |
| Table E.18 | Maximum and Minimum Index Density Test Results | 125 |
| Table H.1 | Input parameters and model results – test box model, uniform conductivity solution method | 140 |
| Table H.2 | Input parameters and model results – riverbed model, uniform conductivity solution method | 140 |
| Table H.3 | Input parameters and model results – riverbed model, rigorous solution method | 143 |

## LIST OF FIGURES


| | | |
|---|---|---|
| Figure 2.1 | HDD drill bit with housing | 30 |
| Figure 2.2 | Potential HDD drill path for potable water production | 30 |
| Figure 2.3 | Horizontal collector well and infiltration gallery | 30 |
| Figure 2.4 | Test equipment schematic diagram | 31 |
| Figure 2.5 | Test box dimensions | 31 |
| Figure 2.6 | Particle size distribution of granular materials used in test boxes | 32 |
| Figure 2.7 | Wellscreen filtrate turbidity vs. raw water turbidity (2001) | 32 |
| Figure 2.8 | Raw water turbidity vs. time (2001) | 33 |
| Figure 2.9 | Wellscreen filtrate turbidity vs. time: Sandblocker and Vee-wire drive point wellscreens only (2001) | 33 |
| Figure 2.10 | Percentiles of percent turbidity reduction by wellscreen type (2001) | 34 |
| Figure 2.11 | Flow rate vs. time: Vee-Wire Drive Point and Schumasoil 80 wellscreens (South Box) (2001) | 34 |
| Figure 2.12 | Flow rate vs. time: Sandblocker and Schumasoil 200 wellscreens (North Box) (2001) | 35 |
| Figure 2.13 | Percentiles of flow rate by wellscreen type (2001) | 35 |
| Figure 2.14 | Particle size distributions for clean and dirty sand samples collected at decommissioning (2001) | 36 |
| Figure 2.15 | Dry density profiles measured at decommissioning (2001) | 36 |
| Figure 2.16 | Measured hydraulic conductivity and empirical correlations | 37 |
| Figure 3.1 | HDD drill bit with housing | 66 |
| Figure 3.2 | Potential HDD drill path for potable water production | 66 |
| Figure 3.3 | Test equipment schematic diagram | 66 |
| Figure 3.4 | Particle size distribution of granular materials used in test boxes | 67 |
| Figure 3.5 | Wellscreen flow rate comparison: percentiles of flow rate by wellscreen type | 67 |
| Figure 3.6 | Particle size distributions for clean and dirty sand samples collected at decommissioning | 68 |

| | | |
|---|---|---|
| Figure 3.7 | Dry density profiles measured at decommissioning | 68 |
| Figure 3.8 | Measured hydraulic conductivity and empirical correlations | 69 |
| Figure 3.9 | Test box model dimensions | 70 |
| Figure 3.10 | Riverbed model dimensions | 70 |
| Figure 3.11 | Solution mesh generated by FlexPDE: NGRID = 30 | 70 |
| Figure 3.12 | Solution mesh generated by FlexPDE at z = 2.43m: NGRID = 30 | 71 |
| Figure 3.13 | Contours of total head at z = 1.22m (midpoint of wellscreen) | 71 |
| Figure 3.14 | Contours of total head at y = 0.1m (center of wellscreen) | 72 |
| Figure 3.15 | Contours of total head at x = 0.4m (center of wellscreen) | 72 |
| Figure 3.16 | Profile of axial velocity along axis of wellscreen | 73 |
| Figure 3.17 | Profile of total head along axis of wellscreen and connecting pipe | 73 |
| Figure 3.18 | Flow rate vs. length: hydraulic conductivity ($k_h$) = $10^{-3}$ m/s, depth = 5m | 74 |
| Figure 3.19 | Flow rate vs. length: hydraulic conductivity ($k_h$) = $10^{-4}$ m/s, depth = 5m | 74 |
| Figure 3.20 | Flow rate vs. length: hydraulic conductivity ($k_h$) = $10^{-5}$ m/s, depth = 5m | 75 |
| Figure 3.21 | Flow rate vs. length: hydraulic conductivity ($k_h$) = $10^{-6}$ m/s, depth = 5m | 75 |
| Figure 3.22 | Flow rate vs. depth: hydraulic conductivity ($k_h$) = $10^{-3}$ m/s, diameter = 300mm, length = 250m | 76 |
| Figure 3.23 | Riverbed model output: solution mesh generated by FlexPDE at z = 0m: NGRID = 60 | 76 |
| Figure 3.24 | Riverbed model output: solution mesh generated by FlexPDE at z = 0m (zoomed to region around wellscreen): NGRID = 60 | 77 |
| Figure 3.25 | Riverbed model output: transverse view of contours of total head at z = 125m: L = 250m, Ø = 300mm, $k_h$ = $10^{-3}$ m/s | 77 |
| Figure 3.26 | Riverbed model output: plan view of contours of total head at y = 5m: L = 250m, Ø = 300mm, $k_h$ = $10^{-3}$ m/s | 78 |
| Figure 3.27 | Riverbed model output: longitudinal section view of contours of total head at x = 0m: L = 250m, Ø = 300mm, $k_h$ = $10^{-3}$ m/s | 78 |

Figure 3.28 Riverbed model output: profile of total head along axis of wellscreen: L = 250m, Ø = 300mm, $k_h = 10^{-3}$ m/s 79

Figure 3.29 Profile of axial velocity along axis of wellscreen: L = 250m, Ø = 300mm, $k_h = 10^{-3}$ m/s 79

Figure 3.30 Profile of hydraulic conductivity along axis of wellscreen: L = 250m, Ø = 300mm, $k_h = 10^{-3}$ m/s 80

Figure I.1 Example model output: contours of total head at z = 25m; L = 50m, Ø = 300mm, $k_h = 10^{-3}$ m/s 145

Figure I.2 Example model output: contours of total head at y = 5m; L = 50m, Ø = 300mm, $k_h = 10^{-3}$ m/s 145

Figure I.3 Example model output: contours of total head at x = 0m; L = 50m, Ø = 300mm, $k_h = 10^{-3}$ m/s 146

Figure I.4 Example model output: profile of total head along axis of wellscreen; L = 50m, Ø = 300mm, $k_h = 10^{-3}$ m/s 146

Figure I.5 Example model output: profile of axial velocity along axis of wellscreen; L = 50m, Ø = 300mm, $k_h = 10^{-3}$ m/s 147

Figure I.6 Example model output: profile of hydraulic conductivity along axis of wellscreen; L = 50m, Ø = 300mm, $k_h = 10^{-3}$ m/s 147

Figure I.7 Example model output: contours of total head at z = 250m; L = 250m, Ø = 200mm, $k_h = 10^{-3}$ m/s 148

Figure I.8 Example model output: contours of total head at y = 5m; L = 250m, Ø = 200mm, $k_h = 10^{-3}$ m/s 148

Figure I.9 Example model output: contours of total head at x = 0m; L = 250m, Ø = 200mm, $k_h = 10^{-3}$ m/s 149

Figure I.10 Example model output: profile of total head along axis of wellscreen; L = 250m, Ø = 200mm, $k_h = 10^{-3}$ m/s 149

Figure I.11 Example model output: profile of axial velocity along axis of wellscreen; L = 250m, Ø = 200mm, $k_h = 10^{-3}$ m/s 150

Figure I.12 Example model output: profile of hydraulic conductivity along axis of wellscreen; L = 250m, Ø = 200mm, $k_h = 10^{-3}$ m/s 150

Figure I.13 Example model output: contours of total head at z = 125m; L = 250m, Ø = 300mm, $k_h = 10^{-3}$ m/s 151

Figure I.14 Example model output: contours of total head at y = 5m; L = 250m, Ø = 300mm, $k_h = 10^{-3}$ m/s 151

Figure I.15 Example model output: contours of total head at x = 0m; L = 250m, Ø = 300mm, $k_h = 10^{-3}$ m/s 152

Figure I.16 Example model output: profile of total head along axis of wellscreen; L = 250m, Ø = 300mm, $k_h = 10^{-3}$ m/s 152

Figure I.17 Example model output: profile of axial velocity along axis of wellscreen; L = 250m, Ø = 300mm, $k_h = 10^{-3}$ m/s 153

Figure I.18 Example model output: profile of hydraulic conductivity along axis of wellscreen; L = 250m, Ø = 300mm, $k_h = 10^{-3}$ m/s 153

Figure I.19 Example model output: contours of total head at z = 125m; L = 250m, Ø = 300mm, $k_h = 10^{-5}$ m/s 154

Figure I.20 Example model output: contours of total head at y = 5m; L = 250m, Ø = 300mm, $k_h = 10^{-5}$ m/s 154

Figure I.21 Example model output: contours of total head at x = 0m; L = 250m, Ø = 300mm, $k_h = 10^{-5}$ m/s 155

Figure I.22 Example model output: profile of total head along axis of wellscreen; L = 250m, Ø = 300mm, $k_h = 10^{-5}$ m/s 155

Figure I.23 Example model output: profile of axial velocity along axis of wellscreen; L = 250m, Ø = 300mm, $k_h = 10^{-5}$ m/s 156

Figure I.24 Example model output: profile of hydraulic conductivity along axis of wellscreen; L = 250m, Ø = 300mm, $k_h = 10^{-5}$ m/s 156

Figure I.25 Example model output: contours of total head at z = 250m; L = 500m, Ø = 300mm, $k_h = 10^{-3}$ m/s 157

| | | |
|---|---|---|
| Figure I.26 | Example model output: contours of total head at y = 5m; L = 500m, Ø = 300mm, $k_h = 10^{-3}$ m/s | 157 |
| Figure I.27 | Example model output: contours of total head at x = 0m; L = 500m, Ø = 300mm, $k_h = 10^{-3}$ m/s | 158 |
| Figure I.28 | Example model output: profile of total head along axis of wellscreen; L = 500m, Ø = 300mm, $k_h = 10^{-3}$ m/s | 158 |
| Figure I.29 | Example model output: profile of axial velocity along axis of wellscreen; L = 500m, Ø = 300mm, $k_h = 10^{-3}$ m/s | 159 |
| Figure I.30 | Example model output: profile of hydraulic conductivity along axis of wellscreen; L = 500m, Ø = 300mm, $k_h = 10^{-3}$ m/s | 159 |
| Figure J.1 | Sandblocker and Schumasoil 200 wellscreens during placement (July 2001) | 161 |
| Figure J.2 | Forklift used to handle sand bags; filling south test box (July 2001) | 161 |
| Figure J.3 | Filling the south test box with clean sand – Vee-Wire Drive Point and Schumasoil 80 wellscreens shown (July 2001) | 162 |
| Figure J.4 | Test boxes full of clean sand (July 2001) | 163 |
| Figure J.5 | Start of water circulation – north test box (July 2001) | 164 |
| Figure J.6 | South test box filled with water; turbidity approximately 20 NTU (July 2001) | 164 |
| Figure J.7 | V-notch weir box; water flowing from north test box, south test box closed (July 2001) | 165 |
| Figure J.8 | V-notch weir box; baffle used to reduce surface disturbance at v-notch (July 2001) | 165 |
| Figure J.9 | V-notch weir flowing full; ruler for measuring water level at right edge of plastic face (July 2001) | 166 |
| Figure J.10 | Overall arrangement of test equipment at E.L. Smith Water Treatment Plant (September 2001) | 166 |
| Figure J.11 | Shelby tube and steel plate for measuring density (October 2001) | 167 |
| Figure J.12 | Close-up of broken joint in Schumasoil 80 wellscreen (October 2001) | 167 |
| Figure J.13 | Schumasoil 80 wellscreen upon decommissioning (October 2001) | 168 |

Figure J.14 Close-up of Vee-Wire Drive Point wellscreen (October 2001) 168

Figure J.15 Vee-Wire Drive Point wellscreen upon decommissioning (October 2001) 168

## LIST OF SYMBOLS

| | |
|---|---|
| $\alpha$ | constant of proportionality: 10 for rough wellscreens |
| C | constant of proportionality: 274.4 for v-notch weirs with apex angles of 22.5°, water levels measured in metres, and flow rates measured in litres per second |
| $D_{10}$ | diameter of sieve allowing 10% of soil sample to pass (mm) |
| e | void ratio |
| $\varepsilon$ | pipe roughness (m) |
| f | particle angularity |
| f | friction factor |
| g | acceleration due to gravity: 9.81 $m/s^2$ |
| $\Delta h_f$ | head loss due to friction (m) |
| H | water level in v-notch weir (m) |
| i | hydraulic gradient |
| k | hydraulic conductivity (m/s) |
| $k_h$ | horizontal hydraulic conductivity (m/s) |
| L | pipe length (m) |
| v | kinematic viscosity of water ($m^2/s$) |
| Ø | pipe diameter (m) |
| F | fraction of open area of wellscreen surface |
| $q_i$ | flow rate of water entering wellscreen radially ($m^3/s/m$) |
| Q | flow rate measured in v-notch weir (L/s) |
| $R_e$ | Reynold's number |
| S | specific surface ($mm^{-1}$) |
| u | velocity of water flowing through wellscreen axially (m/s) |
| v | velocity of water entering wellscreen radially (m/s) |
| V | velocity (m/s) |
| V(z) | axial velocity in wellscreen as a function of z (m/s) |
| V'(z) | first derivative of function describing axial velocity in wellscreen (m/s) |

| | |
|---|---|
| z | coordinate parallel to wellscreen axis in numerical models (m) |

## LIST OF ABBREVIATIONS

| | |
|---|---|
| HDPE | high density polyethylene |
| HDD | horizontal directional drilling |
| NTU | nephelometric turbidity units |
| PVC | polyvinyl chloride |

# 1 INTRODUCTION

## 1.1 Background

The research conducted in this study focused on the potential for horizontal wells installed in riverbed sediments using horizontal directional drilling (HDD) to be sources of water for water treatment plants. In order to evaluate the viability of these wells, two studies were necessary: the available improvement in water quality, and the quantity of water produced by the wells. To that end, pilot-scale field experiments were carried out, and numerical models of ground water flow into horizontal wells were developed. The available literature was reviewed for similar examples of previous work which could be compared to the results of this research. The following is an introduction to the work conducted for this study.

Horizontal directional drilling is a technology originally developed by the petroleum industry to improve productivity in thin or highly anisotropic reservoirs (Vicente *et al.*, 2002). More recently, it has been applied to a range of civil and environmental engineering applications, including utility crossings and contaminated site remediation. The crux of the technology in either field is a manoeuvrable drill bit that allows the placement of pipes or wells along any path in three dimensions, with some restrictions on length, depth and curvature. While drill bit designs can vary greatly, a common trait is that the shape of the drill bit assembly causes it to follow a curved path when the bit is advanced without rotating. A straight segment is formed by rotating the drill bit while advancing. The pilot bores formed by the drill bit are then reamed to their final diameter by several passes with reamers of increasing size, and the product pipe or wellscreen is pulled into place following the final reaming. Drilling fluids are pumped through the drill stem, out of the drill bit or reamer, and back to the surface to carry cuttings, support the borehole walls, and to cool and lubricate the down-hole equipment.

To apply horizontal directional drilling to the needs of water treatment plants, horizontal wells may be placed in the saturated sediments beneath rivers. These wells will draw river water through the riverbed sediments, where suspended solids in the river water will be partially removed by filtration. Because water treatment plants must purchase chemicals (e.g., alum) to aid in the

removal of these suspended solids (EPCOR Water Services Inc., 2002), reducing the concentration of suspended solids in the raw water supply should reduce the cost of treating water. Also, if there is less variability in the raw water turbidity, the operation of the treatment system will be simplified.

## 1.2 Examples of Similar Work

A review of the available literature did not reveal any previous uses of horizontal directional drilling in riverbed sediments for the provision of potable water, but a number of similar technologies have been used in the past. Ray *et al.* (2002), Mikels (1992) and Obst (1974) have described the design, installation and use of horizontal collector wells (sometimes referred to as Ranney or Fehlmann wells) for supplying water to treatment plants in North America. Karanth (1997) described the use of infiltration galleries by communities in peninsular India. The results of these case studies have been compared to the results of this research to help evaluate the effectiveness of directionally drilled horizontal wells.

## 1.3 Objectives

The evaluation of horizontal wells as a source of water focussed on two determinations: the potential improvement in water quality, and the flow rates of water available from horizontal wells with a range of design parameters. Pilot-scale field tests and numerical models were used to aid in making these determinations.

## 1.4 Methodology

The test equipment used in the physical testing in this study was located at the E.L. Smith Water Treatment Plant in Edmonton, Alberta. Two plywood test boxes, each containing two sample wellscreens and a backfill of granular material, were supplied with river water over two summers (2000 and 2001). To quantify the improvement in water quality, turbidity and particle concentrations were measured in the raw river water and the filtrate produced by each of the four wellscreens. Wellscreen filtrate flow rates were also measured.

A three-dimensional finite-element model of a test box was developed to confirm the accuracy of the numerical modelling software used in this study. Using the material properties measured from the test boxes (particle-size distributions, density and hydraulic conductivity) in the numerical model, the wellscreen filtrate flow rate was computed. When the predicted flow rate came sufficiently close to the measured values, the model was considered to be verified.

After confirming the suitability of the numerical modelling software to the problem of flow to horizontal wells, a finite-element model was developed to model groundwater flow to a horizontal well placed beneath a river. This model was used to examine the effect of several design variables (well length, well diameter, well depth, and aquifer hydraulic conductivity) and pipe hydraulics on the flow rates available from horizontal wells. The simulation of pipe hydraulics in the wellscreen was not straightforward; no single value of hydraulic conductivity could correctly represent the frictional head losses at every point along the wellscreen's length. Two methods for assigning equivalent hydraulic conductivities to the wellscreen were developed – a simpler, less-rigorous method requiring less time, and a more comprehensive and accurate method requiring more time. The results from both methods were compared to each other to judge their accuracy.

Based on the results of the experimental and numerical modelling work performed in this study, several important recommendations are made. Wellscreen selection, and the importance of aquifer hydraulic conductivity and well diameter on the optimization of well length are discussed.

### 1.5 Organization of Thesis

This thesis has been written in paper format. Chapter 1 introduces the reader to the reasons why this study has been conducted, and outlines the structure of the research. Chapter 2 presents the pilot-scale field tests, stating the types of measurements carried out, the results of these tests, and estimating the water quality improvement that could be expected from full-scale horizontal well installations. Chapter 3 explains the development and solution of two numerical models – the test boxes described in Chapter 2, and a hypothetical horizontal well placed in riverbed sediments. Chapter 4 concludes and summarizes the results of this study, and presents the need for further work.

Appendices A, B, C contain the flow rate, turbidity and particle count measurements taken during the summer of 2001. Appendix D describes the laboratory procedures performed on the granular materials used in the 2001 testing program, and Appendix E presents the results of those tests. Appendix F explains the procedures used in the solution of the numerical models. Samples of the text input files from the numerical models are presented in Appendix G. Appendix H lists the input parameters and results of the numerical models. Samples of the graphical output of the numerical modelling software are shown in Appendix I. Finally, photographs from the pilot-scale field test program and decommissioning are presented in Appendix J.

### 1.6 References

EPCOR Water Services Inc. Monthly Water Treatment Plant Report: May 2002. Edmonton, Alberta, Canada. pp. 9-17.

Karanth, K. R. 1997. On sustainable yield of infiltration gallery in valley fills of peninsular India. Journal of Applied Hydrology, 10(3, 4): 86-98.

Mikels, M. S. 1992. Characterizing the influence of surface water on water produced by collector wells. Journal of the American Water Works Association, 84(9): 77-84.

Obst, C. E. 1974. Horizontal groundwater collectors, 'Canada's largest water well'. Proceedings of the Annual Conference of the British Columbia Water and Waste Association, Vancouver, British Columbia, April 9-11, pp. 107-123.

Ray, C., Grischek, T., Schubert, J., Wang, J., and Speth, T. 2002. A perspective of riverbank filtration. Journal of the American Water Works Association, 94(4): 149-160.

Vicente, R., Sarica, C., and Ertekin, T. 2002. A Numerical Model Coupling Reservoir and Horizontal Well-Flow Dynamics: Transient Behaviour of Single-Phase Liquid and Gas Flow . Society of Petroleum Engineers Journal, March 2002, pp. 70-77.

# 2 HORIZONTAL DIRECTIONAL DRILLING FOR POTABLE WATER: EXPERIMENTAL EVAULATION

## 2.1 Introduction

Horizontal wells placed in the high-permeability sand and gravel sediments beneath rivers should possess some advantages over the intake structures commonly used by water treatment plants. The quality and variability of the water pumped from an intake structure is identical to river water; it contains the same concentration of suspended solids and pathogens, and fluctuates between the same extremes of quality. Horizontal wells installed by directional drilling could improve some of the characteristics (e.g., turbidity) of the water supplied to treatment plants. Water would flow from the river to the horizontal well through the sand and gravel in the riverbed, where the concentration of suspended solids and pathogens would be reduced by filtration (particle straining and adsorption) and dilution with groundwater (Ray *et al.*, 2002). In addition, the volume of the riverbed sediment should buffer changes in river water quality, leading to a more uniform raw water supply. Because significant amounts of chemicals, such as alum, are used to remove suspended solids from the raw water supply (EPCOR Water Services Inc., 2002), a cleaner water supply should reduce required dosages and costs to treat. Less variability in the quality of the water should mean that fewer operators will be needed to run treatment plants, further reducing operating costs. Predicting the potential improvement in water quality from horizontal wells is an important step in evaluating the technology.

Horizontal directional drilling (HDD) is a technology originally developed by the petroleum industry to improve production in thin or highly anisotropic reservoirs (Vicente *et al.*, 2002). More recently, it has been applied to a range of civil and environmental engineering applications, including utility crossings and contaminated site remediation, and it holds potential to aid in water treatment applications. In a typical HDD installation, the drill stem enters the ground at an angle of 10°-25° to the horizontal (Case Corporation, 2002). The shape of the drill bit (see Figure 2.1) allows the drill stem to be steered along a desired path while underground. The drill bit can be advanced while rotating the drill string to produce a straight segment, whereas advancement with no drill

string rotation will produce a curved segment. This manoeuvrability allows the placement of pipelines or wells in areas inaccessible through other means, for example beneath existing structures (roads or buildings, for example) or bodies of water (Figure 2.2), and with great precision. The drill path is usually restricted by several factors: the allowable bending radius of the drill stem or product pipe, soil properties and stratigraphy, and the required borehole length and depth. After the drill bit surfaces at a predetermined location, the pilot bore is reamed to the final diameter. Several passes with reamers of increasing size may be necessary, and on the final reaming the product pipe or wellscreen is pulled into place. During drilling, specially designed drilling fluids are pumped through the drill stem to the bit or reamer and back to the surface (Birch *et al.*, 2001). Drilling fluids are used to remove cuttings, support the borehole wall, and to clean, cool and lubricate the underground equipment. In the case of a well installation, where the permeability of the surrounding soil must be maintained to ensure productivity, the drilling fluid may be designed to resist seeping into the soil or to biodegrade following well completion. Control over drilling fluid pressure is also important – if the pressure is too low, the borehole walls may collapse, and if the pressure is too high, the fluid may hydraulically fracture the surrounding soil and escape to the surface.

### 2.1.1 Research Objectives

The testing program was designed to estimate the improvement in water quality (i.e., the reduction in turbidity and particle counts from raw water to filtered water) that could be expected from a full-scale horizontal well installation, and to examine the sensitivity of the results to several factors: soil type, wellscreen type, and raw water quality. Turbidity is commonly used by water treatment plants as an indicator of the concentration of suspended solids, which in turn is taken as indicative of the presence and concentration of micro-organisms (Ray *et al.*, 2002). Particle counts were used to measure the reduction of particles larger than two microns in diameter. The rate of flow of wellscreen filtrate was also measured as an additional approach to evaluate the performance of the test equipment.

### 2.1.2 Examples of Horizontal Wells Used for Potable Water Supply

A review of the available literature has not revealed any examples of identical uses of horizontal directionally drilled wells in the past, but several examples of similar work were found. Infiltration galleries and radial horizontal collector wells (Figure 2.3) have been placed beneath rivers, at depths from 6m to 27m below the surface, to supply water to municipalities. These installations have been described by several authors. Ray *et al.* (2002) detailed the effectiveness of riverbank filtration (including both horizontal wells beneath and vertical wells beside rivers) at removing chemical and biological contaminants. In the case studies presented by Ray *et al.*, the various measures of water quality, including particulates, pathogens and disinfection by-product precursors, show that riverbank filtration is useful as a pre-treatment technology for water treatment plants. Mikels (1992) focussed on the degree of independence of horizontal collector well filtrate from river water by examining turbidity, temperature and the presence of indicator organisms (pathogens and invertebrates) in both water sources. While the temperature data indicated the influence of surface water on collector well filtrate, turbidity and water-borne particulate data suggested that this influence was indirect, i.e., the collector well filtrate was not subject to *Giardia* contamination. Joshi *et al.* (1985) described the filtering performance of an infiltration gallery by measuring turbidity, chemical oxygen demand (COD) and bacteriological counts. All were significantly reduced. Karanth (1997), and Obst (1974) focus on the prediction and measurement of yield from infiltration galleries and collector wells. Horizontal directionally drilled wells have been placed in aquifers to supply potable water (Rash, 2002), but installations in the saturated sediment beneath rivers were not found in the literature. Where appropriate, the conclusions of these case studies will be used to help predict the performance of directionally drilled horizontal wells in the riverbed sediments.

## 2.2 Experimental Setup

### 2.2.1 Test Equipment

All of the work performed for this study was carried out at the E.L. Smith Water Treatment Plant, which is located on the North Saskatchewan River in Edmonton, Alberta. Water quality tests were

carried out in the summers of 2000 and 2001, with the majority of data recorded in the period between July and September 2001.

Raw water was pumped from the Low Lift Pump-house to the testing equipment on an adjacent tarmac. The two plywood test boxes shown schematically in Figures 2.4 and 2.5 (referred to below as the North Box and South Box) measured 1.20m deep x 1.20m wide x 2.43m long; each contained two 0.91m long wellscreen segments, a plastic-tarp lining for water-tightness and a backfill of 0.8m of granular material. Raw water entered the box at one end through a diffuser placed just above the sand, then flowed either to overflow pipes at the other end of the box or through the soil to an open wellscreen. Wellscreen filtrate flowed through PVC pipes down a short hill (7:1 slope, 15m long) to a box containing a v-notch weir, and was then discharged back into the river.

Four wellscreens were used: from MAASS Midwest, a Sandblocker screen; and from Johnson Screens, a Vee-Wire Drive Point and two Schumasoil screens. The Sandblocker wellscreen was constructed of two perforated stainless-steel tubes, one inside the other, separated by stainless-steel fibre wool. The Vee-Wire Drive Point consisted of a triangular-shaped wire, the base facing outward, wrapped around longitudinal stainless-steel ribs arranged in a circular formation around the wellscreen axis. The two Schumasoil wellscreens were constructed of HDPE beads sintered together to form a porous structure. Bead sizes were controlled to provide specific pore-throat diameters; 200 microns and 80 microns in the wellscreens used. Both Schumasoil wellscreens consisted of three 300mm segments of screen, connected with PVC couplers and bonded with a solvent adhesive. These wellscreens were used in both testing years. Table 2.1 lists the important properties of each wellscreen. Photos presented in Appendix J show the wellscreens before and after placement.

In 2000, the two boxes were filled with a sand and a sandy gravel backfill. The combination of unusually low turbidity in the raw water supplied to the test boxes and the presence of fines in the soil backfills caused problems in the measurement of filtration – the turbidity of the wellscreen filtrate was often higher than the turbidity of the raw water. To remedy this problem, a triple-

washed silica sand (containing no fines) was used in both boxes in 2001. A summary of the characteristics of each of the soil types is provided in Table 2.2. Figure 2.6 shows the granular materials' particle-size distributions before placement. In both years, the granular materials were placed in a loose and dry state, either by shovelling or pouring from supply bags. The test boxes were then filled with water to the level of the overflow pipes when pumping began.

### 2.2.2 Test Box Operation

During normal operation, only one wellscreen in each box was allowed to flow. It was felt that running two wellscreens from the same box simultaneously would change the flow conditions in the single outlet pipe shared by both screens and thus interfere with free drainage from either or both screens. To allow all four wellscreens to run for approximately equal lengths of time (approximately 50% of the total test duration), the two open wellscreens were closed after sampling and flow from the other two wellscreens was permitted.

While the tests performed in 2001 were carried out over a three month period, the test boxes did not operate continuously. To carry out maintenance on the test equipment (e.g. patching leaks) or to cooperate with plant operations, the raw water supply to the test boxes was occasionally turned off (six times in total throughout the summer).

Whenever the test equipment operated overnight, a thin layer of fine sediment would settle out of the raw water onto the surface of the sand in the test boxes. The most likely reason for this build up was a decrease in water velocity from the river to the test boxes, however no measurements of velocity in the river or the boxes were made. This layer of sediment would reduce the flow rate of water flowing through the soil in the test boxes, so before sampling this layer was broken up by stirring the surface of the sand with a garden rake. Experience showed that after a period of 30 minutes flow rates and turbidity re-established at normal levels. This settling was observed at all levels of raw water turbidity, but was more pronounced during times of high turbidity.

### 2.2.3 Turbidity and Particle Count Sampling and Testing Methods

Water samples were collected throughout the program to monitor the filtering ability of the experimental system. Two samples were taken for each data point to quantify a reduction in turbidity or particle counts – one sample of raw water and one sample of wellscreen filtrate. Raw water samples were collected by dipping a clean sample bottle into the water circulating above the sand in each box. Filtrate samples were collected by filling a bottle under the outlet of the wellscreen filtrate pipes where they entered the v-notch weir box. For turbidity analysis, a 200mL sample of raw water was paired with each 200mL sample of filtrate, or with two samples of filtrate if they were collected within fifteen minutes of each other. For particle counts, a single 1000mL sample of raw water was used as a reference for all four 1000mL wellscreen filtrate samples. Turbidity samples from each wellscreen were taken approximately twice daily during the testing period; due to restrictions on instrument availability, particle counts were taken once daily during the final week of operation.

When testing turbidity, the sample was used to double-rinse and fill a small (10mL) vial to the top. After being capped, beads of water and fingerprints were wiped off, and the vial was placed into a Hach 2100N™ turbidimeter. A digital display showed the turbidity in NTU to three significant digits. Fluctuations in the exact measurement of turbidity were always present, so the reading was given one or two minutes to stabilize before being recorded. If the readings did not stabilize, the lowest reading was recorded (following the water treatment plant's testing procedure). Because the turbidimeter gave continuous readings of sample turbidity, no duplicates were tested.

Before conducting particle counts, a sample of distilled water was run through the Hach WGS267™ particle count meter to remove any residual particles and to confirm the meter's correct operation. A 100mL sample of wellscreen filtrate or raw water was then diluted with 400mL of distilled water to reduce the particle concentration to one-fifth of the original concentration. The dilute sample was pumped through the meter at 100 mL/min. and analyzed.

Counts of particles in several size ranges (2-3μm, 3-5μm, 5-7μm, 7-10μm, 10-15μm and larger than 15μm) per millilitre of water were printed and averaged by the instrument when complete.

### 2.2.4 Flow Rate Measurement

The flow rate of wellscreen filtrate was measured using a v-notch weir with an apex angle of 22.5° in a small waterproof plywood box (see Appendix J). The PVC pipes carrying the wellscreen filtrate from the test boxes discharged the filtrate a short distance above the weir box so that the flow conditions in the filtrate pipes would be unaffected by the water level in the weir. The height of water above the apex of the v-notch was recorded and converted to flow rates using the following relationship (Grant and Dawson, 1995):

$$Q = C \cdot H^{2.5} \qquad [2.1]$$

where Q is flow rate (L/s); C is a constant, equal to 274.4 for apex angles of 22.5° and the given units; and H is the height of water above the v-notch apex (m). Flow rates were measured at the v-notch weir with a single wellscreen flowing. After measurement, the wellscreen was closed and the other wellscreen in the same test box was opened. Fifteen to thirty minutes elapsed before the next flow rate measurement was taken. Experience showed that this time was sufficient for flow rates measured at the v-notch weir to reach steady-state conditions.

## 2.3 Experimental Results

### 2.3.1 Turbidity Removal

Figure 2.7 shows the wellscreen filtrate turbidity versus raw water turbidity for all four wellscreens. Wellscreen filtrate turbidity rose as raw water turbidity increased, but remained approximately one order of magnitude lower. Raw water turbidity varied from 1.40 to 3030 NTU (with a median value of 8.0 NTU), while wellscreen filtrate turbidity ranged from 0.18 to 342 NTU (with a median value of 1.2 NTU).

The variations in raw water and filtrate turbidity over the duration of the test are shown in Figures 2.8 and 2.9. Approximately 250 hours into the test (July 30, 2001) a brief (70 hour) high-turbidity

event was observed. After this event, a constant and gradual decrease in raw water turbidity was observed until the end of testing. No samples were taken from 802 hours until 1138 hours of testing, a period corresponding to September 11 to September 24, 2001, when increased security measures at the water treatment plant prevented access to the test equipment.

From the perspective of a water treatment plant, the ability of a filtering system to remove suspended solids from the water supply is important. Figure 2.10 shows the percentiles of turbidity reduction for the four wellscreens. Two of the wellscreens, the Sandblocker and Schumasoil 200 screens, were nearly identical in reducing turbidity by a large amount (median reductions of 86%), with the Schumasoil 80 screen performing almost as well (median reduction of 83%). The Vee-Wire Drive Point wellscreen consistently delivered the smallest reductions in turbidity (median reduction of 74%).

### 2.3.2 Particle Counts

Water samples were analyzed for particle concentrations in the last week of testing. Table 2.3 shows the average number of particles greater than two microns per millilitre for the raw water supply and the filtrate from all four wellscreens. (Particle counts for all size ranges and for all dates tested are given in Appendix C). The four wellscreens removed small particles well – the Sandblocker and Schumasoil 200 screens performed almost identically, removing approximately 90.8% and 89.2% of the particles from the raw water supply, respectively. The Vee-Wire Drive Point performed poorly in comparison (48.1%), and the Schumasoil 80 placed between the two extremes (80.2%). Average turbidity readings and percent reductions in turbidity from the same period have been included for comparison.

### 2.3.3 Flow Rates

Filtering ability alone does not provide sufficient information to properly evaluate the performance of the wellscreens used in this test; the flow rate of filtered water produced by the screens must also be considered. Figure 2.11 shows the flow rate measurements for each of the four wellscreens made throughout the 2001 test program. From high readings initially, flow rates decrease for approximately the first 200 hours. The high-turbidity event 250 hours into testing

was accompanied by very low filtrate flow rates, after which the measured flow rates rebound slightly and then remain relatively constant for the remainder of the test program. These trends are most noticeable in the Schumasoil 200 and Sandblocker wellscreens, but are present to a lesser extent in the Schumasoil 80 and Vee-wire Drive Point screens.

In Figure 2.13 the four wellscreens are compared by percentiles of flow rate. Again, the Sandblocker and Schumasoil 200 wellscreens delivered nearly identical performance (median flow rates of 0.37 L/s and 0.40 L/s respectively). The Vee-Wire Drive Point produced consistently higher flows (median flow rate of 0.78 L/s), and the flows measured from the Schumasoil 80 wellscreen were approximately one order of magnitude lower than the other three (median flow rate of 0.02 L/s).

The differences in soil and wellscreen properties can be seen in their effects on the flow measurements. In Table 2.4, a distinct increase (approximately one order of magnitude) in mean flow rates was observed after replacing the sand and sandy gravel used in 2000 with the clean uniform sand used in 2001. There was even a two- to three-fold difference between the flows measured from the wellscreens in 2000; the two wellscreens placed in the sandy gravel backfill (the Vee-Wire Drive Point and Schumasoil 80) delivered lower flow rates than the two screens used with the sand backfill.

### 2.3.4 Decommissioning of Test Equipment

At the conclusion of the 2001 testing program, the test equipment was disassembled and removed from the site. Some useful observations were made on the condition of the sand and wellscreens.

Two distinct layers of sand were present in both test boxes. A layer of dirty sand 50mm to 75mm deep covering the entire surface of the boxes had developed. From a visual inspection, it appeared that fine suspended solids present in the raw water supply had been filtered from the water as it seeped through this granular material. The increased fines content had made the sand in this layer darker and more cohesive than the remaining sand (the bottom 725mm to 750mm).

This thicker underlying layer of clean sand appeared to be relatively unchanged from the condition in which it had been placed. Figure 2.14 shows the difference in grain size distributions between the clean and dirty sand layers. Only 0.4% of the clean sand passed a #200 sieve (75µm openings), compared to 2.8% of the dirty sand.

As the wellscreens were removed from the boxes their condition was assessed. Three of the four wellscreens (the Vee-Wire Drive Point, Schumasoil 200 and Sandblocker screens) appeared to be in good condition, free of fine material and unclogged (i.e., no visible sediment or particulates in the pores or openings). The surface of the Schumasoil 80 wellscreen had become darkened, suggesting the pores had become clogged with suspended solids from the raw water. After sectioning the wellscreen, it became apparent that most of the discolouration was confined to the exterior surface of this wellscreen. Except for the exterior surface, the cross-section colour remained very close to the original white (see Figures J.12 and J.13).

Density measurements of the sand in both boxes were taken as excavation progressed. Density was determined by extracting a known volume of soil (1501 $cm^3$) and measuring the mass and water content in the laboratory. The samples were collected by pushing a 201mm long, 97.5mm diameter Shelby Tube downward into the soil, excavating the soil around the tube, and sliding a steel plate beneath to lift the tube without losing any soil. In each box, samples were taken along the same vertical plane, but at different positions laterally to allow for some overlap in the depths covered by consecutive samples. Because the sand in the test boxes was unsaturated during decommissioning, the dry densities of the samples were calculated using the bulk densities and water contents. Figure 2.15 shows the profiles of dry densities calculated for both boxes. Dry densities ranged from 1521 $kg/m^3$ to 1706 $kg/m^3$.

### 2.3.5 Laboratory Testing

Constant-head permeability tests were conducted on bulk samples of clean and dirty sand prepared at loose and dense states (using wet pluviation and vibro-compaction, respectively, as described in Appendix D). The hydraulic conductivity measurements determined from these tests

are plotted against void ratio in Figure 2.16, along with the empirical predictions of hydraulic conductivity reached using Hazen's equation:

$$k = 0.01(D_{10})^2 \qquad [2.2]$$

and the Kozeny-Carman equation:

$$k = \frac{2}{f \cdot S^2}\left(\frac{e^3}{1+e}\right) \qquad [2.3]$$

where k is hydraulic conductivity (m/s), $D_{10}$ is the diameter of sieve that allows 10% of the soil to pass (mm), f is a constant representing particle angularity, S is specific surface ($mm^{-1}$), and e is void ratio. In the calculation of hydraulic conductivity for both soil types, a value of 1.25 was used for f. The specific surface, S, was calculated as 210 $mm^{-1}$ for the clean sand, and 570 $mm^{-1}$ for the dirty sand, based on the measured particle-size distributions shown in Figure 2.6. The reader is referred to Head (1992) for a more detailed explanation of these two equations. The Kozeny-Carman equation, which uses the soil's entire particle-size distribution curve as input, clearly does a superior job of matching the measured hydraulic conductivity across a range of void ratios compared to Hazen's equation, which uses only the soil's $D_{10}$ value.

## 2.4 Discussion of Results

### 2.4.1 Turbidity Removal

The turbidity reduction of the raw water supply took place both in the granular backfill of the test boxes and in the wellscreens themselves. Had the granular materials filtered all of the suspended solids from the water supply, the four wellscreens would have produced filtrate of identical quality, which clearly they did not. If the wellscreens had removed all of the suspended solids, the layer of dirty sand (which contained a significant portion of fines not present in the sand before placement) would not have developed. An examination of the curves presented in Figure 2.10 provides a good estimate of the relative contributions of the granular material and wellscreens to turbidity removal.

It can reasonably be assumed (based on its large openings and the condition of the wellscreen at decommissioning, as discussed in Section 2.3.4) that the Vee-Wire Drive Point wellscreen had little or no effect on the turbidity of the water flowing through it. The turbidity reduction between the raw water supply and the Vee-Wire Drive Point filtrate can therefore be attributed almost solely to the filtration provided by the sand during the test. The turbidity reductions observed in the other three wellscreen filtrates are due to the combined effects of filtration in the sand and filtration occurring in the wellscreens themselves. The results of these tests indicate that in addition to the turbidity removed by the sand, the Sandblocker, Schumasoil 200 and Schumasoil 80 wellscreens removed an additional 10% to 20% of the turbidity from the raw water supply (for example see the 50$^{th}$ percentiles of turbidity removal). The smaller turbidity reduction observed in the Schumasoil 80 wellscreen, compared to the Schumasoil 200 wellscreen, is probably attributable to a cracked joint in the Schumasoil 80 wellscreen (see Figures J.12 and J.13) which let water seep into the wellscreen unfiltered. These results suggest the filtering ability of a full-scale horizontal well placed in riverbed sediment will significantly improve the water quality supplied to water treatment plants.

The proper selection of a wellscreen for use in a full-scale horizontal well will depend on the size of particles present in the raw water supply. To operate for long periods of time without clogging, the wellscreen should have openings large enough to allow the largest particles suspended in the water filtered through the riverbed sediment to pass freely through the wellscreen. That the Schumasoil 80 wellscreen clogged in these tests, while the Schumasoil 200 did not, suggests that the particles suspended in the water flowing through the wellscreens were larger than 80 microns and smaller than 200 microns. The wellscreen openings should not be so large that particles in the riverbed sediment passes freely through, or the wellscreen filtrate may contain large amounts of sediment. This may lead to the wellscreen filling with sediment, leading to blockages. If the openings or pores are too small, reductions in flow rate may be expected over time as the screen clogs, which would likely be difficult to reverse.

### 2.4.2 Particle Counts

While the results of the particle count measurements presented in Table 2.3 show a 50% to 90% reduction in particles from the raw water to wellscreen filtrate, these results should be applied with caution when considering the efficiency of the system to remove undesirable micro-organisms from the raw water. The particle count measurements were taken over a five-day period at the end of the 2001 testing program when the raw water turbidity was lowest (approximately 1.5 NTU), and may not represent the filtering performance of the test equipment at other times or levels of turbidity. The filtrate from each of the four wellscreens contained lower concentrations of particles in the size ranges of *Giardia lamblia* and *Cryptosporidium parvum* (2 to 15 microns) than were present in the raw water supply, but the reduction in particle counts show little correlation (0.24) with the reductions in turbidity observed over the same period (see Table 2.3).

Furthermore, a review of the literature indicates that the presence or absence of *Cryptosporidium* is poorly correlated with turbidity, in part due to the similarity in refractive indices of the micro-organisms and clear water (Jakobowski *et al.*, 1996). Some previously reported work has shown that little or no correlation exists between particle counts and the presence or absence of *Cryptosporidium* in either raw or filtered water at treatment plants (Morse *et al.*, 2002), so the reduction of particles should not be applied as an analogue of reduction in protozoan cysts. Particle counts are probably only applicable as indicators of treatment efficiency (as reported by Hargesheimer *et al.*, 1998, for example), and the reduction of particles by soil-wellscreen combinations should be viewed in this context.

### 2.4.3 Flow Rates

Several useful conclusions can be drawn from the flow rate measurements presented in Figures 2.11 to 2.13. The high flows observed at the beginning of the test program (in approximately the first 200 hours) may be attributed to the loose state of the clean sand backfill. Because the sand was placed in the test boxes with no efforts to compact it before testing, it is likely that the void ratio (and therefore hydraulic conductivity) of the sand was higher at this point than subsequently

in the testing program. Two processes are thought to have decreased the hydraulic conductivity of the sand in the test boxes and lowered the flow rates: densification of the sand by the downward seepage of water, and accumulation of fines in the top 50mm to 75mm of sand. The lowest flow rates recorded in the 2001 testing program occurred during the high-turbidity event approximately 250 hours into testing. During this brief period, a large amount of fine sediment settled onto the surface of the sand in the two test boxes, blocking pores and reducing flow rates. As this layer of fine sediment was shovelled away, flow rates increased, until approximately 400 hours had elapsed. From this point until the end of testing, the measured flows remained relatively constant. The flow rates from the Schumasoil 80 and Vee-Wire Drive Point show less response to these events – the Schumasoil 80 produced very low, but relatively consistent, flows during the entire testing program. The flow rates observed from the Vee-Wire Drive Point show some of the same general trends (highest flow at the start of testing, lowest flow at approximately 250 hours). The flows from the Schumasoil 200 and Sandblocker wellscreens showed approximately the same general trends and degrees of variability. These observations are also apparent when comparing the percentiles of measured flow rates in the Figure 2.13.

The difference in the flow rates measured between the four wellscreens is well illustrated in Figure 2.13. From these curves, it is clear that the highest flow rates were measured from the Vee-Wire Drive Point screen, the lowest flow rates were from the Schumasoil 80 screen, and between the two extremes the Sandblocker and Schumasoil 200 screens produced nearly identical results. Because the same backfill surrounded all four wellscreens in 2001, the differences in measured flow rates can be attributed to differences between the wellscreens themselves, in particular the magnitude of head loss across the wellscreen walls. From the flow rate measurements one can conclude that the smallest head losses were caused by the Vee-Wire Drive Point screen, slightly larger head losses in the Sandblocker and Schumasoil 200 screens, and the largest head losses in the Schumasoil 80 wellscreen. Unfortunately, no manufacturer supplied information was available about the head losses inherent in the wellscreens to confirm these conclusions.

With the exception of the results from the Schumasoil 80 wellscreen, the curves shown in Figure 2.13 can be divided into two regions. The upper 20% of the flow rates observed from the Vee-Wire Drive Point, Schumasoil 200 and Sandblocker wellscreens show more variability (steeper slopes) than the lower 80%. Referring back to Figures 2.11 and 2.12, the upper 20% of the flow rates correspond to the measurements taken in the first 200 hours of testing. The lower 80% of the flow rates shown in Figure 2.13 correspond to the readings taken during and after the high-turbidity event. The 80$^{th}$ percentile of measured flow rates (the point separating the two regions) from these three wellscreens is considered to be a good estimate of what the performance of the soil-wellscreen combinations would have been if the high-turbidity event had not caused blinding at the soil surface by the settling out of fine particles.

A reasonable interpretation to draw from these results is that the largest determinant of the flow rate of horizontal wells is the porous medium in which the wells are placed, and to a lesser extent the design of the wellscreens themselves. An accurate and realistic prediction of flow rate from a full-scale horizontal well will have to include a careful evaluation of the hydraulic conductivity, anisotropy and heterogeneity of the riverbed sediment into which the well is placed.

### 2.4.4 Applicability of Data

Problems with the testing method occurred at the higher levels of source water turbidity. During testing, suspended solids from the raw water supply settled on the surface of sand in the test boxes. This occurred at all values of turbidity, but was especially pronounced and problematic at high levels of turbidity and in particular during the high-turbidity event 250 hours into the testing program. The thin layer of fines deposited on the sand resulted in decreased flow rates and improved filtering performance.

These changes are not considered to be representative of conditions in the river when turbidity is high. The water treatment plant collected water from the river directly, so all of the solid materials present in the raw water supply were in suspension in the river. When these particles dropped out of suspension in the test boxes the conditions in the boxes no longer matched the conditions in the river. The measured flow rates and filtering performance of the test boxes would have been

different had the flow conditions in the boxes matched those in the river, so data collected when raw water turbidity was high (>270 NTU) should be considered with caution when compared to measurements taken when turbidity was low. (This arbitrary definition of high turbidity is the 95$^{th}$ percentile of raw water turbidity measurements). The results of these experiments should be applied with caution to raw water turbidity values above this upper limit.

Based on this arbitrary assumption of the 95$^{th}$ percentile representing the appropriate limit, only 5% of the recorded data points during testing would be discarded. Consequently, the measures of average wellscreen performance (in turbidity reduction and flow rate) are relatively unchanged. The discounted data are characterized by high reductions in turbidity and low flow rates; areas where little variability is seen in the original data (see Figures 2.10 and 2.13). Trimming the measured data in this way changes the observed trends and conclusions very little.

## 2.5 Limitations of Test Method

The experimental program was designed to evaluate the effect of different wellscreen and soil combinations on flow and filtration performance, recognizing that the experimental conditions would differ from field conditions. For example, the properties of the granular materials used in the test boxes and the natural deposits in a riverbed would differ. Some speculation is required to appreciate the effects these differences would have on the measured data. What follows is an attempt to identify the important differences between the experimental behaviour of the test equipment and the actual behaviour of a horizontal well.

### 2.5.1 Nature of Porous Medium

For practical reasons the volume of granular material used in the test equipment was kept small, while the volume of riverbed sediment involved in filtering water for a horizontal well would be several orders of magnitude larger. In the test equipment, wellscreen filtrate water quality changed almost simultaneously with raw water quality, whereas in a riverbed the large mass of sediment would likely delay the onset of changes in water quality. The properties of riverbed sediment (grain-size distribution, permeability, anisotropy and heterogeneity) will be different than the properties of the soil used in the test boxes, so it is expected that filtering performance will

differ. Finally, more processes will be involved in improving the quality of horizontal well filtrate, including dilution with groundwater.

Case studies of the successful application of horizontal collector wells suggest that water quality improvement may be better than indicated by the above test results. Ray *et al.* (2002) and Mikels (1992) describe water quality from horizontal collector wells placed between 6m and 15m beneath rivers. Both report significant turbidity removal from source water to well filtrate (approximately 1 to 2 log-units of removal). Mikels reports that no large-diameter pathogens (*Giardia* or *Cryptosporidium*) were found in any well filtrate samples, despite the presence of *Giardia* and coccidia (an indicator organism) in the source water. Ray *et al.* provide several case studies of the reduction of disinfection-by-product (DBP) precursors, microscopic particles and several other indicators of water quality. The infiltration gallery described by Joshi *et al.* (1985) behaved similarly, reducing turbidity and bacteriological levels. The total effect of the differences between the test equipment used in this study and wells installed in riverbed sediment seems to be a positive one.

### 2.5.2 Test Duration

A test lasting for slightly more than 1200 hours, spanning three summer months, cannot adequately capture or simulate the behaviour of a system designed to operate for decades. Seasonal changes in water quality were not included in the experiment. The performance trends identified from the test results were based on limited data; over a longer time-frame other trends may appear, or the long-term data may resist forming easily identifiable trends. It is possible that other processes (e.g. microbial growth on or around the wellscreen) may also affect the performance of a full-scale horizontal well.

Case studies of horizontal collector wells and riverbank filtration may be the only realistic way of estimating the long-term behaviour of a horizontal well. Mikels (1992) reports on the operation of horizontal collector wells at two sites, at the time 14 and 30 years old, over the course of 15 months. Well filtrate water turbidity was in the order of one log-cycle lower than source water, and much more consistent. *Giardia* and coccidia in the source water were often reduced to below

detectable levels in the wellscreen filtrate, and no macro-organisms (e.g., algae, insects, etc.) were detected in the filtrate. Long-term filtrate water quality appeared to be stable and consistently good.

### 2.5.3 The Hyporheic Zone

The proposed horizontal directionally drilled wells considered in this study will be placed in a region of soil known as the hyporheic zone – the volume of saturated sediment beneath a river or stream containing a mixture of surface water and ground water (Woessner, 2000; White, 1993). Because the quality and quantity of water produced by the horizontal wells will be affected by the properties of the hyporheic zone (e.g., the extent of the region, the hydraulic conductivity of the sediments, and the proportions of surface water and ground water at the location of the well) a complete understanding of the hyporheic zone will allow better predictions of well performance.

Because surface water and ground water are different in many standard measures of water quality (American Water Works Association, 1990), the quality of water produced by a horizontal well will depend on the fractions of surface water and ground water entering the well. The relative proportions of surface water and ground water are expected to vary spatially and temporally in the hyporheic zone, and an accurate prediction of the proportions of water from the two sources will require a knowledge of the factors affecting of surface water and ground water interactions. There are two broad categories of factors that will influence the mixture of water entering a horizontal well: the properties of the hyporheic zone (independent of well placement or pumping rate), and the flow patterns that would be established by extracting water from the hyporheic zone by a horizontal well.

A considerable amount of research has already been conducted to determine the natural interaction of surface water and ground water in the hyporheic zone. Some authors have commented on the effect that small-scale features, such as bed topography, porosity and hydraulic conductivity, have on flow patterns in the hyporheic zone (Woessner, 2000; White, 2000; Wondzell and Swanson, 1996; Castro and Hornberger, 1991). Others have focussed on larger-scale surface water and groundwater interactions, including the effects of channel gradient,

sinuosity, width-to-depth ratio, and penetration (Larkin and Sharp, 1992). Temporal variations, such as changes in river stage (elevation) and flow rate seasonally or in response to storm events, have also been studied (Wroblicky *et al.*, 1998; Wondzell and Swanson, 1996). The potential exists to extrapolate from these studies to characterize the properties of the hyporheic zone and to predict the interaction between surface water and ground water for sites where horizontal wells may be used.

As valuable as a complete understanding of the properties of the hyporheic zone at a site would be, the flow regime that develops in this zone as a result of pumping will likely govern the quality and quantity of water produced by horizontal wells. Numerical models, after being verified with field measurements, could be used to predict the flow rates and relative proportions of surface water and ground water produced by a horizontal well.

## 2.6 Conclusions

To evaluate horizontal directionally drilled wells as an alternative source of water for water treatment plants, pilot-scale tests were conducted at the E.L. Smith Water Treatment Plant in Edmonton, Alberta. The testing program measured the change in water quality (as indicated by turbidity and particle counts) and the flow rates from various soil-wellscreen combinations, and examined the sensitivity of the results to soil type, wellscreen type, and raw water turbidity. The two granular soils used in 2000 (a sand and a sandy gravel) were replaced by a triple-washed, uniform sand in the 2001 testing season. Two stainless-steel wellscreens (the Sandblocker and Vee-Wire Drive Point) and two porous HDPE wellscreens (the Schumasoil 200 and Schumasoil 80) were used in both years. Raw water turbidity measurements varied from 1.40 NTU to 3030 NTU.

The filtrate from each of the four wellscreens was significantly less turbid than the raw water supplied to the test equipment. The Schumasoil 200 and Sandblocker wellscreens removed suspended solids most efficiently, reducing turbidity by approximately 86% and particles larger than two microns by approximately 90%. The Schumasoil 80 and Vee-Wire Drive Point wellscreens removed 83% and 74% of the turbidity from the raw water, and reduced particles

larger than two microns by 80% and 48% respectively. Most of the filtration occurred in the top 50mm to 75mm of granular material filling the boxes; a small amount of suspended material was likely removed by the wellscreens themselves.

The flow rate of filtrate produced by the wellscreens varied from a maximum of 1.9 L/s to a minimum of 0.003 L/s. In 2001, the largest flow rates were produced by the Vee-Wire Drive Point wellscreen, with a median value of 0.78 L/s. The Schumasoil 200 and Sandblocker wellscreens produced nearly identical median flow rates, 0.37 L/s and 0.40 L/s respectively. Clogged pores in the Schumasoil 80 wellscreen accounted for the low median flow rate it produced, only 0.02 L/s. The flow rates measured in 2000 were approximately one order of magnitude lower due to the lower hydraulic conductivity of the granular materials used to backfill the test boxes.

A number of factors limit the application of these results. The short duration of these tests, the differences between the granular materials used in the test equipment and riverbed sediments, and the poorly understood nature of the hyporheic zone indicate that these conclusions should be applied with some caution. There are, however, examples in the literature of similar systems (such as infiltration galleries and horizontal collector wells) performing at least as well as these tests estimate, and over longer periods of time (decades).

These results indicate that the potential exists for water quality improvement by using horizontal wells placed in riverbed sediments.

## 2.7 Acknowledgements

Financial support for this work has been provided by NSERC and EPCOR jointly through the Industrial Partnership Scholarship program. Thanks go to Steve Stanley, Craig Bonneville, Charlie Hartery and the rest of the staff of the E.L. Smith Water Treatment Plant for the generous technical and logistical support they provided during the experimental phase of the study. Many thanks are also due to Rob Donahue, Dave Sego and in particular Kevin Biggar for the direction and support they gave from the beginning of this work.

## 2.8 References

American Water Works Association 1990. Water quality treatment: a handbook for community water supplies. McGraw-Hill. pp. 159-161.

Birch, S. M., Biggar, K. W., and Ariaratnam, S. T. Horizontal directional drilling fluids from a geotechnical perspective. Proceedings, 54th Conference of the Canadian Geotechnical Society, Calgary, Alberta, September 16-19, pp. 33-38

Case Corporation. Case Construction Equipment. Web site "http://www.casece.com". Accessed August 29, 2002.

Castro, N. M. and Hornberger, G. M. 1991. Surface-subsurface water interactions in an alluviated mountain stream channel. Water Resources Research, 27(7): 1613-1621.

EPCOR Water Services Inc. Monthly water treatment plant report: May 2002. Edmonton, Alberta, Canada.

Grant, D. M. and Dawson, B. D. 1995. ISCO Open channel flow measurement handbook, ISCO, Inc., Lincoln, Nebraska.

Hargesheimer, E. E., McTigue, N. E., Mielke, J. L., Yee, P., and Elford, T. 1998. Tracking filter performance with particle counting. Journal of the American Water Works Association, 90(12): 32-41.

Head, K. H. 1992. Manual of soil laboratory testing, Pentech Press, London.

Jakobowski, W., Boutros, S., Faber, W., Fayer, R., Ghiorse, W., LeChevallier, M., Rose, J., Schaub, S., Singh, A., and Stewart, M. (1996). Environmental methods for cryptosporidium. Journal of the American Water Works Association, 88(9): 107-121.

Joshi, N. S., Dhage, S. S., Kelkar, P. S., Paramasivam, R., and Tajne, D. S. 1985. Performance evaluation of a slow sand filter with pre-treatment by infiltration gallery. Indian Journal of

Environmental Health, 27(2): 118-129.

Karanth, K. R. 1997. On sustainable yield of infiltration gallery in valley fills of peninsular India. Journal of Applied Hydrology, 10(3, 4): 86-98.

Larkin, R. G. and Sharp, J. M. (1992). On the relationship between river-basin geomorphology, aquifer hydraulics, and ground-water flow direction in alluvial aquifers. Geological Society of America Bulletin, 104(12): 1608-1620.

Mikels, M. S. 1992. Characterizing the influence of surface water on water produced by collector wells. Journal of the American Water Works Association, 84(9): 77-84.

Morse, A., Wilson, R., Hull, A., and Simms, J. 2002. Monitoring for cryptosporidium risk: do particle counts help? Water Science and Technology: Water Supply, 2(1): 171-180.

Obst, C. E. 1974. Horizontal groundwater collectors, 'Canada's largest water well'. Proceedings of the Annual Conference of the British Columbia Water and Waste Association, Vancouver, British Columbia, April 9-11, pp. 107-123.

Rash, V. D. 2001. Predicting yield and operating behaviour of a horizontal well. Unpublished.

Ray, C., Grischek, T., Schubert, J., Wang, J., and Speth, T. 2002. A perspective of riverbank filtration. Journal of the American Water Works Association, 94(4): 149-160.

Vicente, R., Sarica, C., and Ertekin, T. 2002. A numerical model coupling reservoir and horizontal well-flow dynamics: transient behaviour of single-phase liquid and gas flow. Society of Petroleum Engineers Journal, March 2002, pp. 70-77.

White, D. S. 1993. Perspectives on defining and delineating hyporheic zones. Journal of the North American Benthological Society, 12(1): 61-69.

Woessner, W. W. (2000). Stream and fluvial plain ground water interactions: rescaling hydrogeologic thought. Ground Water, 38(3): 423-429.

Wondzell, S. M. and Swanson, F. J. 1996. Seasonal and storm dynamics of the hyporheic zone of a 4th-order mountain stream. I: Hydrologic processes. Journal of the North American Benthological Society, 15(1): 3-19.

Wroblicky, G. J., Campana, M. E., Valett, H. M., and Dahm, C. N. 1998. Seasonal variation in surface-subsurface water exchange and lateral hyporheic area of two stream-aquifer systems. Water Resources Research, 34(3): 317-328.

Table 2.1 - Wellscreen properties

| Wellscreen Name | Vee-Wire Drive Point | Schumasoil 80 | Schumasoil 200 | Sandblocker |
|---|---|---|---|---|
| Material | stainless steel | Porous HDPE | Porous HDPE | stainless steel |
| Diameter | 32mm (1.25") | 50mm (2") | 50mm (2") | 75mm (3") |
| Length | 0.91m (36") | 0.91m (36") | 0.91m (36") | 0.91m (36") |
| Construction Type | stainless steel wire wrap: 1.35mm wire, 0.4mm gap | sintered HDPE beads, 80µm average pore size | sintered HDPE beads, 200µm average pore size | perforated stainless steel inner and outer walls, stainless steel fiberwool core |
| Open Area | 22% | 36% | 36% | Not Available |
| Placement | South Box | South Box | North Box | North Box |

Table 2.2 – Granular backfill characteristics

| Granular Material | Sand-2000 | Gravel-2000 | Sand-2001 |
|---|---|---|---|
| Coefficient of Uniformity, $C_U$ | 2.9 | 43.3 | 2.1 |
| Coefficient of Curvature, $C_C$ | 1.0 | 1.0 | 1.2 |
| $D_{10}$ (mm) | 0.17 | 0.30 | 0.35 |
| Fines Content (%) | 3 | 2 | 0 |
| USCS Classification | SP | GW | SP |
| Placement | South Box | North Box | Both Boxes |

Table 2.3 – Particle count results (2001)

| Wellscreen Type | Average No. Particles/mL >2µm | Average Turbidity (NTU) | Percent Reduction of Particles (%) | Percent Reduction of Turbidity (%) |
|---|---|---|---|---|
| Raw Water | 9653, (n=9) | 1.68 | - | - |
| Vee-Wire Drive Point | 5057, (n=9) | 0.35 | 48.1 | 78.4 |
| Schumasoil 80 | 1906, (n=9) | 0.39 | 80.2 | 77.3 |
| Schumasoil 200 | 1047, (n=9) | 0.40 | 89.2 | 76.4 |
| Sandblocker | 884, (n=9) | 0.27 | 90.8 | 83.7 |
| | | | Correlation = 0.24 | |

Table 2.4 – Mean measured flow rate for different backfill materials

| Wellscreen Type | Soil Type | | Mean Flow Rate (L/s) | |
|---|---|---|---|---|
| | 2000 | 2001 | 2000 | 2001 |
| Vee-Wire Drive Point | Sandy Gravel | Clean Sand | 0.015 | 0.838 |
| Schumasoil 80 | Sandy Gravel | Clean Sand | 0.009 | 0.023 |
| Schumasoil 200 | Sand | Clean Sand | 0.031 | 0.530 |
| Sandblocker | Sand | Clean Sand | 0.028 | 0.518 |

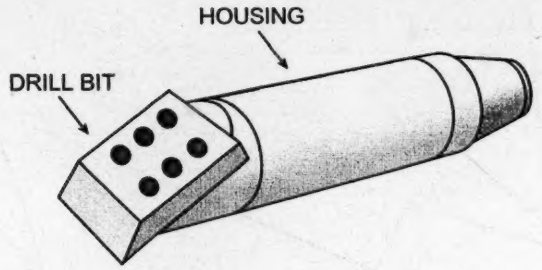


Figure 2.1 – HDD drill bit with housing (not to scale)

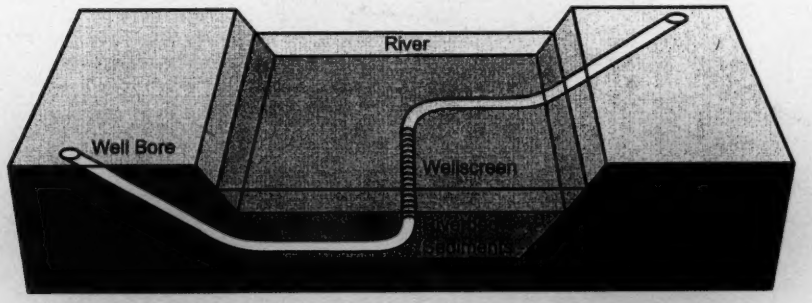


Figure 2.2 – Potential HDD drill path for potable water production (not to scale)

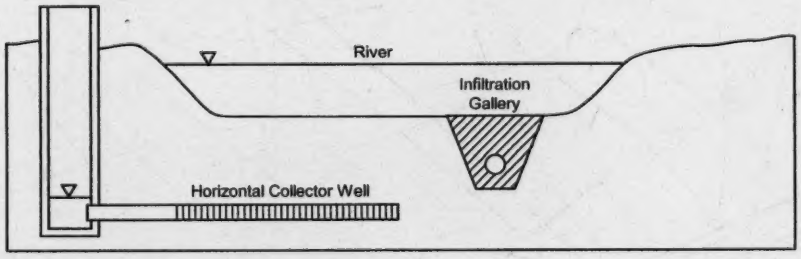


Figure 2.3 – Horizontal collector well and infiltration gallery (not to scale)

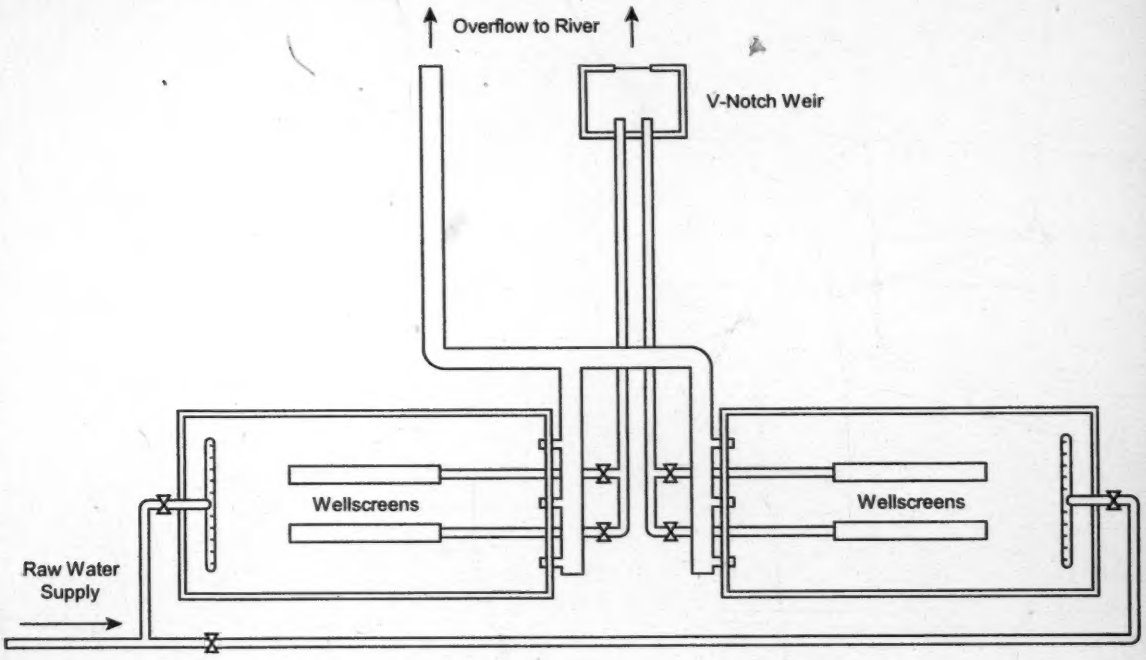


Figure 2.4 – Test equipment schematic diagram (not to scale)

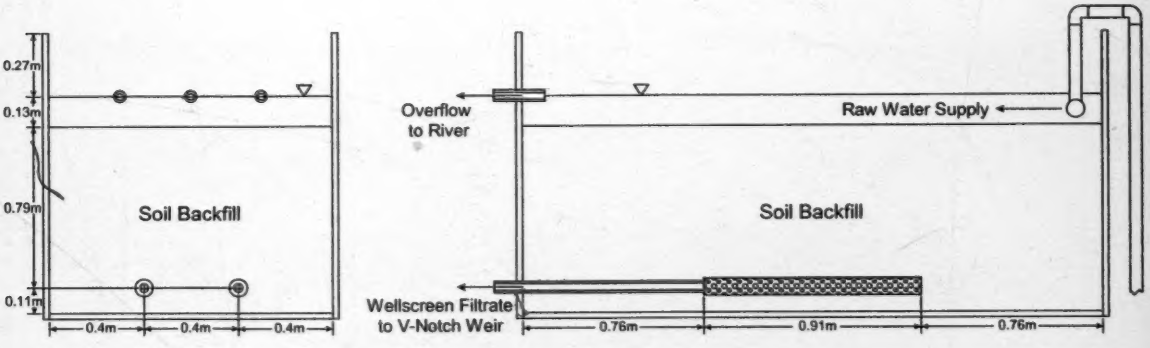


Figure 2.5 - Test box dimensions

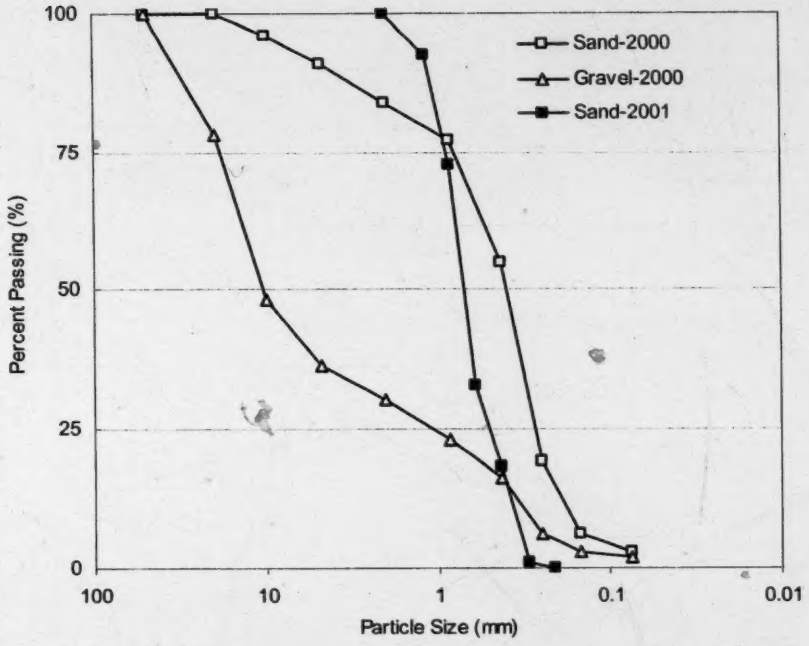


Figure 2.6 – Particle size distribution of granular materials used in test boxes

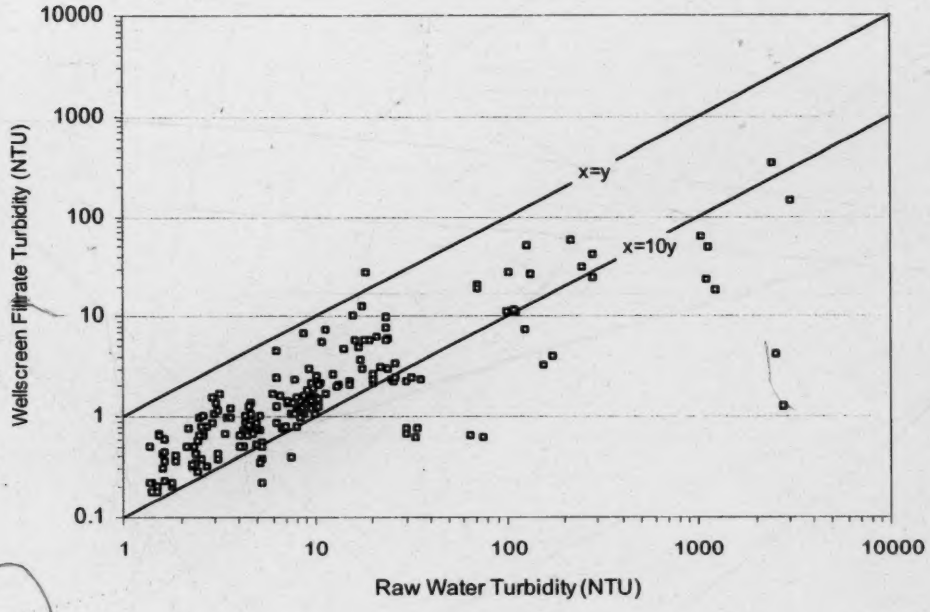


Figure 2.7 – Wellscreen filtrate turbidity vs. raw water turbidity (2001)

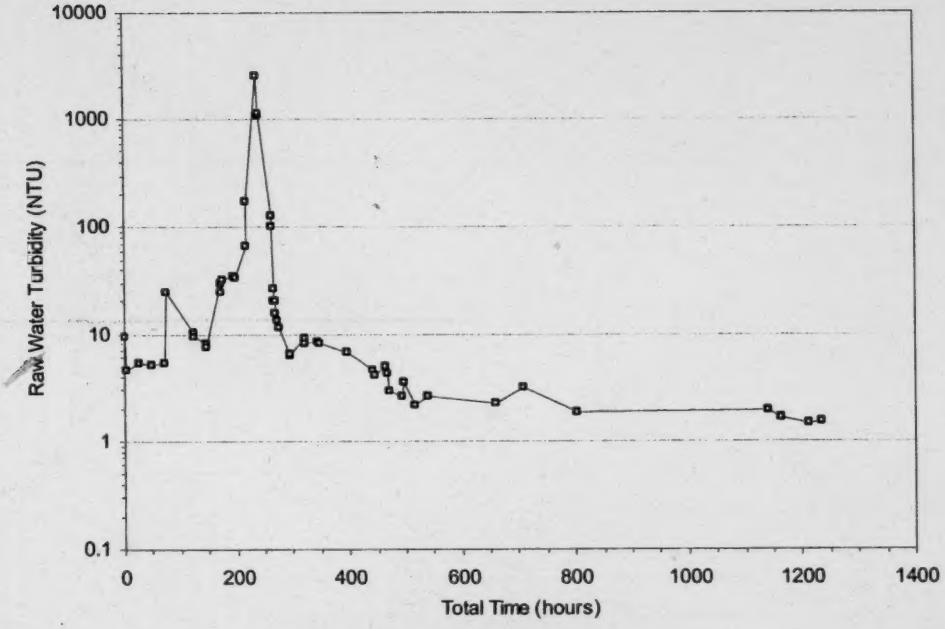


Figure 2.8 – Raw water turbidity vs. time (2001)

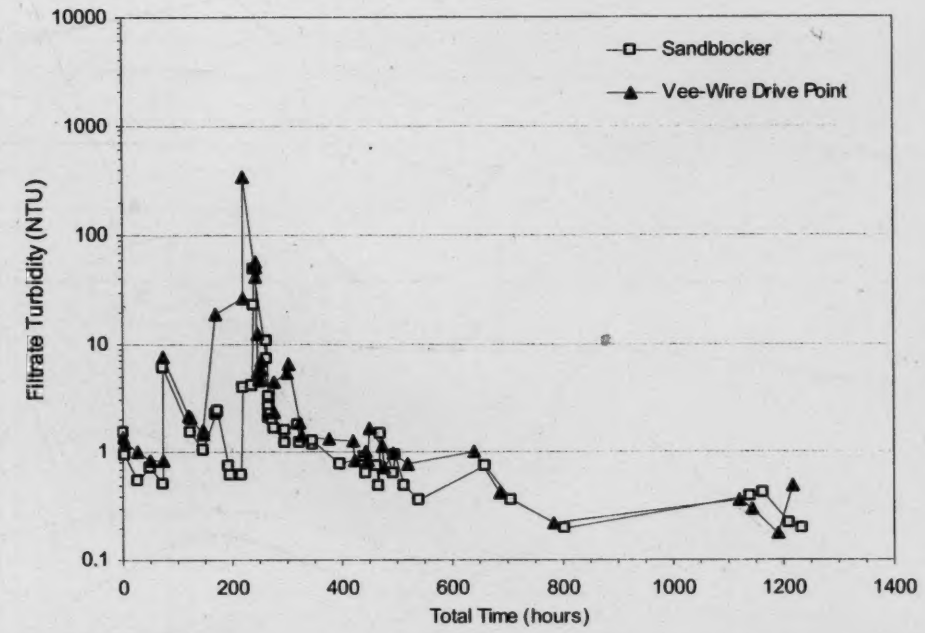


Figure 2.9 – Wellscreen filtrate turbidity vs. time: Sandblocker and Vee-Wire Drive Point wellscreens only (2001)

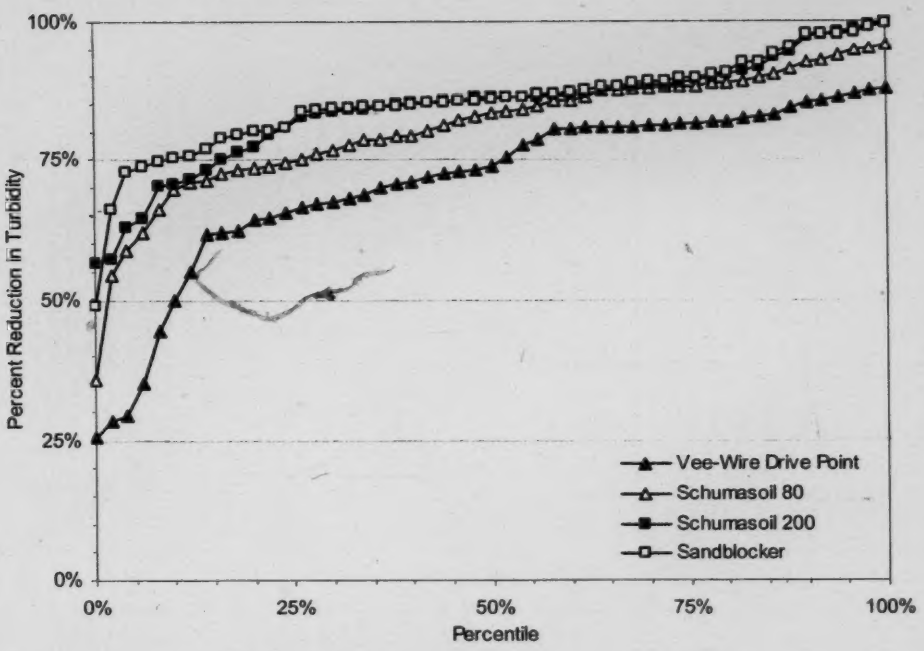


Figure 2.10 – Percentiles of percent turbidity reduction by wellscreen type (2001)

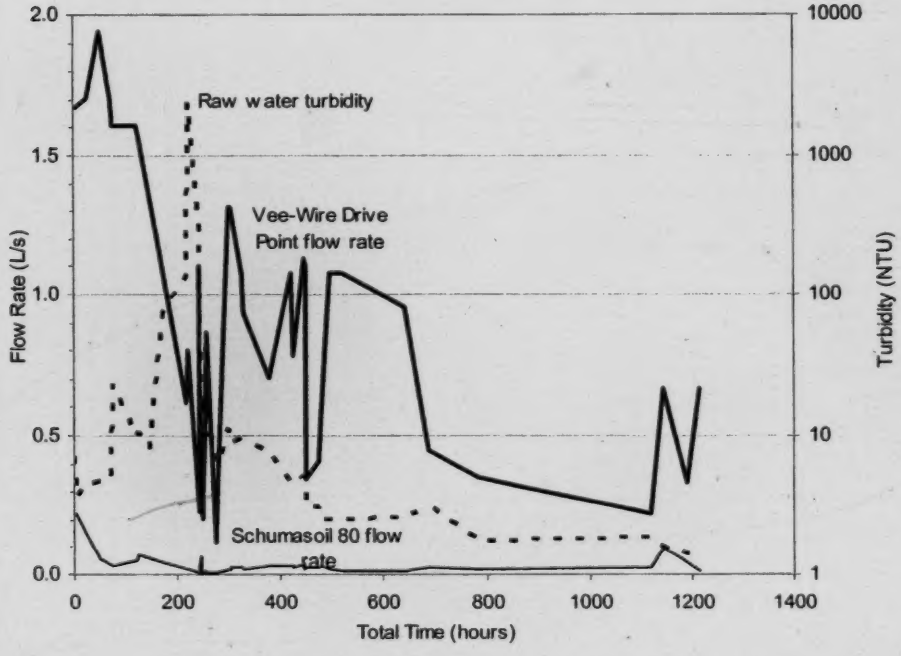


Figure 2.11 – Flow rate vs. time: Vee-Wire Drive Point and Schumasoil 80 wellscreens and raw water turbidity vs. time (South Box) (2001)

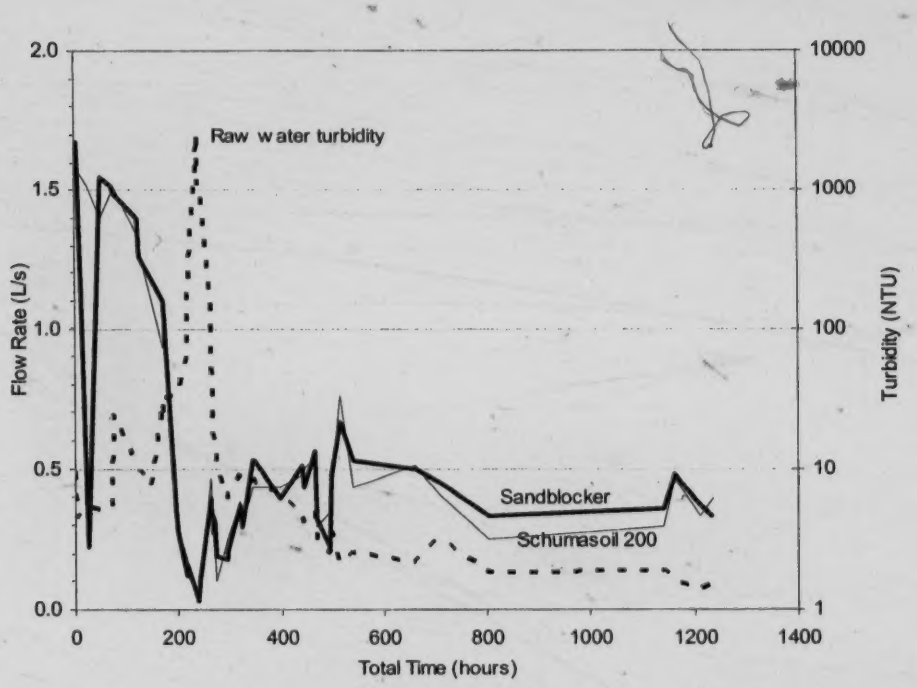


Figure 2.12 – Flow rate vs. time: Sandblocker and Schumasoil 200 wellscreens and raw water turbidity vs. time (North Box) (2001)

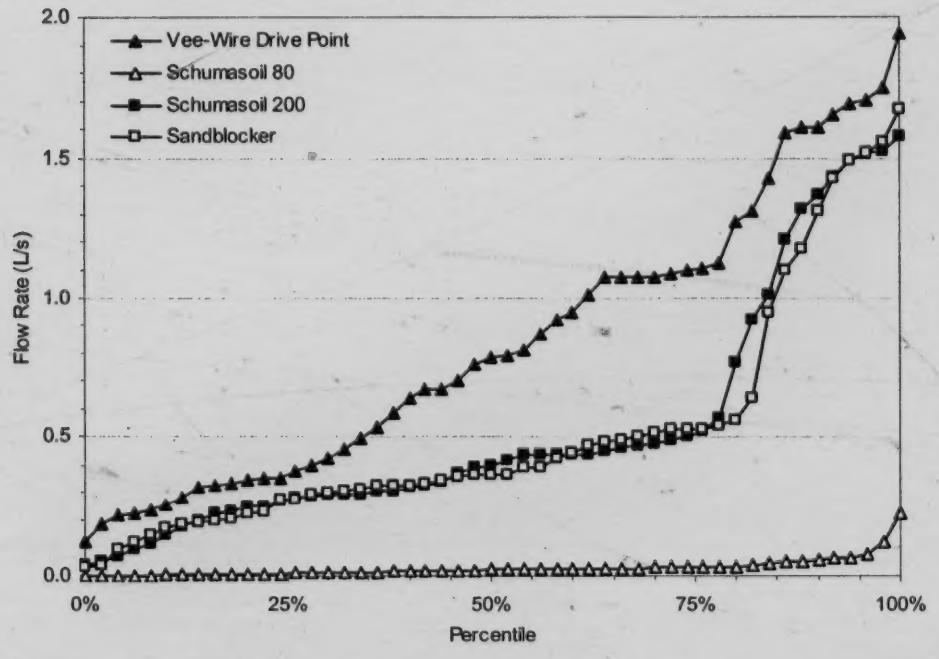


Figure 2.13 – Percentiles of flow rate by wellscreen type (2001)

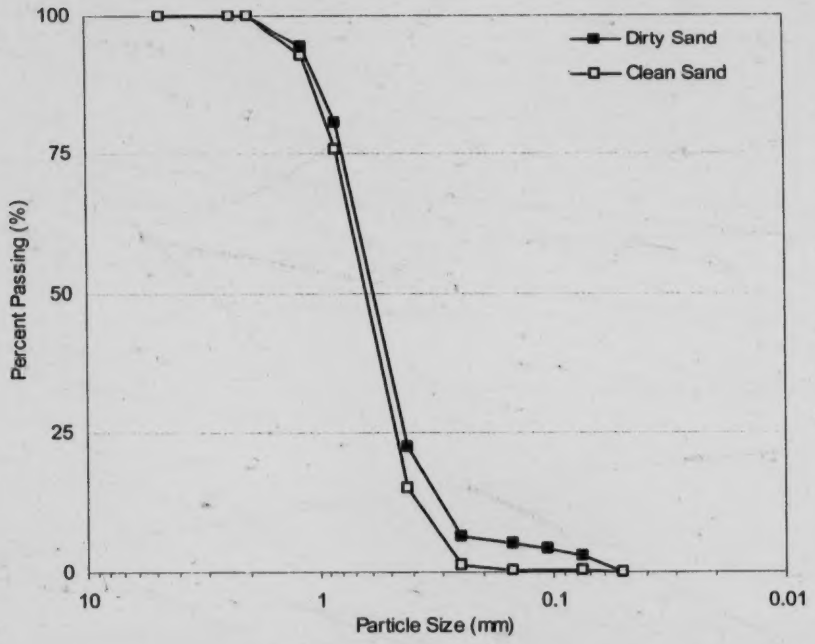


Figure 2.14 – Particle size distributions for clean and dirty sand samples collected at decommissioning (2001)

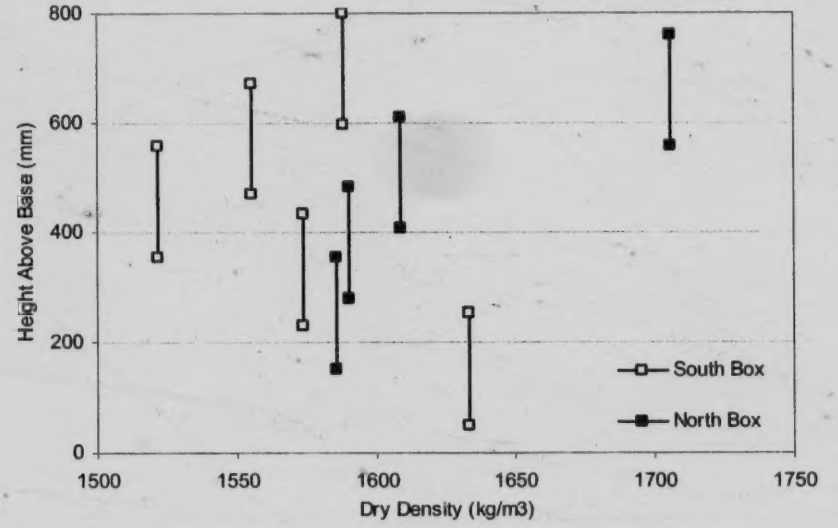


Figure 2.15 – Dry density profiles measured at decommissioning (2001)

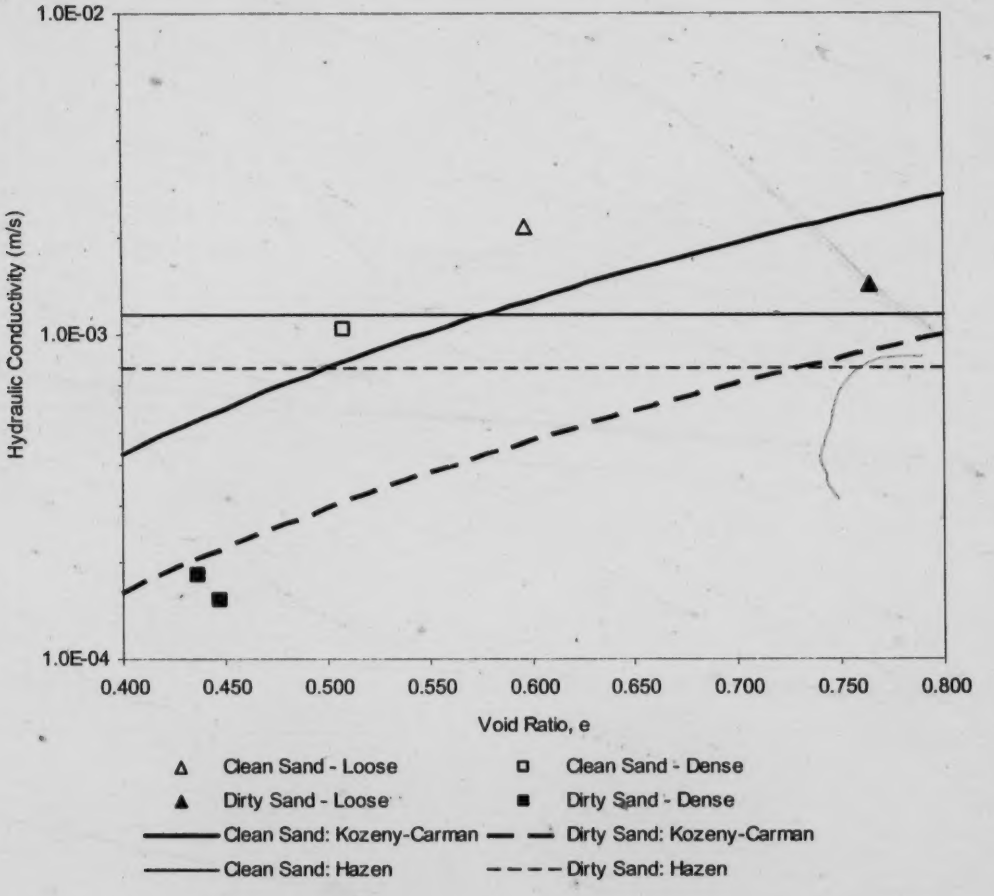


Figure 2.16 – Measured hydraulic conductivity and empirical correlations

# 3 HORIZONTAL DIRECTIONAL DRILLING FOR POTABLE WATER: NUMERICAL MODELLING

## 3.1 Introduction

Horizontal wells placed in the high-permeability sand and gravel sediments beneath rivers should provide some advantages over the intake structures commonly used by water treatment plants. The quality and variability of the water pumped from an intake structure is identical to river water; it contains the same concentration of suspended solids and pathogens, and fluctuates between the same extremes of quality. Horizontal wells installed by directional drilling could improve some of the characteristics (e.g., turbidity) of the water supplied to treatment plants. Water would flow from the river to the horizontal well through the sand and gravel in the riverbed, where the concentration of suspended solids and pathogens would be reduced by filtration (particle straining, adsorption and biological degradation) and dilution with groundwater (Ray *et al.*, 2002; Chapter 2). In addition, the volume of the riverbed sediment should buffer changes in river water quality, leading to a more uniform raw water supply. Because significant amounts of chemicals, such as alum, are used to remove suspended solids from the raw water supply (EPCOR Water Services Inc., 2002), a cleaner water supply should reduce required dosages and cost to treat. Predicting the flow rates available from horizontal wells is an important step in evaluating this technology.

Horizontal directional drilling (HDD) is a technology originally developed by the petroleum industry to improve production in thin or highly anisotropic reservoirs (Vicente *et al.*, 2002). More recently, it has been applied to a range of civil and environmental engineering applications, including utility crossings and contaminated site remediation, and it holds potential to aid in water treatment applications. In a typical HDD installation, the drill stem enters the ground at an angle of 10°-25° to the horizontal (Case Corporation, 2002). The shape of the drill bit (see Figure 3.1) allows the drill stem to be steered along a desired path while underground. The drill bit can be advanced while rotating the drill string to produce a straight segment, whereas advancement without drill string rotation will produce a curved segment. This manoeuvrability allows the placement of

pipelines or wells in areas inaccessible through other means, for example beneath existing structures (roads or buildings, for example) or bodies of water (Figure 3.2), and with great precision. The drill path is usually restricted by several factors: the allowable bending radius of the drill stem or product pipe, soil properties and stratigraphy, and the required borehole length and depth. After the drill bit surfaces at a predetermined location, the pilot bore is reamed to the final diameter. Several passes with reamers of increasing size may be necessary, and on the final reaming the product pipe or wellscreen is pulled into place. During drilling, specially designed drilling fluids are pumped through the drill stem to the bit or reamer and back to the surface (Birch *et al.*, 2001). Drilling fluids are used to remove cuttings, support the borehole wall, and to clean, cool and lubricate the underground equipment. In the case of a well installation, where the permeability of the surrounding soil must be maintained to ensure productivity, the drilling fluid may be designed to resist seeping into the soil or to biodegrade following well completion. Control over drilling fluid pressure is also important – if the pressure is too low, the borehole walls may collapse, and if the pressure is too high, the fluid may hydraulically fracture the surrounding soil and escape to the surface.

### 3.1.1 Research Objectives

The objective of the research presented below was to estimate the flow rates produced by a horizontal well located in the sand and gravel sediments beneath a river, and evaluate the influence of several factors on the yield. The work was conducted in three stages: pilot-scale tests conducted on sample wellscreens, numerical modelling of the flow rates from the pilot-scale test equipment, and numerical modelling of the flow rates from a full-scale horizontal well installation. In the pilot-scale tests, the flow rate of filtrate and filtering performance from several soil-wellscreen combinations was measured (Chapter 2). A three-dimensional finite-element model of the test equipment was developed, using measured material properties to match the measured flow rates. Finally, a second three-dimensional finite-element model was developed to predict the yield from a horizontal well located beneath a river, including a sensitivity analysis of the results to several design parameters and material properties. The effects of wellbore hydraulics were included in both numerical models.

### 3.1.2 Examples of Horizontal Wells Used for Potable Water Supply

Two techniques have traditionally been used to extract water from beneath rivers: infiltration galleries and horizontal collector wells (also known as Ranney or Fehlmann wells). Karanth (1997) describes the use and performance of infiltration galleries for water supply in numerous locations in peninsular India. Reported yields range from $1x10^{-4}$ to $1x10^{-3}$ $m^3/s$ per metre length from infiltration galleries with depths of 6m, lengths of 76m to 762m, diameters of 310mm to 1000mm, and aquifer hydraulic conductivities of $5x10^{-5}$ m/s to $8x10^{-3}$ m/s. Horizontal collector wells have been described recently by Ray *et al.* (2002) and Mikels (1992) and less recently by Obst (1974). Mikels describes collector wells that produced between $1.4x10^{-3}$ and $1.9x10^{-3}$ $m^3/s$ per metre length for well depths of approximately 6m, lengths of 6m to 21m, and aquifer hydraulic conductivities of $1.3x10^{-3}$ m/s to $3.1x10^{-3}$ m/s. Ray *et al.* focus primarily on the filtration ability of horizontal collector wells, but describe several collector wells with depths of 15m to 25m, lengths of 41m to 72m, diameters of 200mm to 300mm, and yields between $1.1x10^{-3}$ and $1.9x10^{-3}$ $m^3/s$ per metre length. Obst describes the design, construction and operation of a single Fehlmann-type horizontal collector well with a yield of approximately $4.5x10^{-4}$ $m^3/s$ per metre length. The well's 15 radial laterals had average lengths of 36m, were 200mm in diameter, and were placed in an aquifer with a hydraulic conductivity of $1.4x10^{-3}$ m/s. Where possible, the details of these installations (e.g. well length, depth, diameter, aquifer hydraulic conductivity and yield) will be compared to the results of the numerical modelling presented below.

### 3.1.3 Analytical and Numerical Solutions of Flow into Horizontal Wells

Analytical and numerical models of flow into horizontal wells have been used for many years in the petroleum industry. There, the economic benefits of accurate predictions of oil or gas production have warranted the development of various solution techniques. The areas of concern are similar but unfortunately the differences between petroleum production and groundwater extraction make their direct application to groundwater flow problems difficult. Vicente *et al.* (2002) examined the transient behaviour of a horizontal well, including wellbore hydraulics and fluid compressibility. Ouyang *et al.* (1998) modelled steady-state flow from horizontal wells, and included wellbore hydraulics, but aimed for more accurate predictions of pressure drop along the

well by including the effect of radial inflow on frictional head losses. Aziz *et al.* (1999) took a different approach in their modelling, choosing to ignore wellbore hydraulics and focussed instead on the variability in model predictions due to uncertainty in reservoir description. Aziz *et al.* also warned against placing too much confidence in the results of simplified semi-analytical solution techniques. Each of these studies is useful for placing the numerical modelling of groundwater flow into perspective.

Many authors have developed analytical or semi-analytical models of groundwater flow into horizontal wells, each with complexities related to a particular field of interest, or with their own simplifying assumptions. Steward and Jin (2001) used an analytical model to examine losing sections of horizontal remediation wells (segments of the horizontal well where water flows out of the well and into the surrounding aquifer) in aquifers with uniform flow, and related the minimum pumping rate necessary to avoid losing sections to aquifer thickness, well length and radius. The analytical model of steady-state groundwater flow to horizontal wells developed by Zhan *et al.* (2001) was applied to the interpretation of horizontal well pumping tests in anisotropic confined aquifers. Kawecki (2000) adapted analytical solutions of transient flow to horizontal wells originally developed in the petroleum industry to problems of groundwater flow, using units and terminology consistent with groundwater research. The model presented by Tarshish (1992) was the only example found in the groundwater literature of an analytical model combining aquifer and wellbore hydraulics (rather than the common assumptions of uniform-flux or uniform-head boundary conditions). Numerous other equations for flow into horizontal wells exist (see Cullinan (1987) or Karanth (1997) for example), but all are less applicable to the conditions at hand.

Commercially available numerical modelling software packages like MODFLOW have been used to model groundwater flow into horizontal wells, generally focussing on issues related to contaminated site remediation (e.g., Langseth, 1990). Models examining wellbore hydraulics and sensitivity to well placement and design were not found in the literature.

## 3.2 Experimental Setup

### 3.2.1 Test Equipment

All of the field tests performed for this study were carried out at the E.L. Smith Water Treatment Plant, which is located on the North Saskatchewan River in Edmonton, Alberta. Water quality and flow rate measurements were made in the summers of 2000 and 2001, with the majority of data recorded in the period between July and September 2001. A detailed explanation of the tests is contained in Chapter 2, with a brief description of information relevant to this study provided below.

Raw water was pumped from the Low Lift Pump-house to the testing equipment on an adjacent tarmac. The two plywood test boxes shown in Figure 3.3 (referred to below as the North Box and South Box) measured 1.20m deep x 1.20m wide x 2.43m long; each contained two 0.91m long wellscreen segments, a plastic-tarp lining for water-tightness and a backfill of 0.8m of granular material. Raw water entered the box at one end through a diffuser placed just above the sand, then flowed either to overflow pipes at the other end of the box or through the soil to an open wellscreen. Wellscreen filtrate flowed through PVC pipes down a short hill (7:1 slope, 15m long) to a box containing a v-notch weir, after which weir effluent and overflow water were discharged back into the river.

Four wellscreens were used: from MAASS Midwest, a Sandblocker screen; and from Johnson Screens, a Vee-Wire Drive Point and two Schumasoil screens. The Sandblocker wellscreen was constructed of two perforated stainless-steel tubes, one inside the other, separated by stainless-steel fiberwool. The Vee-Wire Drive Point consisted of a triangular-shaped wire, with the base facing outward, wrapped around longitudinal stainless-steel ribs arranged in a circular formation around the wellscreen axis. The two Schumasoil wellscreens were constructed of HDPE beads sintered together to form a porous structure. Bead sizes were controlled to provide specific pore-throat diameters; 200 microns and 80 microns in the wellscreens used. Both Schumasoil wellscreens consisted of three 300mm segments of screen, connected with PVC couplers and

bonded with a solvent adhesive. These wellscreens were used in both testing years. Table 3.1 lists the important properties of each wellscreen.

In 2000, the two boxes were filled with a sand and a sandy gravel backfill. The presence of fines in these soils adversely impacted the evaluation of test results (see Chapter 2), so a triple-washed silica sand was used in both boxes in 2001. A summary of the characteristics of each of the soil types is provided in Table 3.2. Figure 3.4 shows the soils' particle-size distributions. In both years, the soils were placed in a loose and dry state, either by shovelling or pouring from supply bags, and were then saturated when pumping began.

### 3.2.2 Experimental Procedure

Details of the experimental procedure are contained in Chapter 2.

## 3.3 Experimental Results and Discussion

### 3.3.1 Measured Flow Rates

Measurements of flow rates from each of the four wellscreen samples were taken throughout the course of the testing program. These measurements were meant to provide an experimental basis for numerical modelling results to be calibrated against, and help to evaluate the merits of the different wellscreen types. In Figure 3.5 the four wellscreens are compared by percentiles of flow rate from the 2001 tests – a convenient way of displaying the variability of measured flow rates. For example, the 0, 50 and 100 percentiles of each curve represent the minimum, median and maximum flow rates recorded during testing, respectively. The shapes of the curves indicate the distribution of data – flat portions of the curves indicate flow rates recorded more frequently, and steep portions indicate flow rates observed less often. The highest flow rates were measured from the Vee-Wire Drive Point screen, the lowest flow rates were from the Schumasoil 80 screen, and the Sandblocker and Schumasoil 200 screens produced nearly identical results. Because the same backfill surrounded all four wellscreens, the differences in measured flow rates can be attributed to differences between the wellscreens, in particular the magnitude of head loss across the wellscreen walls. From the flow rate measurements one can conclude that the smallest head losses occurred in the Vee-Wire Drive Point screen, with slightly larger head losses in the

Sandblocker and Schumasoil 200 screens, and the largest head losses in the Schumasoil 80 wellscreen. Unfortunately, no manufacturer-supplied information about the head losses inherent in the wellscreens was available to confirm these conclusions.

The difference in flow rates measured in the 2000 and 2001 testing seasons is presented in Table 3.3. A distinct increase in flow rate (approximately one order of magnitude) was observed when replacing the soils used in 2000 with the clean sand used in 2001. There was even a two- to three-fold difference in flows measured in the two granular materials of 2000 with the gravel backfill paired with the Vee-Wire Drive Point and Schumasoil 80 screens delivered lower flow rates than the sand backfill used with the other two screens.

A reasonable interpretation to draw from these results is that the largest determinant of the flow rate of horizontal wells is the porous medium in which the wells are placed, and to a lesser extent the design of the wellscreens themselves. An accurate and realistic prediction of flow rate from a full-scale horizontal well will have to include a careful evaluation of the hydraulic conductivity, anisotropy and heterogeneity of the riverbed sediment into which the well is placed.

### 3.3.2 Decommissioning of Test Equipment

At the conclusion of the 2001 testing program, the test equipment was disassembled and removed from the site. Some useful observations were made on the condition of the sand and wellscreens.

Two distinct layers of sand were present in both test boxes. A layer of dirty sand 50mm to 75mm deep covering the entire surface of the boxes had developed. From a visual inspection, it appeared that fine suspended solids present in the raw water supply had been filtered from the water as it seeped through this granular material. The increased fines content had made the sand in this layer darker and more cohesive than the remaining sand (the bottom 725mm to 750mm). This thicker underlying layer of clean sand appeared to be relatively unchanged from the condition in which it had been placed. Figure 3.6 shows the difference in grain size distributions

between the clean and dirty sand layers. Only 0.4% of the clean sand passed a #200 sieve (75μm), compared to 2.8% of the dirty sand.

As the wellscreens were removed from the boxes their condition was assessed. Three of the four wellscreens (the Vee-Wire Drive Point, Schumasoil 200 and Sandblocker screens) appeared to be in good condition, free of fine material and relatively unclogged (i.e., no visible sediment or particulates in the pores or openings). The surface of the Schumasoil 80 wellscreen had become darkened, suggesting the pores had become clogged with suspended solids from the raw water. After sectioning the wellscreen, it became apparent that most of the discolouration was confined to the exterior surface of this wellscreen. Except for the exterior surface, the cross-section colour remained very close to the original white.

Density measurements of the sand in both boxes were taken as excavation progressed (see Appendix D for the testing procedure). Figure 3.7 shows the profiles of dry densities calculated for both boxes, which ranged from 1521 kg/m$^3$ to 1706 kg/m$^3$.

### 3.3.3 Laboratory Testing

Constant-head permeability tests were conducted on bulk samples of clean and dirty sand prepared at loose and dense states (using wet pluviation and vibro-compaction, respectively, as described in Appendix D). The hydraulic conductivity measurements determined from these tests are plotted against void ratio in Figure 3.8, along with the empirical predictions of permeability obtained using Hazen's equation:

$$k = 0.01(D_{10})^2 \qquad [1]$$

and the Kozeny-Carman equation:

$$k = \frac{2}{f \cdot S^2}\left(\frac{e^3}{1+e}\right) \qquad [2]$$

where k is hydraulic conductivity (m/s), $D_{10}$ is the diameter of sieve that allows 10% of the soil to pass (mm), f is a constant representing particle angularity, S is specific surface ($mm^{-1}$), and e is void ratio. Head (1992) provides a detailed explanation of these two equations. The Kozeny-Carman equation, which can use a soil's entire particle-size distribution curve as input, clearly does a better job of matching the measured hydraulic conductivity across a range of void ratios than does Hazen's equation, which uses only the soil's $D_{10}$ value.

## 3.4 Numerical Model Setup

### 3.4.1 Software

Numerical modelling for this study was performed with two commercially available software packages: FlexPDE™ (PDE Solutions, 2002) and SVFlux™ (SoilVision Systems Ltd., 2002). SVFlux was used to generate the text input files (which were then modified) used by FlexPDE. FlexPDE, a solver and post-processor, uses the finite-element method (FEM) to solve partial differential equations. The program automatically generates and refines the mesh, with user control over mesh density and solution accuracy. The three-dimensional numerical models were constructed by extruding two-dimensional regions into multiple layers with variable material properties and boundary conditions in each layer.

### 3.4.2 Test Box Model Geometry

The test boxes measured 1.20m x 1.20m x 2.43m, but because only the soil and wellscreens needed to be modelled, the model domain (shown in Figure 3.9) was 0.80m high, 1.20m wide and 2.43m long. The model was constructed with two layers of sand: a top layer of dirty sand 0.075m thick and a bottom layer of clean sand 0.725m thick. A single 0.91m long wellscreen, oriented along the axis of the test box, was connected to the end of the box with a 0.76m long pipe. The axis of the wellscreen and connecting pipe was located 0.11m above the base of the test box, and 0.40m from the side of the box. The radius of the wellscreen was 0.016m; the connecting pipe had an inside radius of 0.016m and an outside radius of 0.030m.

### 3.4.3 Riverbed Model Geometry

In the hypothetical riverbed under consideration, the horizontal well was located directly below the center of the river. Because this simple conceptual model was symmetric, the domain of the numerical model (Figure 3.10) used to represent it consisted of one-half of the aquifer, river and wellscreen. The half-width riverbed model measured 12m high, 65m wide and from 250m to 700m long, depending on the length of the wellscreen (the model domain always extended 100m beyond the ends of the proposed wellscreen). A 25m wide river was incised 2m into the top of the aquifer. The wellscreen varied from 50 to 500m in length (L), from 100 to 300mm in diameter (Ø), and was located between 2.5 and 9.5m below the riverbed surface (D).

### 3.4.4 Test Box Model Boundary Conditions

In the test box model (Figure 3.9), the top surface of the domain was represented by a constant head boundary, with a head value of 0.93m to match measured water levels. The opening of the connecting pipe at the end of the box was also represented by a constant-head boundary, with the head of 0.22m calculated to equal the sum of the elevation head (0.11m), velocity head (0.11m) and pressure head (zero) at the opening. (An iterative procedure was used to determine the velocity head. Details are discussed in Appendix F). All other exterior surfaces (the sides and bottom of the test box) were represented by zero-flux boundaries.

### 3.4.5 Riverbed Model Boundary Conditions

The model of the horizontal well and riverbed (Figure 3.10) was constructed to generalize riverbed geometry and minimize computation time. The river channel surfaces (the side and bottom of the river) and the upstream and downstream faces of the model domain were represented by constant-head boundaries (using head values of 12m on these faces). The open end of the wellscreen was also modelled as a constant-head surface, using a head value equal to the elevation of the wellscreen (i.e., zero pressure and zero velocity head). All other exterior surfaces of the model domain were represented by zero-flux boundaries.

### 3.4.6 Test Box Model Material Properties

The hydraulic conductivities of the sand layers in the numerical model of the test box were based on measured values of density and hydraulic conductivity (see Figures 3.7 and 3.8). Given the range of dry densities measured during decommissioning, a dry density of 1600 kg/m$^3$, which corresponds to a void ratio of 0.65, was selected. From the Kozeny-Carman equation, hydraulic conductivities of $1.6 \times 10^{-3}$ m/s and $5.9 \times 10^{-4}$ m/s were assigned to the clean and dirty sand layers, respectively. The hydraulic conductivities were assumed to be isotropic within each layer.

To model the connecting pipe correctly, the pipe walls had to be considered perfectly impermeable. Rather than using a very low hydraulic conductivity, which caused numerical instability with the software, the pipe walls were treated as a void. Voids are regions of the model where the mesh is not created, so no flow can occur through them, and are therefore treated as perfectly impermeable materials. Examination of the model results confirmed that the void region functioned as intended.

Because FlexPDE does not solve different constitutive equations in different regions of the model domain (i.e., one equation governing flow through porous media and another equation governing flow through pipes), modelling head losses due to friction in the wellscreen required assigning values of hydraulic conductivity along the length of the wellscreen that would simulate the head losses associated with pipe flow. Assigning the properties of the wellscreen and the inside of the connecting pipe to accurately simulate frictional head losses was somewhat complicated. From Darcy's equation,

$$k = \frac{V}{i} \qquad [3]$$

where V is velocity (m/s), i is gradient, and the hydraulic conductivity, k, is a constant for a homogeneous and isotropic porous medium. In pipe flow, however, the gradient ($\Delta hf/L$) is proportional to the square of the velocity, as seen after rearranging the Darcy-Weisbach equation:

$$\frac{\Delta h_f}{L} = \frac{fV^2}{2g\emptyset} \qquad [4]$$

where $\Delta h_f$ is head loss due to friction (m), L is pipe length (m), f is friction factor, g is gravitational acceleration (9.81 m/s$^2$), and Ø is the pipe diameter (m). Adding to the differences between pipe flow and flow through porous media, the friction factor, f, is usually calculated as a function of the Reynold's number, $R_e$, as seen in Haaland's equation (Haaland, 1983):

$$f = \left[1.8\log_{10}\left(\frac{6.9}{R_e} + \left(\frac{\varepsilon}{3.7\emptyset}\right)^{1.11}\right)\right]^{-2} \qquad [5]$$

where

$$R_e = \frac{V\emptyset}{\nu} \qquad [6]$$

with $\nu$ as kinematic viscosity (m$^2$/s). Combining Equations [3] through [6] yields

$$k = \frac{2g\emptyset}{V}\left[1.8\log_{10}\left(\frac{6.9\nu}{V\emptyset} + \left(\frac{\varepsilon}{3.7\emptyset}\right)^{1.11}\right)\right]^{2} \qquad [7]$$

where $\varepsilon$ is pipe roughness (m). The kinematic viscosity of water, ν, was set at $10^{-6}$ m$^2$/s for all model runs. Pipe roughness, ε, was set differently for the two materials subject to pipe flow: $10^{-3}$ m for the wellscreen, and $10^{-5}$ m for the connecting pipe.

From Equation [7], the hydraulic conductivity at any point in the wellscreen was a function of several constants (diameter, Ø, roughness, ε, and viscosity, ν) and one unknown variable (velocity, V). Two ways of approximating the equivalent hydraulic conductivity along the wellscreen were considered: first by using the average velocity of water in the wellscreen to calculate the hydraulic conductivity using Equation [7], and secondly by using a simple function, V(z), in Equation [7] to calculate a function describing the hydraulic conductivity along the

wellscreen. The first method, which was employed for the model of the test box equipment, is described briefly below and in detail in Appendix F. Because the pipes used in this experiment were short, this was deemed a reasonable approach. The second method is described in detail with the description of material properties for the riverbed model.

Using a uniform hydraulic conductivity for the entire wellscreen was a simple and efficient approximate solution to the problem of modelling pipe hydraulics with porous media. The mean velocity of water in the wellscreen, as computed by the numerical model, was used in Equation [7] to calculate the equivalent hydraulic conductivity of the wellscreen. A simple iterative procedure, described in Appendix F, was used to converge on the correct values of mean velocity and hydraulic conductivity.

### 3.4.7 Riverbed Model Material Properties

Horizontal hydraulic conductivity ($k_h$) in the riverbed model was varied from $10^{-3}$ m/s to $10^{-6}$ m/s to cover the range of values reported in the literature (e.g., Karanth (1997), Mikels (1992) and Ray *et al.* (2002)). Anisotropy ($k_h/k_v$) was set at 10 for all cases.

All computations were undertaken using the uniform conductivity solution method described above. A more exact solution method was also used, in a small number of cases, to check the accuracy of this simpler approach. The rigorous approach assumed that velocity in the well, rather than being constant, was a function of the location along the wellscreen (z). This approach also included the effect of radial inflow on the calculation of friction factor along the wellscreen length.

Rather than using the values of velocity computed by FlexPDE to calculate permeability at every point along the length of the well, a function approximating the distribution of velocity along the well, V(z), was used. A linear function, such as

$$V(z) = az + b \qquad [8]$$

or an exponential function of the form

$$V(z) = \exp(az + b) - \exp(b) + c \qquad [9]$$

was used to approximate the velocity distribution within the well, where a, b, and c were constants. The choice to use linear or exponential functions was based on the results of the uniform conductivity solution (in particular, the shape of the profiles of velocity along the axis of the well as seen in Figure 3.16). An iterative procedure (described in Appendix F) was used to determine the values of the constants a, b and c. This process was very time consuming, so it was not used for all parameter combinations, but instead was compared against the uniform conductivity solution previously described for particular representative parameter combinations to establish its influence on the results.

To accurately compute the friction factor in the horizontal well, the effect of radial inflow must be considered. Shulkes *et al.* (1999) show how radial inflow reduces friction, and express the corrected friction factor as:

$$\tilde{f} = f \times \left[1 - 4\alpha\Phi\frac{v}{u}\right] \qquad [10]$$

where $\alpha$ is an experimentally determined parameter, $\Phi$ is the percentage of open area in a wellscreen, v (m/s) is the velocity of fluid flowing radially into the pipe, and u (m/s) is the velocity of fluid flowing through the pipe. Schulkes *et al.* point out that this correction factor is only valid for situations where v/u << 1 (and refer to experimental work concluding that radial inflow ceases to act as lubrication, and starts to obstruct flow, when v/u approaches 1). In this rigorous solution method, the corrected friction factor was constrained to be not less than one-quarter of the uncorrected friction factor. Transforming the variables in Equation [10] to variables consistent with Equations [3] to [9] yields:

$$\Phi\frac{v}{u} = \frac{q_i(z)}{\pi\emptyset \cdot V(z)} = \frac{\pi\emptyset^2}{4}\frac{\frac{\partial V(z)}{\partial z}}{\pi\emptyset \cdot V(z)} = \frac{\emptyset}{4}\frac{\frac{\partial V(z)}{\partial z}}{V(z)} \qquad [11]$$

where $q_i(z)$ is the rate of inflow per metre length along the wellscreen ($m^3/s/m$). Using a conservative value of $\alpha$ = 10 (appropriate for rough pipes like the Vee-Wire Drive Point), the corrected friction factor can be expressed as a function of position along the well:

$$\tilde{f}(z) = f \times \left[ 1 - 10 \left( \frac{\frac{\partial V(z)}{\partial z}}{V(z)} \right) \varnothing \right] \qquad [12]$$

### 3.5 Numerical Model Results and Discussion

#### 3.5.1 Test Box Model

Using the input parameters outlined above and summarized in Table 3.4, the steady-state flow rate predicted by the numerical model of the test box was 1.16 L/s. Comparing this flow rate with the percentiles of measured flows in Figure 3.5, the model's predicted flow rate is larger than 78% of the measured flow rates from the Vee-Wire Drive Point wellscreen, 86% of flow rates from the Schumasoil 200 wellscreen, and 87% of flow rates from the Sandblocker wellscreen. The numerical model result is larger than all measured flow rates from the Schumasoil 80 wellscreen.

Clearly the numerically modelled test box predicts a flow rate consistent with some of the measured values from the pilot-scale test equipment; however, as the numerical model's material properties are based on measurements made during decommissioning, the computed flow rates should match the measured flow rates at the conclusion of the pilot-scale testing program. Average flow rates measured in the final week of testing were 0.47 L/s for the Vee-Wire Drive Point, 0.37 L/s for the Schumasoil 200, and 0.38 L/s for the Sandblocker wellscreen. Errors in the densities measured during decommissioning (and thus the calculated hydraulic conductivities used to define material properties for the numerical model) may be responsible for the nearly three-fold difference between the computed and measured flow rates.

When the clean and dirty sand layers in the test box were assigned hydraulic conductivities of $5.96 \times 10^{-4}$ m/s and $2.21 \times 10^{-4}$ m/s respectively (which are predicted by the Kozeny-Carman equation when using a void ratio of 0.45 and the grain-size distributions shown in Figure 3.6), the

computed flow rate decreased to 0.53 L/s. While the density measurements shown in Figure 3.7 suggest that a void ratio of 0.45 is low, these hydraulic conductivities are within the range of values measured in the laboratory (see Appendix E). The predicted flow rate would also have been lower if the numerical model had included head losses across the walls of the wellscreen. This head loss could have been simulated by modelling the walls of the wellscreen as an equivalent porous medium and assigning a hydraulic conductivity based on the wellscreen type. The head loss across the Vee-Wire Drive Point wellscreen would have been negligible, whereas the head loss across the Schumasoil 80 screen would have been much more significant. Unfortunately, the equivalent hydraulic conductivity was not available for all of the wellscreens used, and conducting laboratory testing to measure this material property was beyond the scope of this investigation. Consequently, the numerical model was run without this component of head loss, and the predicted flow rate is understood to be slightly high. The simulated flow rate (0.53 L/s) is considered to be sufficiently close to the measured flow rates to verify the model's accuracy.

In addition to the calculated flow rates, the model output included the solution mesh generated by the program (Figures 3.11 and 3.12), contours of total head in the test box (Figures 3.13 to 3.15), and profiles of velocity and total head in the wellscreen and connecting pipe (Figures 3.16 and F3.17). The two views of the solution mesh illustrate the typical meshes generated by FlexPDE and the mesh refinement that occurs closer to the wellscreen. The contours of total head, as seen in Figures 3.13 to 3.15, show total head decreasing towards the wellscreen. The profile of axial velocity in the wellscreen (Figure 3.16) shows an approximately linear increase from approximately zero at the toe of the wellscreen (at z = 0.76m) to a maximum at the heel (at z = 1.67m). The slope of the curve is highest near the two ends of the wellscreen, reflecting the greater rate of inflow near the wellscreen's ends and the three-dimensional nature of the flow in the boxes. The profile of total head in the wellscreen and connecting pipe (Figure 3.17) shows a decrease from a maximum of 0.3m (0.3m elevation head, zero velocity head) at the wellscreen toe to a minimum of 0.215m (0.11m elevation head, 0.105m velocity head) at the aperture of the connecting pipe.

### 3.5.2 Riverbed Model

The numerical model of the riverbed was solved using a range of values for several design variables. From a base case of aquifer horizontal hydraulic conductivity ($k_h$) = $10^{-3}$ m/s, wellscreen diameter (Ø) = 300mm, length (L) = 250m and depth (D) = 5.0m, the following variations were made:

- Horizontal Hydraulic Conductivity – $10^{-3}$, $10^{-4}$, $10^{-5}$, and $10^{-6}$ m/s
- Diameter – 100, 200 and 300mm
- Length – 50, 100, 175, 250 and 500m
- Depth – 2.5, 5.0, 7.5 and 9.5m

Hydraulic conductivities were chosen to cover the range of values reported in the literature from horizontal collector well and infiltration gallery installations. The ranges of diameters and lengths are based on the limitations of HDD installation techniques. The range of depths proceeds from an estimated minimum depth of 2.5m (considering factors such as riverbed scour and hydraulic fracture) to a depth of 9.5m, or 0.5m above the base of the model domain. Using the uniform conductivity solution to calculate frictional head loss along the wellscreen described above, the computed rates of flow at the open end of the well from these combinations are presented versus wellscreen length in Figures 3.18 to 3.22. The check computations presented in Table 3.5 and shown in Figures 3.18 to 3.20 represent instances where variable velocities were used in the calculation of frictional head losses along the wellscreens. The model results provide the rate of flow out of the open end of the well under the condition of atmospheric pressure and zero velocity head at the opening. This would simulate, for example, the well draining into a sump from which water was pumped at a rate sufficient to maintain the water level in the sump at the elevation of the well.

The curves of flow rate vs. length are easily interpreted in the context of wellbore hydraulics. The rate of inflow ($m^3$/s per metre length) at a given point in the well depends (in part) on the total

head in the well at that point – lower head in the well produces more inflow, and higher head produces less inflow. Because water flows toward the open end of the well (and head decreases in the direction of flow due to friction), the head in the well is lowest at the well's open end (the heel) and highest at the well's closed end (the toe). Longer well lengths and smaller well diameters increase the frictional head losses in the well, accentuating the head difference between the heel and toe and reducing the rate of inflow at the toe. Figures 3.18 through 3.21 clearly show this trend: the curves of flow rate vs. length have smaller slopes (?Q/?L, or the rate of inflow at the toe of the well) at longer lengths and smaller diameters. This effect is more pronounced with high aquifer hydraulic conductivity because the peak flow velocities (and thus the total head losses due to friction) are larger.

The plots of flow rate vs. length also lead to some useful conclusions on the optimization of well design, both in terms of length and diameter. From Figures 3.18 through 3.21, it can be seen that frictional head losses act to diminish the additional flow delivered by increasing well lengths. At some optimum length (which can only be accurately determined by analyzing the economics of horizontal well installation, a topic beyond the scope of this work but covered adequately by Cho and Shah, 2002) the additional flow produced by extending the well would not justify the cost of extending the well. In Figure 3.18, where the horizontal hydraulic conductivity in the aquifer is $10^{-3}$ m/s, one can see from the slopes of the curves that the optimum length of a 300mm-diameter well (250m to 300m) is significantly longer than the optimum length of either a 200mm- or 100mm-diameter well (approximately 125m and 75m respectively). At an aquifer hydraulic conductivity of $10^{-6}$ m/s (in Figure 3.21), however, the optimum lengths for the three well diameters are all greater than 500m because even at this length, inflow rates and frictional head losses are too small to be significant. It also appears that horizontal wells should be designed with the largest feasible diameter. In cases where head losses are significant (for example, when aquifer hydraulic conductivity is $10^{-3}$ m/s and length is 500m) it appears that increasing the diameter from 100mm to 300mm more than triples flow from the well. While bigger is better, the best well diameter will be a function of economics and HDD installation techniques as well as production flow rates.

Figure 3.22 shows the response of the model to the depth of the well beneath the river. The increasing head difference with increasing depth results in increased flow rates. As the well location nears the base of the aquifer, simulated by an impermeable boundary, the flow rate levels off. Between 7.5m and 9.5m below the river (i.e., between 2.5m and 0.5m above the base of the aquifer), the effects of the impermeable boundary become significant, as the flow of water into the well from below is restricted. The results indicate that the maximum flow rate is achieved from wells placed as far below the river bottom as possible. In reality though, it is likely that this determination will require an analysis of the construction and operation costs associated with horizontal wells, the limitations of the HDD installation technique, the distribution of hydraulic conductivity in the aquifer, and a better understanding of the boundary conditions acting on the riverbed aquifer.

The check computations show good agreement with the uniform conductivity predictions in most cases. The two solution methods are closest in cases where frictional head losses are small (i.e. where V(z) varies linearly over the length of the well because the rate of inflow along the length of the wellscreen is relatively uniform). In these cases, the rigorous solution tends to predict flow rates within 3% of the uniform conductivity results. Where the head losses in the wellscreen are larger (i.e. where V(z) is non-linear because more inflow occurs near the heel of the well than near the toe), the difference between the uniform conductivity and rigorous solutions increases to as much as 32%. At most points, the two solution techniques predict flow rates close enough to each other to be confident in the results of either calculation approach. The ease of use and time savings associated with the uniform conductivity solution method seem to be worth the potential error in this simplification.

Model output also included the solution mesh generated by FlexPDE, as seen in Figures 3.23 and 3.24, the calculated flow velocity and total head in the aquifer and wellscreen, as seen in Figures 3.25 to 3.29, and the hydraulic conductivity assigned to the wellscreen, shown in Figure 3.30. These figures reveal some useful information not apparent from an examination of the flow rates alone. For example, the contours of total head (also known as equipotentials, or lines

perpendicular to the direction of flow) seen in Figure 3.25 indicate that water flows from the river to the wellscreen through the region of the aquifer not directly beneath the river, and suggest the importance of including this region in future site investigations. The equipotentials in Figures 3.26 and 3.27 show that water flows into the wellscreen from the regions beyond the ends of the wellscreen, and that groundwater in the riverbed flows preferentially towards the heel end of the well. The profile of total head in the wellscreen in Figure 3.28 shows frictional head losses of approximately 5m between the toe and heel of the well. The slope of the profile of axial velocity in the wellscreen (Figure 3.29) increases towards the heel end of the wellscreen (at z = 250m), indicating the greater rate of inflow at that end, where the total head is lowest. Finally, the equivalent hydraulic conductivity assigned to the pipe, seen in Figure 3.30, decreases from a maximum of approximately 1200 m/s at z = 0m (where velocity is lowest) to a minimum of approximately 40 m/s at z = 250m (where velocity is highest).

The results of these numerical models are compared with the reported performance of horizontal collector wells and infiltration galleries in Table 3.6. While none of the cases reported in the literature exactly match the design parameters used in the riverbed model, the ranges of well lengths, depths, diameters and aquifer hydraulic conductivities are approximately the same. The rates of inflow per metre length are very similar between each of the cases reported in the literature and the results of the riverbed numerical model. The maximum rate of inflow per metre length calculated by the numerical model ($3.1 \times 10^{-3}$ $m^3/s/m$) is larger than the largest of the reported inflow rates ($1.9 \times 10^{-3}$ $m^3/s/m$), but the difference is small and is not considered to be significant. The close agreement suggests both that the numerical model is relatively accurate, and that horizontal wells could be economically used for the provision of potable water.

### 3.6 Limitations of Testing and Numerical Modelling

The pilot-scale test equipment worked as intended (to examine flow rates and filtration for various soil-wellscreen combinations), but the design had not considered several important factors. First, due to their short lengths head losses in the wellscreen segments were not significant, and likely had little effect on the total flow rate produced by the test equipment. To better examine how flow

rates were influenced by wellbore hydraulics, several changes could have been made. The wellscreen segments could have been longer, or smaller in diameter to increase the frictional head losses, or placed closer to the surface so that there would have been less difference between the frictional head losses in the wellscreen and the drawdown from the static water level above the sand to the wellscreen. Second, the boundary condition at the wellscreen aperture was poorly understood; treating pressure at the end of the connecting pipe as zero (atmospheric) was a best guess, and it was unclear whether the wellscreens and outlet pipes were full or not. Third, the installation of piezometers to measure pressures at various points in the test boxes could have provided another source of data to compare the numerical model results against. Future work could use test equipment designed to minimize or eliminate these uncertainties.

The numerical riverbed model examined the sensitivity of flow rates to the most important design variables (length, diameter and depth), but several other parameters were not given the same treatment. One would expect the flow rate from a horizontal well to be sensitive to total aquifer thickness, river stage (the elevation of water in the river channel), well placement (distance from the center of the river), well inclination (deviation from horizontal), well orientation (parallel, perpendicular or angled to the direction of flow in the river), and numerous other site-specific details (e.g., material heterogeneity and anisotropy). At present it is unclear how these factors will affect results, but the importance of each should be examined before the installation of a full-scale directionally drilled horizontal well.

### 3.6.1 The Hyporheic Zone

The proposed horizontal directionally drilled wells considered in this study will be placed in a region of soil known as the hyporheic zone – the volume of saturated sediment beneath a river or stream containing a mixture of surface water and ground water (Woessner, 2000; White, 1993). Because the quantity of water produced by the horizontal wells will be affected by the properties of the hyporheic zone (e.g., the extent of the region and the hydraulic conductivity of the sediments) a complete understanding of the hyporheic zone allow better predictions of well

performance. Based on the results shown in Figure 3.22, neglecting groundwater inflow would likely underestimate well production.

In the numerical models presented above, the riverbed aquifer was considered to be recharged by river water alone. In reality, the alluvial sediment in the riverbed is impacted jointly by river water and the local hydrogeologic regime. Horizontal collector wells described by Ray *et al.* (2002) have been shown to draw approximately 30% of their total supply from groundwater. A proper appreciation (and representation in numerical models) of the hyporheic zone will be required to properly understand flow into a horizontal well. This is a complicated system, and one that is beyond the scope of the present study.

## 3.7 Conclusions

Evaluating the potential use of horizontal wells as an alternative intake structure for water treatment plants involved measuring the performance of pilot-scale test equipment, and using numerical modelling to simulate the experimental results and to predict the performance of full-scale horizontal well installations. In the experiments conducted at the E.L. Smith Water Treatment Plant, the flow rates of wellscreen filtrate were examined for their sensitivity to soil type, wellscreen design and raw water turbidity. The two granular materials (a sand and a sandy gravel) used in 2000 were replaced by a triple-washed, uniform sand in the 2001 testing season. Two stainless-steel wellscreens (the Sandblocker and Vee-Wire Drive Point) and two porous HDPE wellscreens (the Schumasoil 200 and Schumasoil 80) were used in both years.

The flow rate of filtrate produced by the wellscreens varied from a maximum of 1.9 L/s to a minimum of 0.003 L/s. In 2001, the largest flow rates were produced by the Vee-Wire Drive Point wellscreen, with a median value of 0.78 L/s. The Schumasoil 200 and Sandblocker wellscreens produced nearly identical median flow rates, 0.37 L/s and 0.40 L/s respectively. Clogged pores in the Schumasoil 80 wellscreen accounted for the low median flow rate it produced, only 0.02 L/s. The flow rates measured in 2000 were approximately one order of magnitude lower due to the lower hydraulic conductivity of the granular materials used to backfill the test boxes.

A three-dimensional finite-element model of the test equipment was constructed using SVFlux™ and FlexPDE™ to try to match the measured flow rates. Using the best estimates of the hydraulic conductivity of the sand from the test boxes, the numerical model predicted flow rates above median measured values, but below experimental maximums. The numerical model results matched the measured flow rates when hydraulic conductivities were lowered to reasonable lower-bound limits.

A three-dimensional finite-element model of a horizontal well placed in the sediment beneath a river was then constructed. The flow rate from the well, under conditions of zero pressure and zero velocity head at the well opening, was computed. The sensitivity of the model results to several parameters – well length, depth and diameter and aquifer hydraulic conductivity – was examined. Two methods of simulating pipe hydraulics in the wellscreen were considered, with generally close agreement. The results indicate the significant effect of frictional head losses in the wellscreen on flow rates, and the importance of optimizing well design. At higher aquifer hydraulic conductivities (above $10^{-4}$ m/s), maximizing well diameter is important, while less difference between computed flow rates is seen at lower hydraulic conductivities. The optimum length for horizontal wells, the length of well above which flow rates increase little, is also seen in the results. Finally, the numerical model results agree well with the rates of inflow per metre length of well reported by several authors.

Only a small number of the many factors affecting the flow rate from a directionally drilled horizontal well were considered in this study. Accurately calculating the flow rates from the installation of a full-scale horizontal well will require a more detailed analysis, including a number of site-specific parameters such as material heterogeneity and aquifer boundary conditions. Assuming the errors in calculating the flow rates in this study are small, this technique of extracting water from a river should be both feasible and practical for water utilities.

### 3.8 Acknowledgements

Financial support for this work has been provided by NSERC and EPCOR jointly through the Industrial Partnership Scholarship program. Thanks go to Steve Stanley, Craig Bonneville,

Charlie Hartery and the rest of the staff of the E.L. Smith Water Treatment Plant for the generous technical and logistical support they provided during the experimental phase of the study. SoilVision, and Murray Fredlund in particular, generously provided financial and technical support with the software used in this study. Many thanks are also due to Rob Donahue, Dave Sego and especially Kevin Biggar for the direction and support they gave from the beginning of this work.

## 3.9 References

Aziz, K., Arbabi, S., and Deutsch, C. V. 1999. Why is it so difficult to predict the performance of horizontal wells. Journal of Canadian Petroleum Technology, 38(10): 37-45.

Birch, S. M., Biggar, K. W., and Ariaratnam, S. T. Horizontal directional drilling fluids from a geotechnical perspective. Proceedings, 54th Conference of the Canadian Geotechnical Society, Calgary, Alberta, September 16-19, pp. 33-38

Case Corporation. Case Construction Equipment. Web Site "http://www.casece.com". Accessed August 29, 2002.

Cho, H. and Shah, S. N. 2002. Optimization of well length for horizontal drilling. Journal of Canadian Petroleum Technology, 41(5): 54-62.

Cleveland, T. G. 1994. Recovery performance for vertical and horizontal wells using semianalytical simulation. Ground Water, 32(1): 103-107.

Cullinan, S. R. 1987. Infiltration galleries: prediction of yield for several hydrogeologic environments. Proceedings, International Conference on Infiltration Development and Application, January 6-9, Manoa, Hawaii.

EPCOR Water Services Inc. Monthly water treatment plant report: May 2002. Edmonton, Alberta, Canada.

Haaland, S. E. 1983. Simple and explicit formulas for the friction factor in turbulent pipe flow. ASME Journal of Fluids Engineering, 105, pp. 89-90.

Head, K. H. 1992. Manual of soil laboratory testing, Pentech Press, London.

Karanth, K. R. 1997. On sustainable yield of infiltration gallery in valley fills of peninsular India. Journal of Applied Hydrology, 10(3, 4): 86-98.

Kawecki, M. W. 2000. Transient flow to a horizontal water well. Ground Water, 38(6): 842-850.

Langseth, D. E. 1990. Hydraulic performance of horizontal wells, Superfund '90. Hazardous Materials Control Research Institute, Washington, D.C., pp. 398-408.

Mikels, M. S. 1992. Characterizing the influence of surface water on water produced by collector wells. Journal of the American Water Works Association, 84(9): 77-84.

Obst, C. E. 1974. Horizontal groundwater collectors, 'Canada's largest water well'. Proceedings of the Annual Conference of the British Columbia Water and Waste Association, Vancouver, British Columbia, April 9-11, pp. 107-123.

Ouyang, L.-B., Arbabi, S., and Aziz, K. 1998. A single-phase wellbore-flow model for horizontal, vertical, and slanted wells. Society of Petroleum Engineers Journal, June 1998, pp. 124-133.

FlexPDE 3.02b1 Professional. PDE Solutions Inc. 2002. 1996-2002.

Ray, C., Grischek, T., Schubert, J., Wang, J., and Speth, T. 2002. A perspective of riverbank filtration. Journal of the American Water Works Association, 94(4): 149-160.

SV Flux 2.28. SoilVision Systems Ltd. 2002.

Steward, D. R. and Jin, W. 2001. Gaining and losing sections of horizontal wells. Water Resources Research, 37(11): 2677-2685.

Tarshish, M. 1992. Combined mathematical model of flow in an aquifer-horizontal well system. Ground Water, 30(6): 931-935.

Vicente, R., Sarica, C., and Ertekin, T. 2002. A numerical model coupling reservoir and horizontal well-flow dynamics: transient behaviour of single-phase liquid and gas flow. Society of Petroleum Engineers Journal, March 2002, pp. 70-77.

Zhan, H., Wang, L. V., and Park, E. 2001. On the horizontal-well pumping tests in anisotropic confined aquifers. Journal of Hydrology, 252, pp. 37-50.

Table 3.1 - Wellscreen properties

| Wellscreen Name | Vee-Wire Drive Point | Schumasoil 80 | Schumasoil 200 | Sandblocker |
|---|---|---|---|---|
| Material | stainless steel | HDPE | HDPE | stainless steel |
| Diameter | 32mm (1.25") | 50mm (2") | 50mm (2") | 75mm (3") |
| Length | 0.9m (36") | 0.9m (36") | 0.9m (36") | 0.9m (36") |
| Construction Type | stainless steel wire wrap: 1.35mm wire, 0.4mm gap | sintered HDPE beads, 80µm average pore size | sintered HDPE beads, 200µm average pore size | perforated stainless steel inner and outer tubes, stainless steel fiberwool core |
| Open Area | 22% | 36% | 36% | N/A |
| Placement | South Box | South Box | North Box | North Box |

Table 3.2 – Granular backfill characteristics

| Granular Material | Sand-2000 | Gravel-2000 | Sand-2001 |
|---|---|---|---|
| Coefficient of Uniformity, $C_U$ | 2.9 | 43.3 | 2.1 |
| Coefficient of Curvature, $C_C$ | 1.0 | 1.0 | 1.2 |
| $D_{10}$ (mm) | 0.17 | 0.30 | 0.35 |
| Fines Content (%) | 3 | 2 | 0 |
| USCS Classification | SP | GW | SP |
| Placement | South Box | North Box | Both |

Table 3.3 – Soil types and mean measured flow rates by testing season

| Wellscreen Type | Soil Type | | Mean Flow Rate (L/s) | |
|---|---|---|---|---|
| | 2000 | 2001 | 2000 | 2001 |
| Vee-Wire Drive Point | Sandy Gravel | Clean Sand | 0.015 | 0.838 |
| Schumasoil 80 | Sandy Gravel | Clean Sand | 0.009 | 0.023 |
| Schumasoil 200 | Sand | Clean Sand | 0.031 | 0.530 |
| Sandblocker | Sand | Clean Sand | 0.028 | 0.518 |

Table 3.4 – Test box model input parameters

| Parameter | Units | First Run | Last Run |
|---|---|---|---|
| Hydraulic Conductivity, Clean Sand | m/s | $1.58 \times 10^{-3}$ | $5.96 \times 10^{-4}$ |
| Hydraulic Conductivity, Dirty Sand | m/s | $5.86 \times 10^{-4}$ | $2.21 \times 10^{-4}$ |
| Kinematic Viscosity of Water | $m^2/s$ | $10^{-6}$ | $10^{-6}$ |
| Wellscreen Roughness | m | $10^{-3}$ | $10^{-3}$ |
| Connecting Pipe Roughness | m | $10^{-5}$ | $10^{-5}$ |
| Wellscreen Hydraulic Conductivity | m/s | 15 | 30 |
| Connecting Pipe Hydraulic Conductivity | m/s | 27 | 57 |
| Total Head at Wellscreen Aperture | m | 0.22 | 0.13 |
| Flow Rate | L/s | 1.155 | 0.527 |

Table 3.5 – Riverbed model flow rate computations for select cases

| Length (m) | Diameter (mm) | Aquifer Permeability (m/s) | Flow Rate ($m^3/s$) | | Difference (%) |
|---|---|---|---|---|---|
| | | | Uniform Permeability | Rigorous Solution (Linear or Exponential) | |
| 50 | 300 | $10^{-3}$ | 0.155 | 0.151 (L) | -2.0 |
| 50 | 300 | $10^{-4}$ | 0.017 | 0.016 (L) | -2.3 |
| 250 | 300 | $10^{-3}$ | 0.371 | 0.305 (E) | -17.9 |
| 250 | 300 | $10^{-4}$ | 0.071 | 0.069 (L) | -2.2 |
| 250 | 300 | $10^{-5}$ | 0.007 | 0.007 (L) | -2.4 |
| 250 | 200 | $10^{-3}$ | 0.204 | 0.139 (E) | -31.7 |
| 250 | 200 | $10^{-4}$ | 0.055 | 0.053 (L) | -2.8 |
| 500 | 300 | $10^{-3}$ | 0.428 | 0.311 (E) | -27.3 |

Table 3.6 – Inflow rates from published studies and select numerical model results

| Source | Well Length (m) | Well Diameter (mm) | Well Depth (m) | Aquifer Hydraulic Conductivity (m/s) | Rate of Inflow ($m^3/s/m$) |
|---|---|---|---|---|---|
| Ray *et al.* (2002) | 41 to 72 | 200 to 300 | 15 to 25 | N/A | $1.1 \times 10^{-3}$ to $1.9 \times 10^{-3}$ |
| Karanth (1997) | 76 to 762 | 310 to 1000 | 6 | $5.0 \times 10^{-5}$ to $8.0 \times 10^{-3}$ | $1.2 \times 10^{-4}$ to $1.1 \times 10^{-3}$ |
| Mikels (1992) | 6 to 21 | N/A | 6 | $1.3 \times 10^{-3}$ to $3.1 \times 10^{-3}$ | $1.4 \times 10^{-3}$ to $1.9 \times 10^{-3}$ |
| Obst (1974) | 36 | 200 | N/A | $1.4 \times 10^{-3}$ | $4.5 \times 10^{-4}$ |
| this study (selected data points only) | 50 to 100 | 200 to 300 | 5 | $1.0 \times 10^{-4}$ to $1.0 \times 10^{-3}$ | $2.8 \times 10^{-4}$ to $3.1 \times 10^{-3}$ |

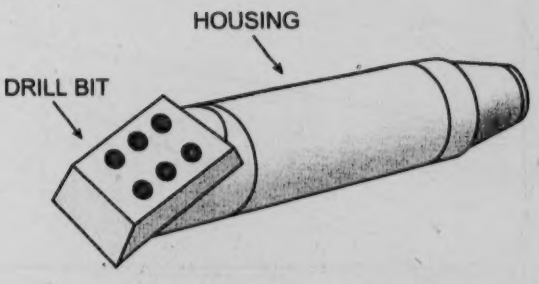


Figure 3.1 – HDD drill bit with housing (not to scale)

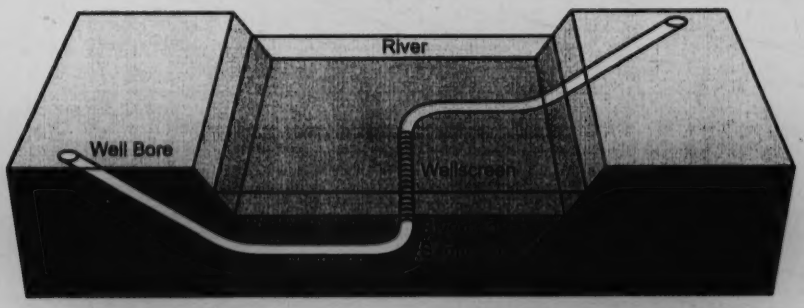


Figure 3.2 – Potential HDD drill path for potable water production (not to scale)

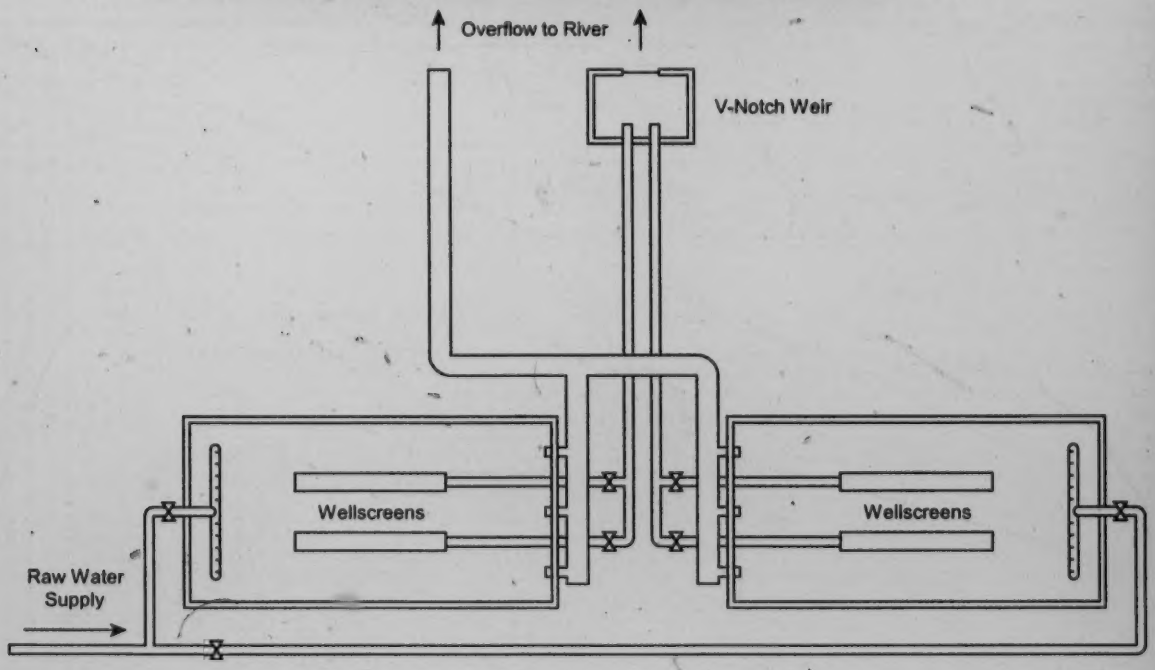


Figure 3.3 – Test equipment schematic diagram (not to scale)

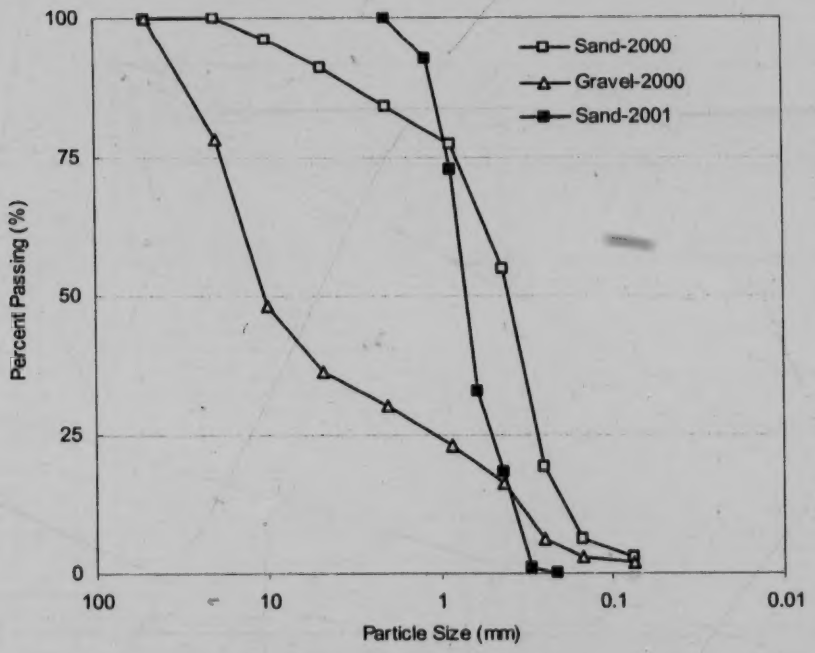


Figure 3.4 – Particle size distribution of soil backfill used in test boxes

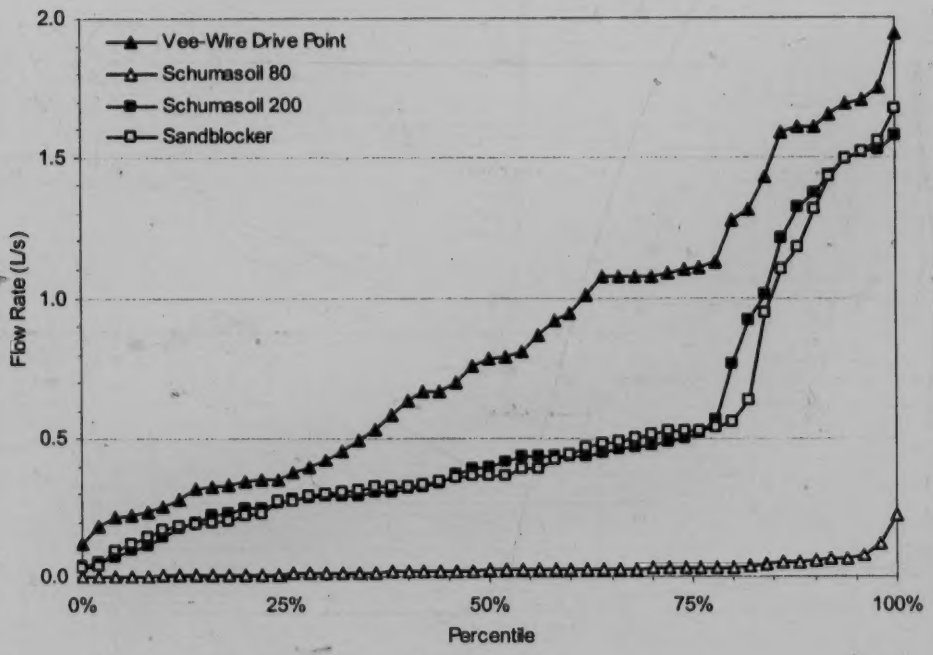


Figure 3.5 – Wellscreen flow rate comparison from 2001 tests: percentiles of flow rate by wellscreen type

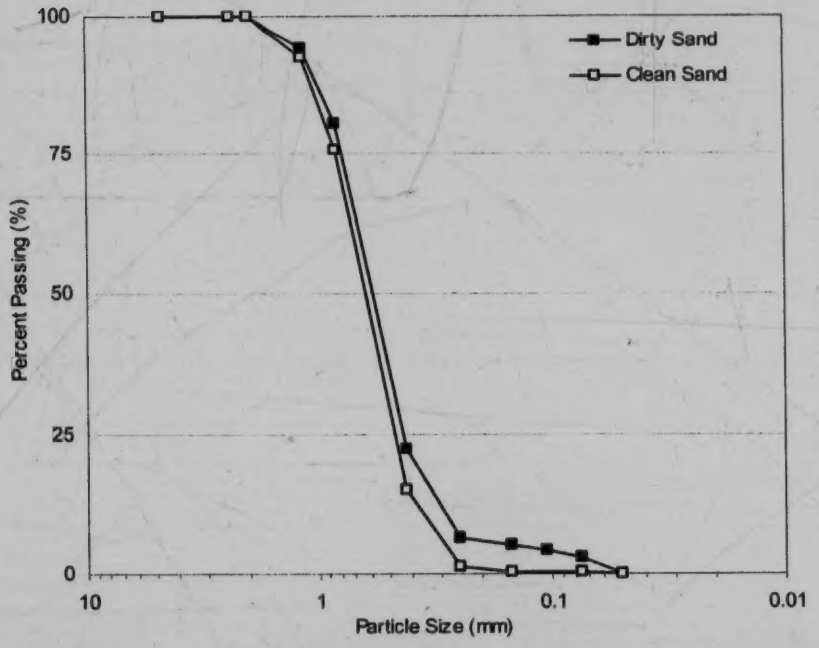


Figure 3.6 – Particle size distributions for clean and dirty sand samples collected at decommissioning

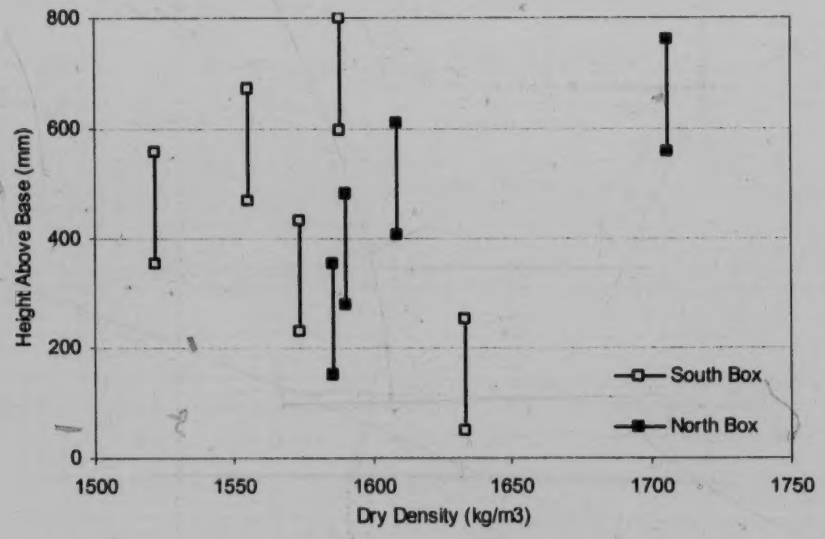


Figure 3.7 – Dry density profiles measured at decommissioning

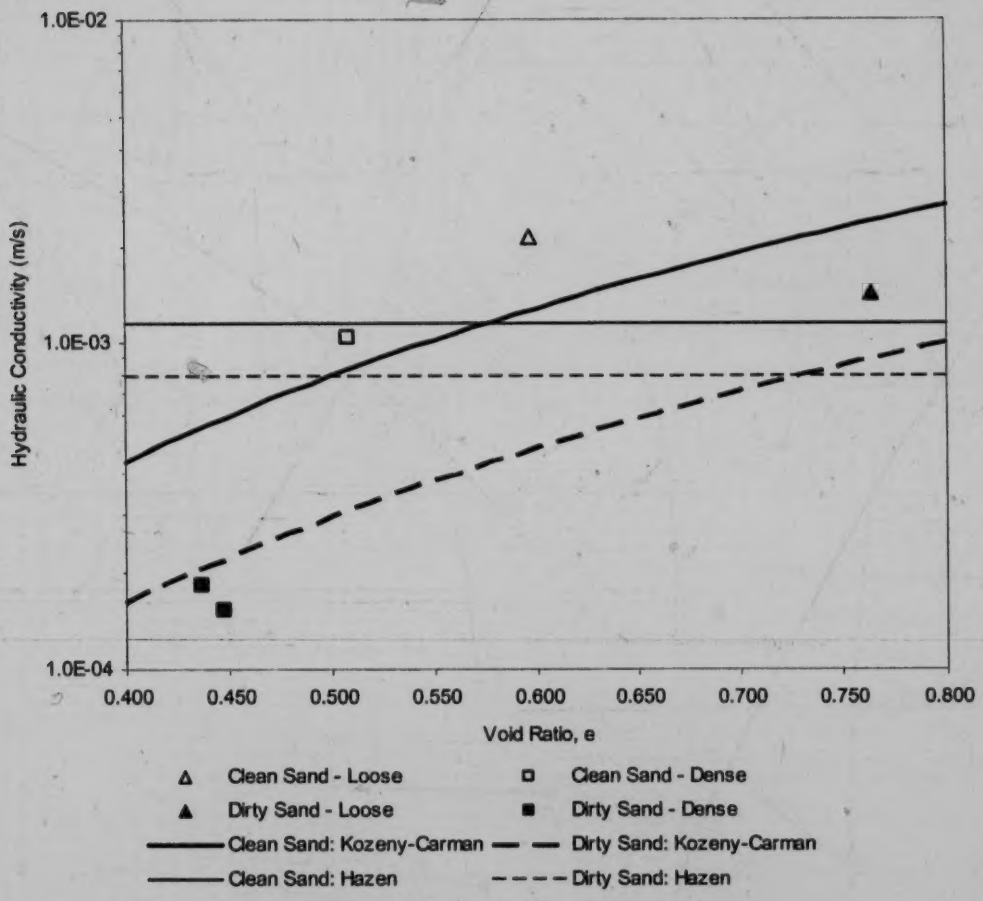


Figure 3.8 – Measured hydraulic conductivity and empirical correlations

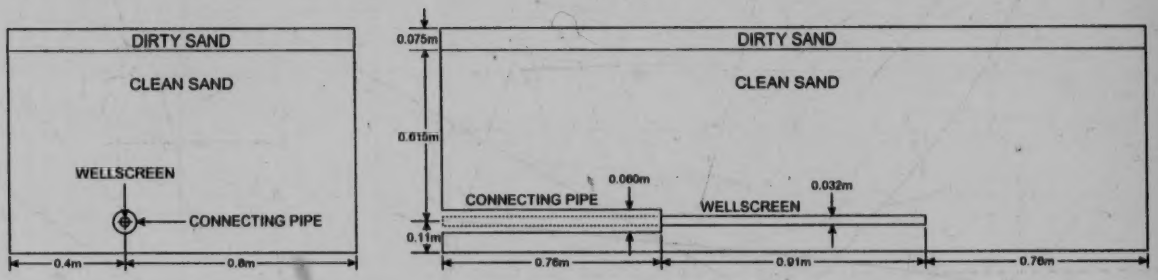


Figure 3.9 – Test box model dimensions (not to scale)

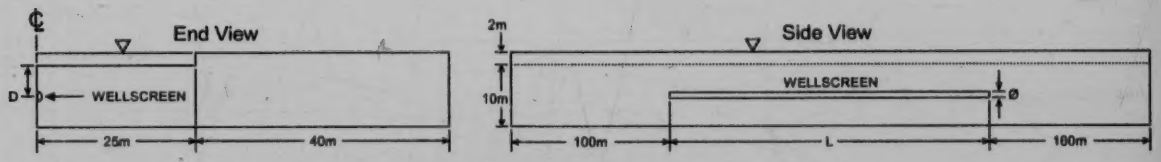


Figure 3.10 – Riverbed model dimensions (not to scale)

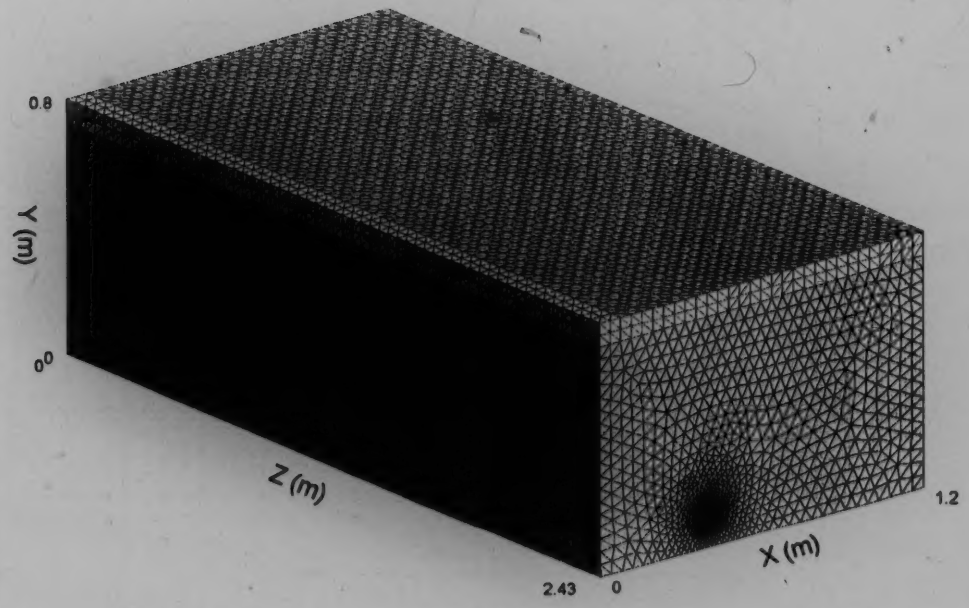


Figure 3.11 – Solution mesh generated by FlexPDE: NGRID = 30

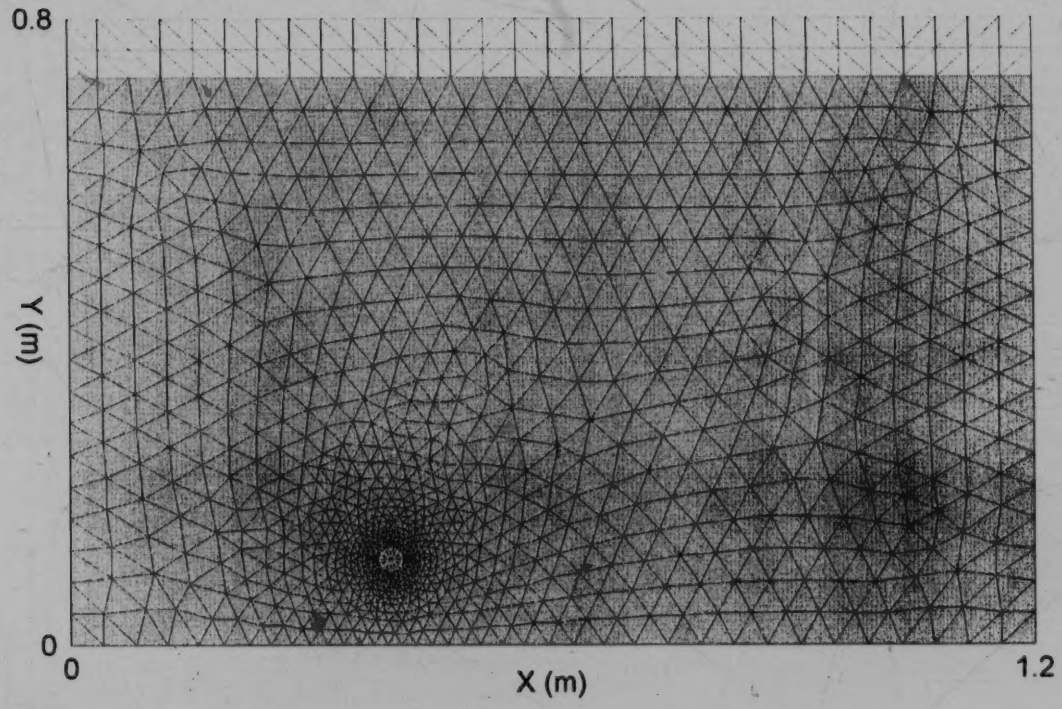


Figure 3.12 – Solution mesh generated by FlexPDE at z = 2.43m: NGRID = 30

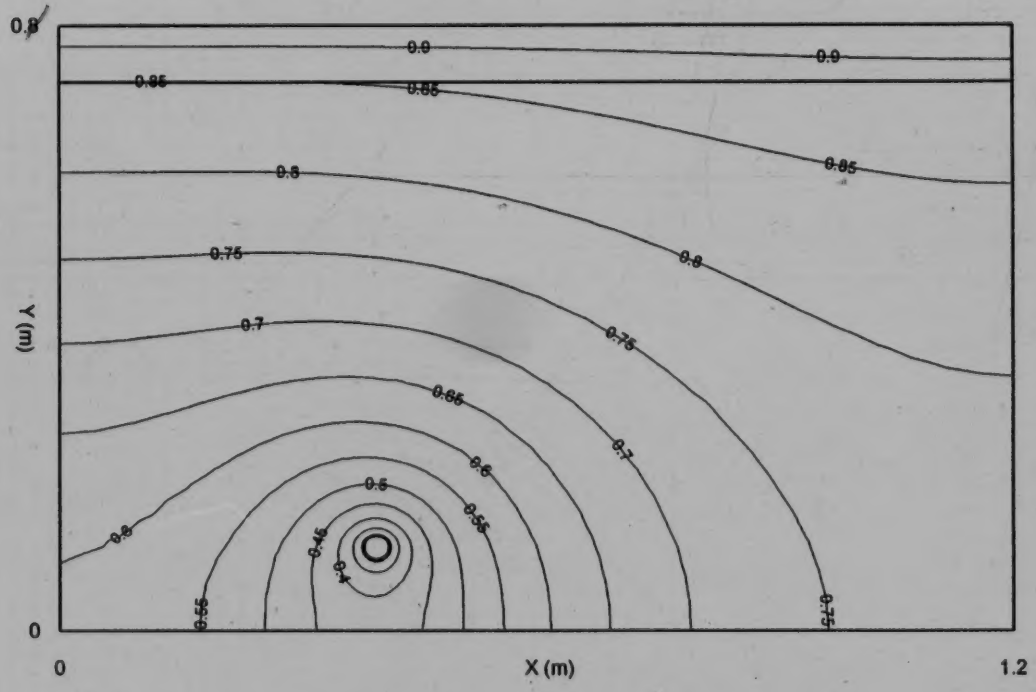


Figure 3.13 – Contours of total head at z = 1.22m (midpoint of wellscreen)

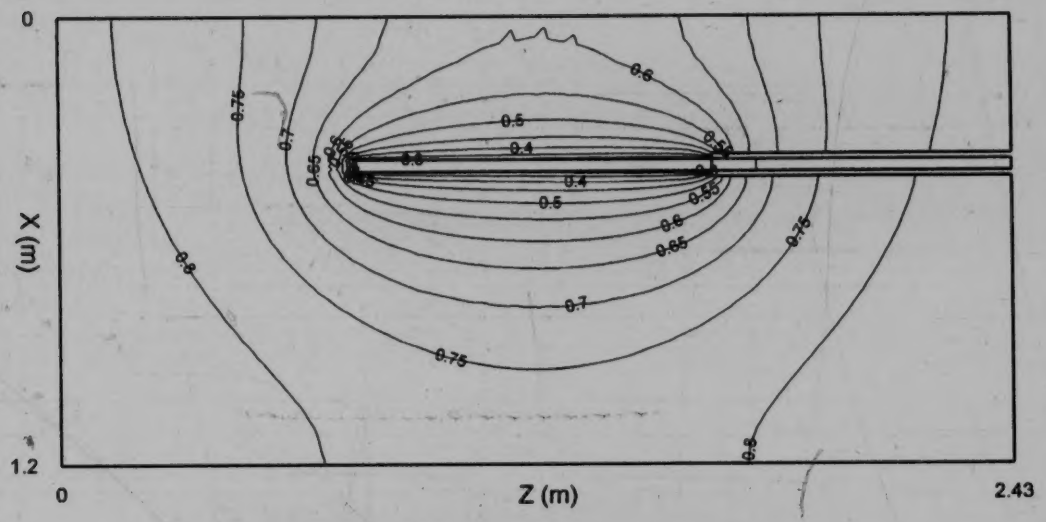


Figure 3.14 – Contours of total head at y = 0.1m (center of wellscreen)

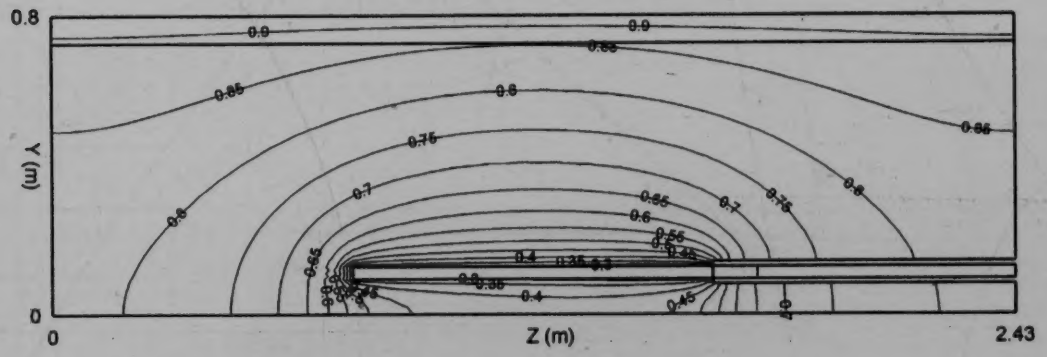


Figure 3.15 – Contours of total head at x = 0.4m (center of wellscreen)

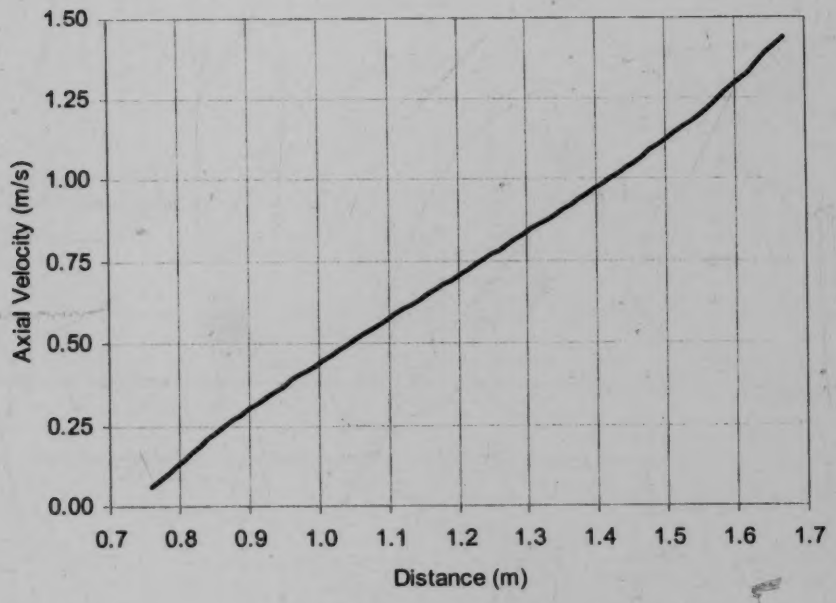


Figure 3.16 – Profile of axial velocity along axis of wellscreen

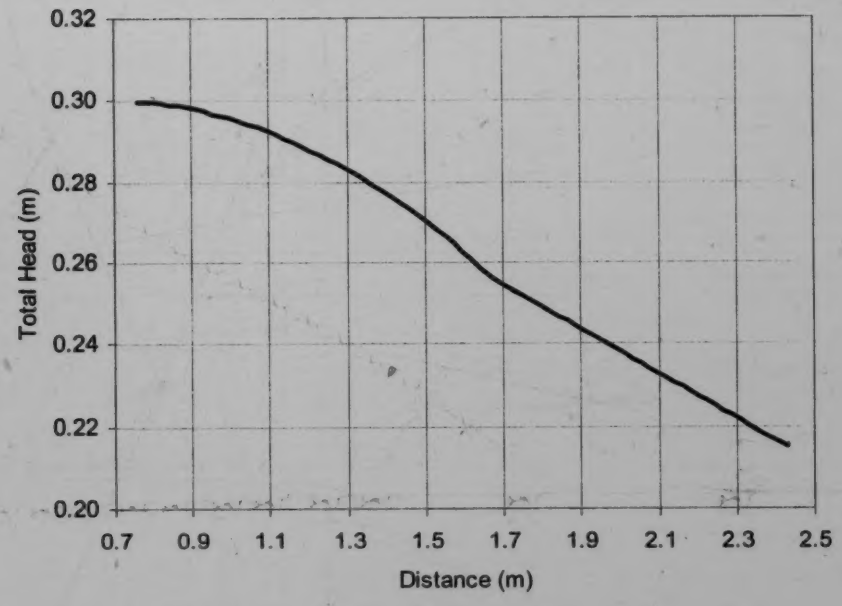


Figure 3.17 – Profile of total head along axis of wellscreen and connecting pipe

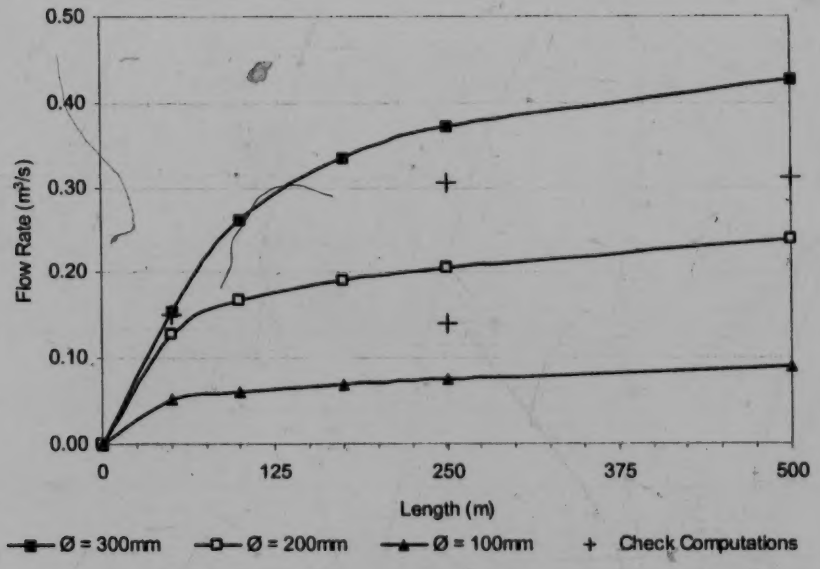


Figure 3.18 – Flow rate vs. length: hydraulic conductivity ($k_h$) = $10^{-3}$ m/s, depth = 5m

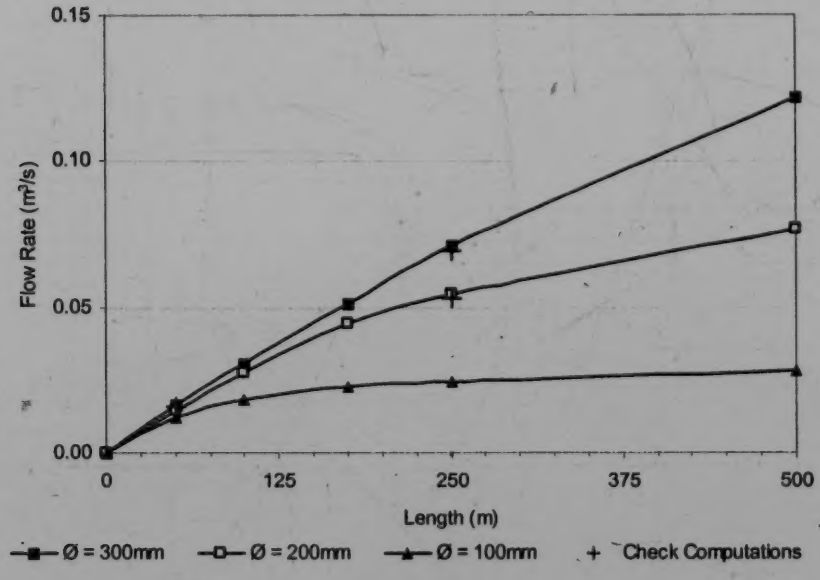


Figure 3.19 – Flow rate vs. length: hydraulic conductivity ($k_h$) = $10^{-4}$ m/s, depth = 5m

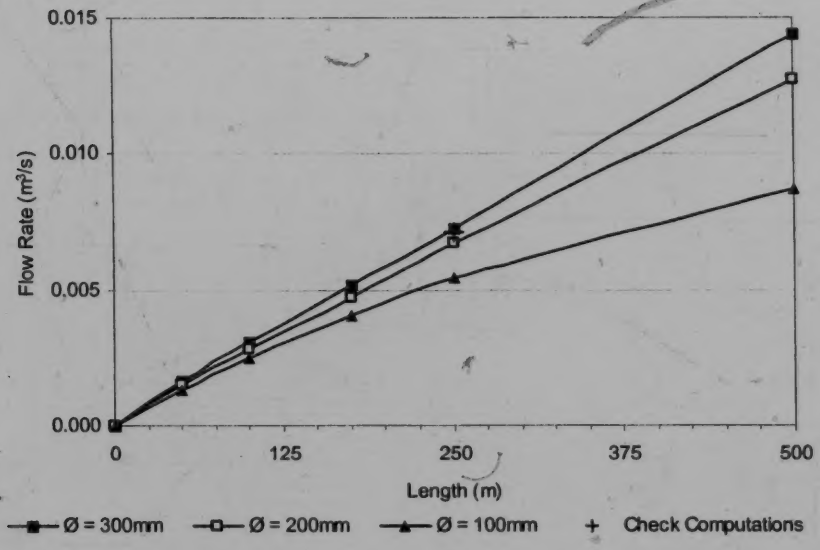


Figure 3.20 – Flow rate vs. length: hydraulic conductivity ($k_h$) = $10^{-5}$ m/s, depth = 5m

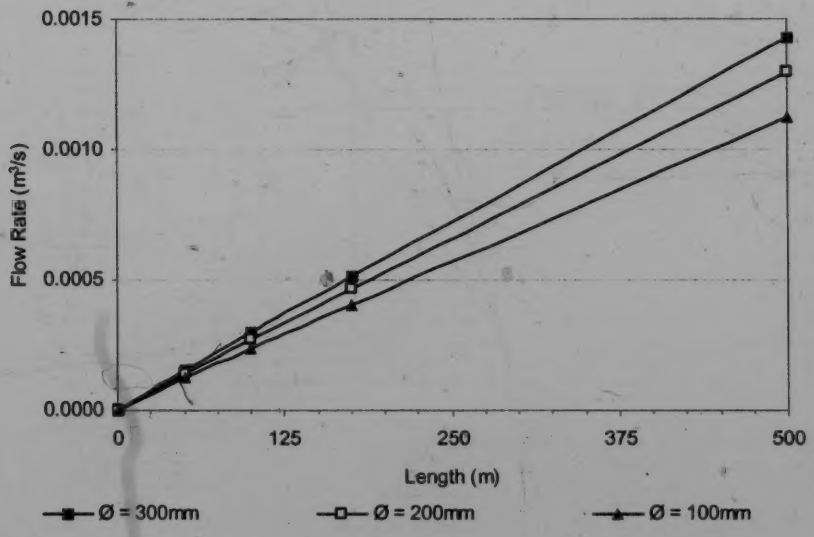


Figure 3.21 – Flow rate vs. length: hydraulic conductivity ($k_h$) = $10^{-6}$ m/s, depth = 5m

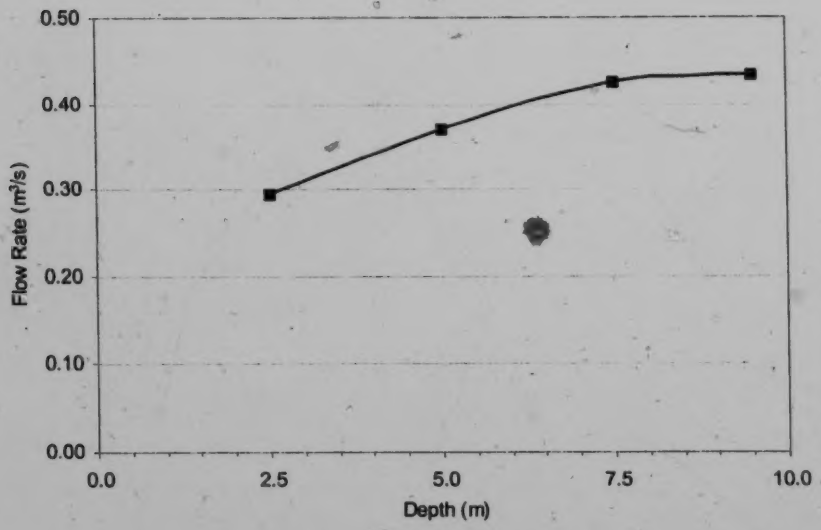


Figure 3.22 – Flow rate vs. depth: hydraulic conductivity ($k_h$) = $10^{-3}$ m/s, diameter = 300mm, length = 250m

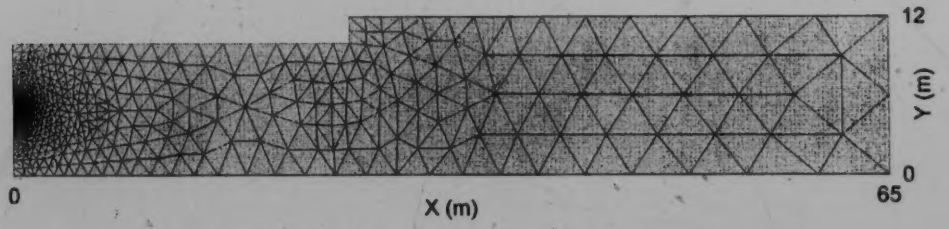


Figure 3.23 – Riverbed model output: solution mesh generated by FlexPDE at z = 0m: NGRID = 60

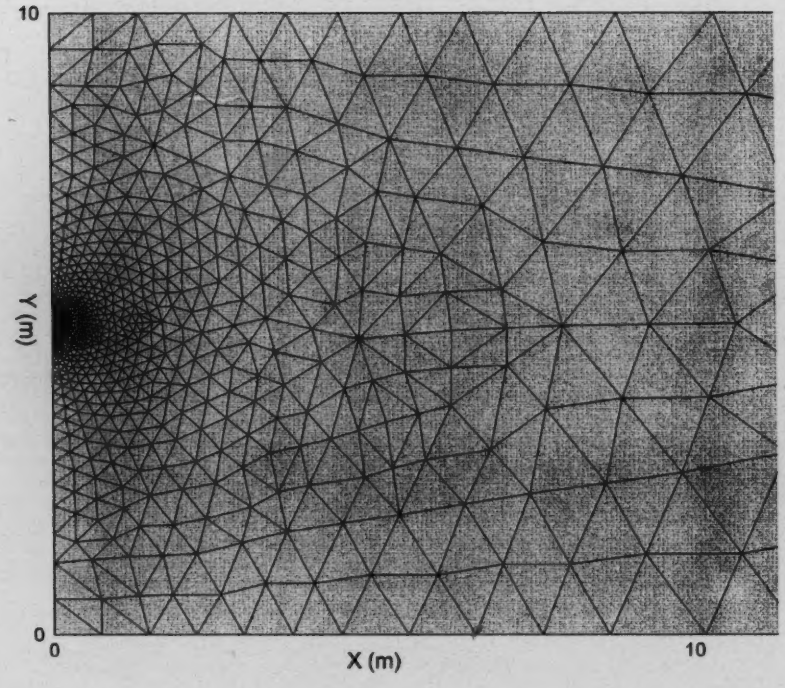


Figure 3.24 – Riverbed model output: solution mesh generated by FlexPDE at z = 0m (zoomed to region around wellscreen): NGRID = 60

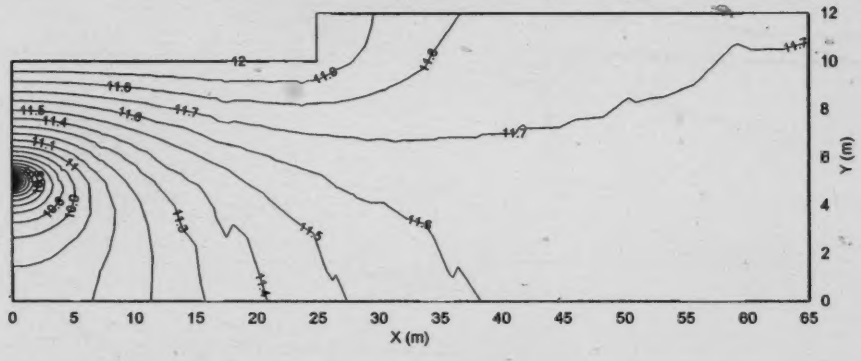


Figure 3.25 – Riverbed model output: transverse view of contours of total head at z = 125m: L = 250m, Ø = 300mm, $k_h$ = $10^{-3}$ m/s

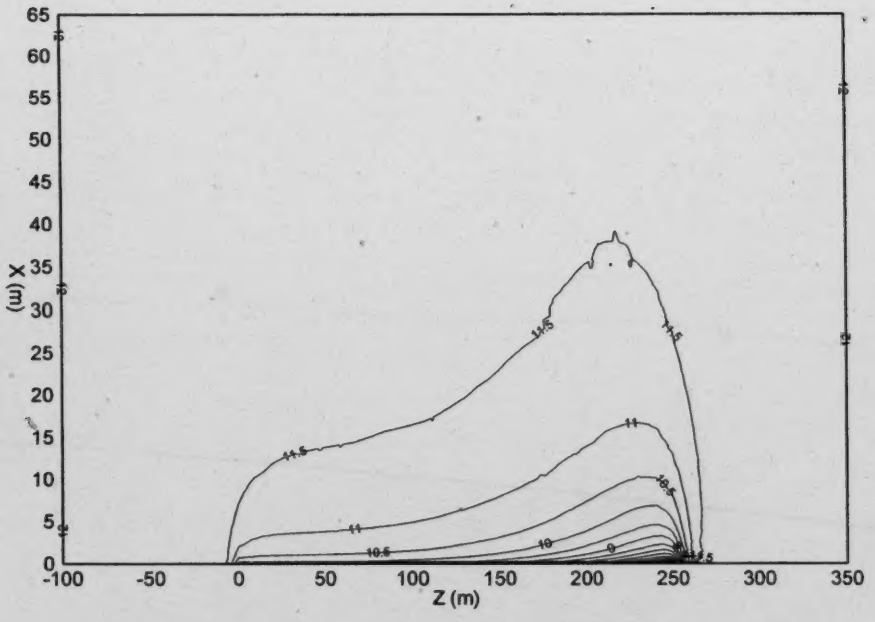


Figure 3.26 – Riverbed model output: plan view of contours of total head at y = 5m: L = 250m, Ø = 300mm, $k_h = 10^{-3}$ m/s

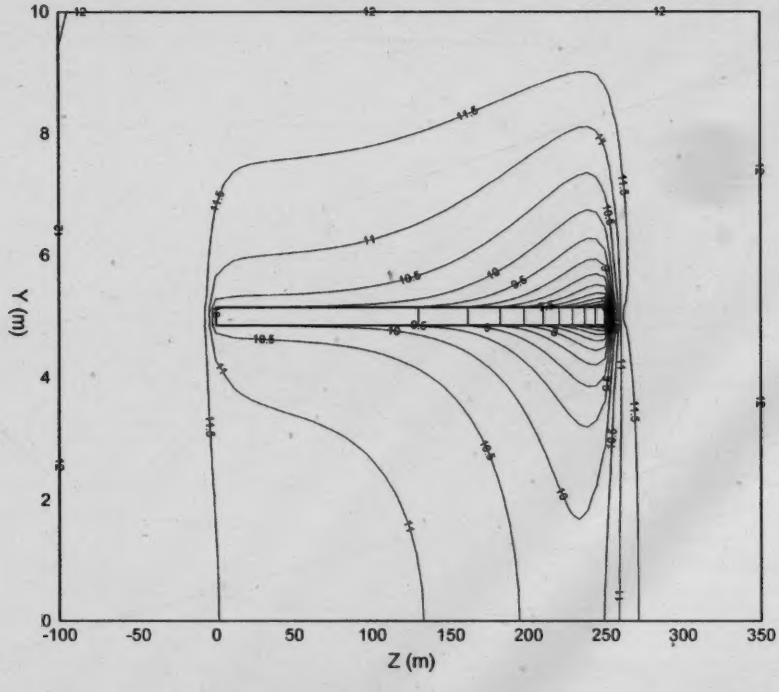


Figure 3.27 – Riverbed model output: longitudinal section view of contours of total head at x = 0m: L = 250m, Ø = 300mm, $k_h = 10^{-3}$ m/s

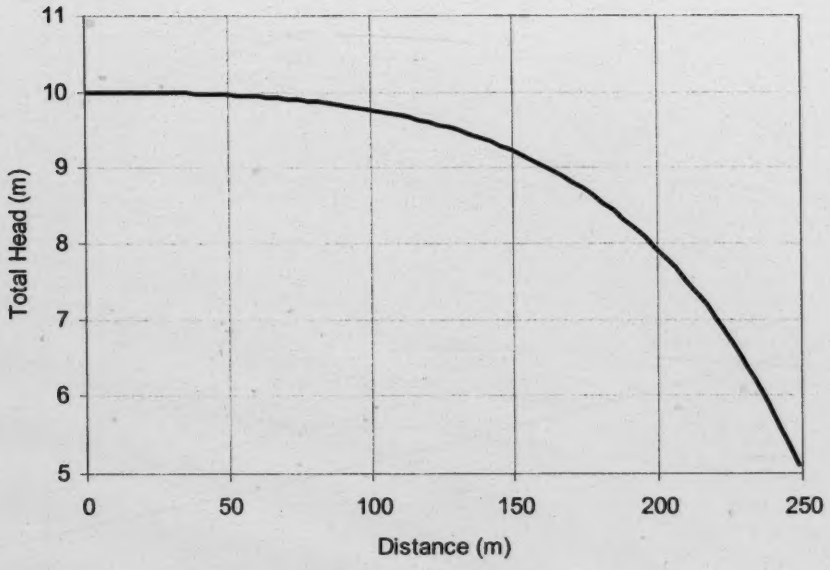


Figure 3.28 – Riverbed model output: profile of total head along axis of wellscreen: L = 250m, Ø = 300mm, $k_h = 10^{-3}$ m/s

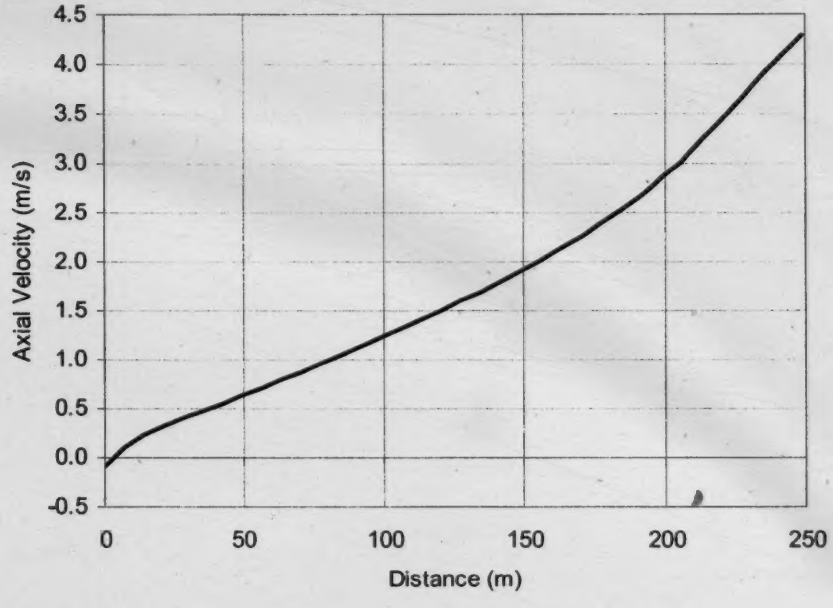


Figure 3.29 – Profile of axial velocity along axis of wellscreen: L = 250m, Ø = 300mm, $k_h = 10^{-3}$ m/s

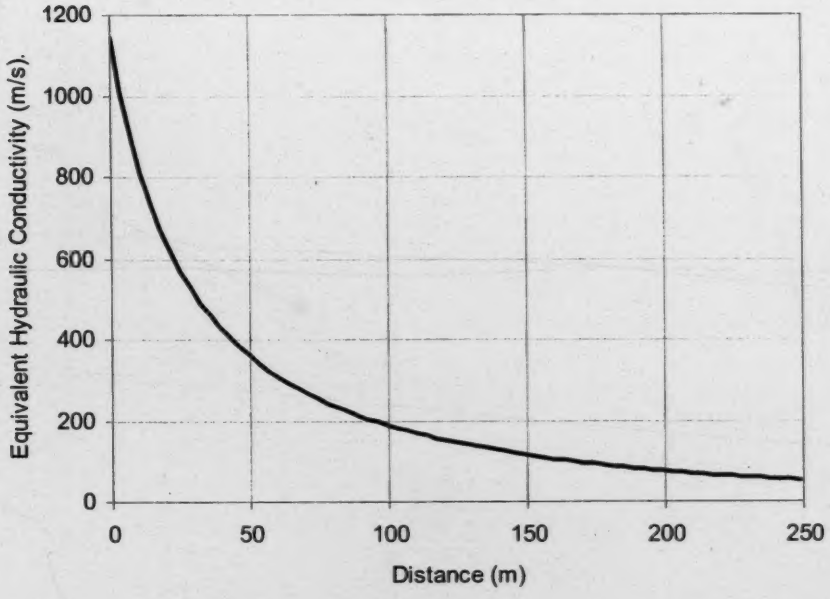


Figure 3.30 – Profile of hydraulic conductivity along axis of wellscreen: L = 250m, Ø = 300mm, $k_h = 10^{-3}$ m/s

# 4 SUMMARY AND CONCLUSIONS

This study focused on the use of horizontal wells in riverbed sediments as an alternate source of water for water treatment plants. Directionally drilled horizontal wells placed in the saturated sediments beneath rivers could supply higher quality water to treatment plants than is available directly from the river. To help evaluate this technology, pilot-scale field tests were conducted to estimate the improvement in water quality that could be expected from full-scale horizontal wells. Numerical models were also used to predict the quantities of water available from such a system. The conclusions reached from this research are presented below.

## 4.1 Field Test Results

Water quality improvement was measured by the reduction in suspended solids from the raw river water to the filtrate of the sample wellscreens used in the test equipment. Nearly identical filtering performance was observed in the filtrate from the Sandblocker and Schumasoil 200 wellscreens, where turbidity reductions of 86% and particle count reductions of approximately 90% were recorded. The Schumasoil 80 wellscreen reduced turbidity and particle counts by slightly less (83% and 80% respectively). The lowest quality filtrate was produced by the Vee-Wire Drive Point wellscreen, with an average turbidity reduction of 74% and a particle count reduction of 48%. The results indicate that most of the filtration occurred in the sand in the test boxes, and the wellscreens themselves were responsible for a small additional amount of filtration. Although turbidity was reduced by approximately the same magnitudes at all levels of raw water turbidity, the test results should only be applied to raw water turbidity levels below 270 NTU (the 95$^{th}$ percentile of raw water turbidity measurements).

The largest flow rates were produced by the Vee-Wire Drive Point wellscreen – 0.78 L/s on average. The Sandblocker and Schumasoil 200 wellscreens again performed nearly identically, producing flow rates of 0.37 L/s and 0.40 L/s respectively. The Schumasoil 80 wellscreen produced very low flows – 0.02 L/s – which can be attributed to clogged pores within the wellscreen.

## 4.2 Numerical Model Results

The numerical models for the test box and riverbed used approximate solutions to account for pipe hydraulics. Because the wellscreens were modelled as porous media, correctly simulating frictional head losses along the wellscreens involved calculating appropriate equivalent hydraulic conductivities. Two methods of calculating hydraulic conductivities were employed – one assigned a uniform conductivity to the entire wellscreen, and the other utilized a variable conductivity along the wellscreen's length. The first method was used in both the test box and riverbed models, while the second method was only used in the latter.

Using laboratory measured values of hydraulic conductivity from the sand taken from the test boxes, the numerical model of the test boxes computed a higher than expected flow rate – above the average flow rate measurements, but less than the maximum measured values. Using a lower estimate of the hydraulic conductivity of the sand backfill, the flow rates computed by the test box model matched the measured flow rates. The hydraulic conductivity required to match the measured and computed flow rates was sufficiently close to the measured conductivity to be considered realistic, and the numerical model was accepted as verified.

The numerical model of flow into a horizontal well placed beneath a river was then solved. The study examined the sensitivity of the model's computed flow rates to several design variables (well length, well diameter, well depth and aquifer hydraulic conductivity) and to the two methods of simulating pipe hydraulics. The factors known to increase head losses in pipes (smaller diameters, greater lengths and higher velocities) were observed to reduce the rate of inflow at the far end of the well, as expected.

The numerical model results also clearly show the effects of aquifer hydraulic conductivity and well diameter on optimum well length. Wells designed with larger diameters tend to have significantly longer optimum lengths, and produce considerably more flow than smaller diameter wells, though this effect is most noticeable when aquifer hydraulic conductivity is high.

The two methods of considering pipe hydraulics (the uniform conductivity and rigorous solution methods) differed very little in most cases – less than 3% difference when head losses were small. The difference between the two solution methods increased to as much as 20% in cases where head losses along the wellscreen were significant. Overall, the modelling time saved by the uniform conductivity method appeared to be worth the potential error.

The rates of inflow per metre length of well calculated by the numerical models agreed closely with the values reported by several authors. The infiltration galleries and horizontal collector wells described by Ray *et al.* (2002), Karanth (1997), Mikels (1992) and Obst (1974) tended to produce $1.2 \times 10^{-4}$ $m^3/s/m$ to $1.9 \times 10^{-3}$ $m^3/s/m$, whereas the horizontal well models in this study predicted inflow rates of $2.8 \times 10^{-4}$ $m^3/s/m$ to $3.1 \times 10^{-3}$ $m^3/s/m$ in cases where well lengths, diameters, depths and aquifer hydraulic conductivities were similar.

### 4.3 Recommendations for Future Work

Future research could take one or two directions: further pilot-scale testing and numerical modelling could be conducted, in an attempt to more accurately predict flow rates from full-scale horizontal wells; or small-scale field installations of horizontal wells could be undertaken to try to confirm or refine the estimates of well performance presented in this study.

Future pilot-scale tests could improve on the tests presented here in several areas:

- Longer-term tests could be conducted. Tests lasting for more than one year would be capable of capturing seasonal variations in water quality and the potential for aquifer clogging.

- Experiments could be designed to better represent the conditions under which a full-scale horizontal well would operate. This would include using granular materials more representative of the sediments found beneath rivers and attempting to match the velocity and depth of water circulating in the test boxes to the velocity and depth of water in the river. Better instrumentation in the test equipment (e.g. using piezometers or

standpipes to measure water pressure in the test boxes and wellscreen) would provide additional data to aid in verifying future numerical models.

Numerical models would be more accurate if the following changes were adopted:

- The model results could be examined for sensitivity to a greater number of factors. Among the variables that are expected to influence flow rates to some degree are: aquifer thickness and width, aquifer heterogeneity and anisotropy, river width, river stage (water depth), well inclination and well orientation. A number of these factors will be site-specific, and may not be amenable to examination in general terms.

- Software that correctly modelled pipe hydraulics (i.e., without the approximate solutions used in this work) would increase confidence in the model's results.

- Numerical models could be developed to distinguish between groundwater and surface water as separate sources of water for horizontal wells. Understanding the fractions of a horizontal well's total production originating from these two sources would aid in accurately predicting wellscreen filtrate quality.

Small-scale installations of horizontal wells would eliminate the need for simplifying assumptions and approximations by displaying the same behaviour as full-scale horizontal wells. Properly instrumented, these wells could provide enough data to develop accurate and reliable estimates of well performance in a broad range of conditions.

The results of this study show the potential value of horizontal wells as an alternate source of potable water. Further work will be necessary before applying the technology to the production of potable water.

### 4.4 References

Karanth, K. R. 1997. On sustainable yield of infiltration gallery in valley fills of peninsular India. Journal of Applied Hydrology, 10(3, 4): 86-98.

Mikels, M. S. 1992. Characterizing the influence of surface water on water produced by collector wells. Journal of the American Water Works Association, 84(9): 77-84.

Obst, C. E. 1974. Horizontal groundwater collectors, 'Canada's largest water well'. Proceedings of the Annual Conference of the British Columbia Water and Waste Association, Vancouver, British Columbia, April 9-11, pp. 107-123.

Ray, C., Grischek, T., Schubert, J., Wang, J., and Speth, T. 2002. A perspective of riverbank filtration. Journal of the American Water Works Association, 94(4): 149-160.

# APPENDIX A FLOW RATE MEASUREMENTS

Table A.1 – Flow Rate Measurements

| Date | Time | Total Hours | Wellscreen Name | Height in Weir (mm) | Flow Rate (L/s) |
|---|---|---|---|---|---|
| 14-Jul | 14:45 | 3.92 | Sandblocker | 130 | 1.672 |
| 15-Jul | 12:15 | 25.42 | Sandblocker | 58 | 0.222 |
| 16-Jul | 13:05 | 50.25 | Sandblocker | 126 | 1.546 |
| 17-Jul | 11:05 | 72.25 | Sandblocker | 125 | 1.516 |
| 21-Jul | 10:45 | 73.33 | Sandblocker | 124 | 1.486 |
| 23-Jul | 11:40 | 122.25 | Sandblocker | 121 | 1.397 |
| 23-Jul | 12:55 | 123.50 | Sandblocker | 116 | 1.258 |
| 25-Jul | 12:15 | 170.83 | Sandblocker | 110 | 1.101 |
| 25-Jul | 13:15 | 171.83 | Sandblocker | 110 | 1.101 |
| 26-Jul | 12:15 | 194.83 | Sandblocker | 69 | 0.343 |
| 26-Jul | 14:45 | 197.33 | Sandblocker | 63 | 0.273 |
| 27-Jul | 11:20 | 217.92 | Sandblocker | 46 | 0.125 |
| 29-Jul | 14:15 | 218.42 | Sandblocker | 51 | 0.161 |
| 30-Jul | 10:10 | 238.33 | Sandblocker | 28 | 0.036 |
| 31-Jul | 10:00 | 239.67 | Sandblocker | 27 | 0.033 |
| 31-Jul | 10:40 | 240.33 | Sandblocker | 44 | 0.111 |
| 02-Aug | 10:10 | 263.83 | Sandblocker | 73 | 0.395 |
| 02-Aug | 10:50 | 264.50 | Sandblocker | 71 | 0.369 |
| 07-Aug | 13:50 | 266.00 | Sandblocker | 66 | 0.307 |
| 07-Aug | 14:40 | 266.83 | Sandblocker | 63 | 0.273 |
| 08-Aug | 11:15 | 268.17 | Sandblocker | 68 | 0.331 |
| 08-Aug | 11:50 | 268.75 | Sandblocker | 66 | 0.307 |
| 10-Aug | 10:45 | 272.67 | Sandblocker | 55 | 0.195 |
| 10-Aug | 13:15 | 275.17 | Sandblocker | 55 | 0.195 |
| 14-Aug | 9:40 | 295.33 | Sandblocker | 53 | 0.177 |
| 14-Aug | 10:30 | 296.17 | Sandblocker | 56 | 0.204 |
| 15-Aug | 11:00 | 320.67 | Sandblocker | 71 | 0.369 |
| 15-Aug | 12:50 | 322.50 | Sandblocker | 65 | 0.296 |
| 16-Aug | 11:45 | 345.42 | Sandblocker | 82 | 0.528 |
| 16-Aug | 13:05 | 346.75 | Sandblocker | 82 | 0.528 |
| 18-Aug | 15:15 | 396.92 | Sandblocker | 73 | 0.395 |
| 20-Aug | 12:00 | 441.67 | Sandblocker | 81 | 0.512 |
| 20-Aug | 14:40 | 444.33 | Sandblocker | 76 | 0.437 |
| 21-Aug | 10:55 | 464.58 | Sandblocker | 84 | 0.561 |
| 21-Aug | 12:55 | 466.58 | Sandblocker | 83 | 0.545 |
| 27-Aug | 13:00 | 469.58 | Sandblocker | 67 | 0.319 |
| 28-Aug | 13:50 | 494.42 | Sandblocker | 58 | 0.222 |
| 28-Aug | 15:35 | 496.17 | Sandblocker | 79 | 0.481 |

| Date | Time | Total Hours | Wellscreen Name | Height in Weir (mm) | Flow Rate (L/s) |
|---|---|---|---|---|---|
| 29-Aug | 10:20 | 514.92 | Sandblocker | 90 | 0.667 |
| 30-Aug | 11:30 | 540.08 | Sandblocker | 82 | 0.528 |
| 04-Sep | 11:35 | 660.17 | Sandblocker | 80 | 0.497 |
| 06-Sep | 11:00 | 707.58 | Sandblocker | 77 | 0.451 |
| 10-Sep | 9:35 | 802.17 | Sandblocker | 68 | 0.331 |
| 24-Sep | 10:20 | 1138.92 | Sandblocker | 70 | 0.356 |
| 25-Sep | 10:15 | 1162.83 | Sandblocker | 79 | 0.481 |
| 27-Sep | 10:30 | 1211.08 | Sandblocker | 71 | 0.369 |
| 28-Sep | 9:45 | 1234.33 | Sandblocker | 68 | 0.331 |
| 14-Jul | 13:45 | 2.92 | Schumasoil 200 | 127 | 1.577 |
| 15-Jul | 13:10 | 26.33 | Schumasoil 200 | 125 | 1.516 |
| 16-Jul | 12:20 | 49.50 | Schumasoil 200 | 121 | 1.397 |
| 17-Jul | 11:20 | 72.50 | Schumasoil 200 | 124 | 1.486 |
| 21-Jul | 11:45 | 74.33 | Schumasoil 200 | 125 | 1.516 |
| 23-Jul | 11:05 | 121.67 | Schumasoil 200 | 119 | 1.340 |
| 23-Jul | 12:35 | 123.17 | Schumasoil 200 | 117 | 1.285 |
| 25-Jul | 12:45 | 171.33 | Schumasoil 200 | 103 | 0.934 |
| 25-Jul | 13:45 | 172.33 | Schumasoil 200 | 107 | 1.028 |
| 26-Jul | 13:40 | 196.25 | Schumasoil 200 | 67 | 0.319 |
| 26-Jul | 15:30 | 198.08 | Schumasoil 200 | 64 | 0.284 |
| 27-Jul | 10:40 | 217.25 | Schumasoil 200 | 53 | 0.177 |
| 29-Jul | 14:45 | 218.92 | Schumasoil 200 | 45 | 0.118 |
| 30-Jul | 9:40 | 237.83 | Schumasoil 200 | 28 | 0.036 |
| 31-Jul | 10:15 | 239.92 | Schumasoil 200 | 32 | 0.050 |
| 31-Jul | 11:00 | 240.67 | Schumasoil 200 | 38 | 0.077 |
| 02-Aug | 10:30 | 264.17 | Schumasoil 200 | 78 | 0.466 |
| 02-Aug | 11:10 | 264.83 | Schumasoil 200 | 65 | 0.296 |
| 07-Aug | 14:15 | 266.42 | Schumasoil 200 | 66 | 0.307 |
| 07-Aug | 14:55 | 267.08 | Schumasoil 200 | 63 | 0.273 |
| 08-Aug | 12:50 | 269.75 | Schumasoil 200 | 54 | 0.186 |
| 08-Aug | 13:30 | 270.42 | Schumasoil 200 | 59 | 0.232 |
| 10-Aug | 9:50 | 271.75 | Schumasoil 200 | 58 | 0.222 |
| 10-Aug | 12:30 | 274.42 | Schumasoil 200 | 43 | 0.105 |
| 14-Aug | 10:10 | 295.83 | Schumasoil 200 | 61 | 0.252 |
| 15-Aug | 11:40 | 321.33 | Schumasoil 200 | 72 | 0.382 |
| 15-Aug | 13:30 | 323.17 | Schumasoil 200 | 66 | 0.307 |
| 16-Aug | 11:15 | 344.92 | Schumasoil 200 | 76 | 0.437 |
| 16-Aug | 12:35 | 346.25 | Schumasoil 200 | 76 | 0.437 |
| 18-Aug | 15:45 | 397.42 | Schumasoil 200 | 76 | 0.437 |

| Date | Time | Total Hours | Wellscreen Name | Height in Weir (mm) | Flow Rate (L/s) |
|---|---|---|---|---|---|
| 20-Aug | 12:40 | 442.33 | Schumasoil 200 | 79 | 0.481 |
| 20-Aug | 14:00 | 443.67 | Schumasoil 200 | 80 | 0.497 |
| 21-Aug | 11:35 | 465.25 | Schumasoil 200 | 83 | 0.545 |
| 21-Aug | 13:35 | 467.25 | Schumasoil 200 | 77 | 0.451 |
| 27-Aug | 13:30 | 470.08 | Schumasoil 200 | 65 | 0.296 |
| 28-Aug | 14:35 | 495.17 | Schumasoil 200 | 69 | 0.343 |
| 28-Aug | 15:55 | 496.50 | Schumasoil 200 | 76 | 0.437 |
| 29-Aug | 10:50 | 515.42 | Schumasoil 200 | 95 | 0.763 |
| 30-Aug | 11:00 | 539.58 | Schumasoil 200 | 76 | 0.437 |
| 04-Sep | 12:05 | 660.67 | Schumasoil 200 | 81 | 0.512 |
| 06-Sep | 11:20 | 707.92 | Schumasoil 200 | 74 | 0.409 |
| 10-Sep | 10:10 | 802.75 | Schumasoil 200 | 61 | 0.252 |
| 24-Sep | 10:40 | 1139.25 | Schumasoil 200 | 65 | 0.296 |
| 25-Sep | 10:10 | 1162.75 | Schumasoil 200 | 78 | 0.466 |
| 27-Sep | 10:50 | 1211.42 | Schumasoil 200 | 68 | 0.331 |
| 28-Sep | 10:20 | 1234.92 | Schumasoil 200 | 73 | 0.395 |
| 14-Jul | 14:45 | 3.92 | Schumasoil 80 | 58 | 0.222 |
| 15-Jul | 12:15 | 25.42 | Schumasoil 80 | | 0.000 |
| 16-Jul | 13:05 | 50.25 | Schumasoil 80 | 34 | 0.058 |
| 17-Jul | 11:05 | 72.25 | Schumasoil 80 | | 0.000 |
| 21-Jul | 10:45 | 73.33 | Schumasoil 80 | 27 | 0.033 |
| 23-Jul | 11:40 | 122.25 | Schumasoil 80 | 32 | 0.050 |
| 23-Jul | 12:55 | 123.50 | Schumasoil 80 | 36 | 0.067 |
| 30-Jul | 11:10 | 219.67 | Schumasoil 80 | | 0.000 |
| 01-Aug | 11:00 | 242.50 | Schumasoil 80 | 12 | 0.004 |
| 01-Aug | 11:30 | 243.00 | Schumasoil 80 | 27 | 0.033 |
| 02-Aug | 12:35 | 244.08 | Schumasoil 80 | 35 | 0.063 |
| 07-Aug | 10:45 | 244.83 | Schumasoil 80 | 10 | 0.003 |
| 07-Aug | 11:45 | 245.83 | Schumasoil 80 | 19 | 0.014 |
| 07-Aug | 13:00 | 247.08 | Schumasoil 80 | 16 | 0.009 |
| 08-Aug | 11:30 | 248.58 | Schumasoil 80 | 13 | 0.005 |
| 08-Aug | 12:10 | 249.25 | Schumasoil 80 | 14 | 0.006 |
| 10-Aug | 11:10 | 253.25 | Schumasoil 80 | 19 | 0.014 |
| 10-Aug | 12:10 | 254.25 | Schumasoil 80 | 16 | 0.009 |
| 14-Aug | 9:55 | 275.75 | Schumasoil 80 | 13 | 0.005 |
| 15-Aug | 11:20 | 301.17 | Schumasoil 80 | 22 | 0.020 |
| 15-Aug | 13:10 | 303.00 | Schumasoil 80 | 24 | 0.024 |
| 16-Aug | 11:30 | 325.33 | Schumasoil 80 | 24 | 0.024 |
| 16-Aug | 12:50 | 326.67 | Schumasoil 80 | 23 | 0.022 |

| Date | Time | Total Hours | Wellscreen Name | Height in Weir (mm) | Flow Rate (L/s) |
|---|---|---|---|---|---|
| 18-Aug | 15:30 | 377.33 | Schumasoil 80 | 26 | 0.030 |
| 20-Aug | 12:20 | 422.17 | Schumasoil 80 | 27 | 0.033 |
| 20-Aug | 14:20 | 424.17 | Schumasoil 80 | 25 | 0.027 |
| 21-Aug | 11:15 | 445.08 | Schumasoil 80 | 28 | 0.036 |
| 21-Aug | 12:35 | 446.42 | Schumasoil 80 | 22 | 0.020 |
| 27-Aug | 13:15 | 450.00 | Schumasoil 80 | 24 | 0.024 |
| 28-Aug | 14:20 | 475.08 | Schumasoil 80 | 24 | 0.024 |
| 28-Aug | 15:45 | 476.50 | Schumasoil 80 | 26 | 0.030 |
| 29-Aug | 10:35 | 495.33 | Schumasoil 80 | 22 | 0.020 |
| 30-Aug | 11:15 | 520.00 | Schumasoil 80 | 17 | 0.010 |
| 04-Sep | 11:50 | 640.58 | Schumasoil 80 | 20 | 0.016 |
| 06-Sep | 11:20 | 688.08 | Schumasoil 80 | 24 | 0.024 |
| 10-Sep | 10:00 | 782.75 | Schumasoil 80 | 21 | 0.018 |
| 24-Sep | 10:40 | 1119.42 | Schumasoil 80 | 24 | 0.024 |
| 25-Sep | 10:30 | 1143.25 | Schumasoil 80 | 41 | 0.093 |
| 27-Sep | 10:45 | 1191.50 | Schumasoil 80 | 31 | 0.046 |
| 28-Sep | 9:55 | 1214.67 | Schumasoil 80 | 18 | 0.012 |
| 14-Jul | 13:45 | 2.92 | Vee-Wire Drive Point | 130 | 1.672 |
| 15-Jul | 13:10 | 26.33 | Vee-Wire Drive Point | 131 | 1.704 |
| 16-Jul | 12:20 | 49.50 | Vee-Wire Drive Point | 138 | 1.941 |
| 17-Jul | 11:20 | 72.50 | Vee-Wire Drive Point | 131 | 1.704 |
| 21-Jul | 11:45 | 74.33 | Vee-Wire Drive Point | 128 | 1.608 |
| 23-Jul | 11:05 | 121.67 | Vee-Wire Drive Point | 128 | 1.608 |
| 23-Jul | 12:35 | 123.17 | Vee-Wire Drive Point | 127 | 1.577 |
| 29-Jul | 13:30 | 218.75 | Vee-Wire Drive Point | 87 | 0.613 |
| 30-Jul | 10:40 | 219.17 | Vee-Wire Drive Point | 97 | 0.804 |
| 01-Aug | 10:35 | 242.08 | Vee-Wire Drive Point | 59 | 0.232 |
| 01-Aug | 11:15 | 242.75 | Vee-Wire Drive Point | 110 | 1.101 |
| 02-Aug | 12:25 | 243.92 | Vee-Wire Drive Point | 96 | 0.784 |
| 07-Aug | 11:15 | 245.33 | Vee-Wire Drive Point | 73 | 0.395 |
| 07-Aug | 12:20 | 246.42 | Vee-Wire Drive Point | 61 | 0.252 |
| 07-Aug | 13:30 | 247.58 | Vee-Wire Drive Point | 56 | 0.204 |
| 08-Aug | 13:10 | 250.25 | Vee-Wire Drive Point | 70 | 0.356 |
| 08-Aug | 13:50 | 250.92 | Vee-Wire Drive Point | 64 | 0.284 |
| 10-Aug | 10:20 | 252.42 | Vee-Wire Drive Point | 80 | 0.497 |
| 10-Aug | 12:50 | 254.92 | Vee-Wire Drive Point | 100 | 0.868 |
| 14-Aug | 9:25 | 275.25 | Vee-Wire Drive Point | 46 | 0.125 |
| 14-Aug | 10:20 | 276.17 | Vee-Wire Drive Point | 68 | 0.331 |
| 15-Aug | 10:40 | 300.50 | Vee-Wire Drive Point | 118 | 1.312 |

| Date | Time | Total Hours | Wellscreen Name | Height in Weir (mm) | Flow Rate (L/s) |
|---|---|---|---|---|---|
| 15-Aug | 12:30 | 302.33 | Vee-Wire Drive Point | 118 | 1.312 |
| 16-Aug | 11:00 | 324.83 | Vee-Wire Drive Point | 109 | 1.076 |
| 16-Aug | 12:20 | 326.17 | Vee-Wire Drive Point | 103 | 0.934 |
| 18-Aug | 15:00 | 376.83 | Vee-Wire Drive Point | 92 | 0.704 |
| 20-Aug | 11:40 | 421.50 | Vee-Wire Drive Point | 109 | 1.076 |
| 20-Aug | 13:40 | 423.50 | Vee-Wire Drive Point | 96 | 0.784 |
| 21-Aug | 10:35 | 444.42 | Vee-Wire Drive Point | 111 | 1.126 |
| 21-Aug | 13:15 | 447.08 | Vee-Wire Drive Point | 110 | 1.101 |
| 27-Aug | 12:45 | 449.50 | Vee-Wire Drive Point | 69 | 0.343 |
| 28-Aug | 14:05 | 474.83 | Vee-Wire Drive Point | 74 | 0.409 |
| 28-Aug | 15:25 | 476.17 | Vee-Wire Drive Point | 83 | 0.545 |
| 29-Aug | 10:05 | 494.83 | Vee-Wire Drive Point | 109 | 1.076 |
| 30-Aug | 11:45 | 520.50 | Vee-Wire Drive Point | 109 | 1.076 |
| 04-Sep | 12:15 | 641.00 | Vee-Wire Drive Point | 104 | 0.957 |
| 06-Sep | 11:00 | 687.75 | Vee-Wire Drive Point | 77 | 0.451 |
| 10-Sep | 9:40 | 782.42 | Vee-Wire Drive Point | 70 | 0.356 |
| 24-Sep | 10:20 | 1119.08 | Vee-Wire Drive Point | 58 | 0.222 |
| 25-Sep | 10:20 | 1143.08 | Vee-Wire Drive Point | 90 | 0.667 |
| 27-Sep | 10:30 | 1191.25 | Vee-Wire Drive Point | 68 | 0.331 |
| 28-Sep | 10:15 | 1215.00 | Vee-Wire Drive Point | 90 | 0.667 |

## APPENDIX B TURBIDITY MEASUREMENTS

Table B.1 – Turbidity Measurements

| Date | Time | Total Hours | Wellscreen Name | Influent Turbidity (NTU) | Effluent Turbidity (NTU) |
|---|---|---|---|---|---|
| 12-Jul | 11:05 | 1.00 | Sandblocker | 9.5 | 1.54 |
| 14-Jul | 14:40 | 3.83 | Sandblocker | 4.55 | 0.93 |
| 15-Jul | 12:10 | 25.33 | Sandblocker | 5.32 | 0.55 |
| 16-Jul | 13:00 | 50.17 | Sandblocker | 5.2 | 0.72 |
| 17-Jul | 11:00 | 72.17 | Sandblocker | 5.32 | 0.51 |
| 21-Jul | 10:40 | 73.25 | Sandblocker | 24.4 | 6.03 |
| 23-Jul | 11:35 | 122.17 | Sandblocker | 10.1 | 1.55 |
| 23-Jul | 12:55 | 123.50 | Sandblocker | 9.66 | 1.53 |
| 24-Jul | 11:40 | 146.25 | Sandblocker | 8.07 | 1.05 |
| 24-Jul | 12:15 | 146.83 | Sandblocker | 7.57 | 1.05 |
| 25-Jul | 12:10 | 170.75 | Sandblocker | 30.2 | 2.22 |
| 25-Jul | 13:15 | 171.83 | Sandblocker | 25.1 | 2.32 |
| 25-Jul | 15:30 | 174.08 | Sandblocker | 32.2 | 2.39 |
| 26-Jul | 12:15 | 194.83 | Sandblocker | 34.2 | 0.75 |
| 26-Jul | 14:45 | 197.33 | Sandblocker | 34 | 0.61 |
| 27-Jul | 11:20 | 217.92 | Sandblocker | 65.6 | 0.63 |
| 29-Jul | 14:15 | 218.42 | Sandblocker | 175 | 3.96 |
| 30-Jul | 10:10 | 238.33 | Sandblocker | 2550 | 4.08 |
| 31-Jul | 10:00 | 239.67 | Sandblocker | 1100 | 23.1 |
| 31-Jul | 10:40 | 240.33 | Sandblocker | 1130 | 49.1 |
| 2-Aug | 10:10 | 263.83 | Sandblocker | 127 | 7.42 |
| 2-Aug | 10:50 | 264.50 | Sandblocker | 101 | 10.9 |
| 7-Aug | 13:50 | 266.00 | Sandblocker | 26.3 | 3.31 |
| 7-Aug | 14:40 | 266.83 | Sandblocker | 20.2 | 2.09 |
| 8-Aug | 11:15 | 268.17 | Sandblocker | 20.1 | 2.58 |
| 8-Aug | 11:50 | 268.75 | Sandblocker | 15.4 | 2.22 |
| 10-Aug | 10:45 | 272.67 | Sandblocker | 13.4 | 2.04 |
| 10-Aug | 13:15 | 275.17 | Sandblocker | 11.4 | 1.66 |
| 14-Aug | 9:40 | 295.33 | Sandblocker | 6.28 | 1.25 |
| 14-Aug | 10:30 | 296.17 | Sandblocker | 6.55 | 1.58 |
| 15-Aug | 11:00 | 320.67 | Sandblocker | 9.19 | 1.81 |
| 15-Aug | 12:50 | 322.50 | Sandblocker | 8.26 | 1.22 |
| 16-Aug | 11:45 | 345.42 | Sandblocker | 8.54 | 1.19 |
| 16-Aug | 13:05 | 346.75 | Sandblocker | 8 | 1.26 |
| 18-Aug | 15:15 | 396.92 | Sandblocker | 6.82 | 0.77 |
| 20-Aug | 12:00 | 441.67 | Sandblocker | 4.62 | 0.89 |
| 20-Aug | 14:40 | 444.33 | Sandblocker | 4.07 | 0.64 |

| Date | Time | Total Hours | Wellscreen Name | Influent Turbidity (NTU) | Effluent Turbidity (NTU) |
|---|---|---|---|---|---|
| 21-Aug | 10:55 | 464.58 | Sandblocker | 4.99 | 0.75 |
| 21-Aug | 12:55 | 466.58 | Sandblocker | 4.24 | 0.50 |
| 27-Aug | 13:00 | 469.58 | Sandblocker | 2.95 | 1.51 |
| 28-Aug | 13:50 | 494.42 | Sandblocker | 2.59 | 0.65 |
| 28-Aug | 15:35 | 496.17 | Sandblocker | 3.51 | 0.95 |
| 29-Aug | 10:20 | 514.92 | Sandblocker | 2.17 | 0.50 |
| 30-Aug | 11:30 | 540.08 | Sandblocker | 2.6 | 0.37 |
| 4-Sep | 11:35 | 660.17 | Sandblocker | 2.22 | 0.75 |
| 6-Sep | 11:00 | 707.58 | Sandblocker | 3.15 | 0.37 |
| 10-Sep | 9:35 | 802.17 | Sandblocker | 1.83 | 0.20 |
| 24-Sep | 10:20 | 1138.92 | Sandblocker | 1.89 | 0.40 |
| 25-Sep | 9:40 | 1162.25 | Sandblocker | 1.61 | 0.42 |
| 27-Sep | 10:20 | 1210.92 | Sandblocker | 1.43 | 0.22 |
| 28-Sep | 9:45 | 1234.33 | Sandblocker | 1.52 | 0.20 |
| 12-Jul | 11:45 | 1.67 | Schumasoil 200 | 7.3 | 1.37 |
| 14-Jul | 13:40 | 2.83 | Schumasoil 200 | 3.65 | 0.97 |
| 15-Jul | 13:05 | 26.25 | Schumasoil 200 | 4.67 | 1.37 |
| 16-Jul | 12:15 | 49.42 | Schumasoil 200 | 4.73 | 0.7 |
| 17-Jul | 11:15 | 72.42 | Schumasoil 200 | 4.98 | 0.53 |
| 21-Jul | 11:40 | 74.25 | Schumasoil 200 | 23.5 | 5.82 |
| 23-Jul | 11:00 | 121.58 | Schumasoil 200 | 9.58 | 1.54 |
| 23-Jul | 12:30 | 123.08 | Schumasoil 200 | 10.6 | 1.46 |
| 24-Jul | 11:15 | 145.83 | Schumasoil 200 | 8.1 | 1.12 |
| 24-Jul | 12:50 | 147.42 | Schumasoil 200 | 8.78 | 1.05 |
| 25-Jul | 12:45 | 171.33 | Schumasoil 200 | 25.6 | 2.21 |
| 25-Jul | 13:45 | 172.33 | Schumasoil 200 | 26.3 | 2.36 |
| 25-Jul | 15:15 | 173.83 | Schumasoil 200 | 36.3 | 2.31 |
| 26-Jul | 13:40 | 196.25 | Schumasoil 200 | 30.4 | 0.77 |
| 26-Jul | 15:30 | 198.08 | Schumasoil 200 | 30.2 | 0.66 |
| 27-Jul | 10:40 | 217.25 | Schumasoil 200 | 76.8 | 0.61 |
| 29-Jul | 14:45 | 218.92 | Schumasoil 200 | 158 | 3.19 |
| 30-Jul | 9:40 | 237.83 | Schumasoil 200 | 2820 | 1.24 |
| 31-Jul | 10:15 | 239.92 | Schumasoil 200 | 1250 | 17.8 |
| 31-Jul | 11:00 | 240.67 | Schumasoil 200 | 1050 | 62.8 |
| 2-Aug | 10:30 | 264.17 | Schumasoil 200 | 113 | 11.2 |
| 2-Aug | 11:10 | 264.83 | Schumasoil 200 | 110 | 11.3 |
| 7-Aug | 14:15 | 266.42 | Schumasoil 200 | 17.7 | 2.92 |

| Date | Time | Total Hours | Wellscreen Name | Influent Turbidity (NTU) | Effluent Turbidity (NTU) |
|---|---|---|---|---|---|
| 7-Aug | 14:55 | 267.08 | Schumasoil 200 | 20.3 | 2.3 |
| 8-Aug | 12:50 | 269.75 | Schumasoil 200 | 13.2 | 1.93 |
| 8-Aug | 13:30 | 270.42 | Schumasoil 200 | 22.1 | 3.03 |
| 10-Aug | 9:45 | 271.67 | Schumasoil 200 | 15.3 | 2.06 |
| 10-Aug | 12:30 | 274.42 | Schumasoil 200 | 10.7 | 2.12 |
| 14-Aug | 10:10 | 295.83 | Schumasoil 200 | 6.39 | 2.36 |
| 15-Aug | 11:40 | 321.33 | Schumasoil 200 | 9.34 | 1.42 |
| 15-Aug | 13:30 | 323.17 | Schumasoil 200 | 9.07 | 1.32 |
| 16-Aug | 11:15 | 344.92 | Schumasoil 200 | 8.23 | 1.08 |
| 16-Aug | 12:35 | 346.25 | Schumasoil 200 | 7.95 | 1.04 |
| 18-Aug | 15:45 | 397.42 | Schumasoil 200 | 6.36 | 0.85 |
| 20-Aug | 12:40 | 442.33 | Schumasoil 200 | 4.26 | 0.72 |
| 20-Aug | 14:00 | 443.67 | Schumasoil 200 | 4.37 | 0.70 |
| 21-Aug | 11:35 | 465.25 | Schumasoil 200 | 4.36 | 1.02 |
| 21-Aug | 13:35 | 467.25 | Schumasoil 200 | 4.11 | 0.49 |
| 27-Aug | 13:30 | 470.08 | Schumasoil 200 | 3.07 | 1.33 |
| 28-Aug | 14:35 | 495.17 | Schumasoil 200 | 2.96 | 0.87 |
| 28-Aug | 15:55 | 496.50 | Schumasoil 200 | 2.75 | 0.78 |
| 29-Aug | 10:50 | 515.42 | Schumasoil 200 | 2.47 | 0.56 |
| 30-Aug | 11:00 | 539.58 | Schumasoil 200 | 2.73 | 0.32 |
| 4-Sep | 12:05 | 660.67 | Schumasoil 200 | 2.41 | 0.35 |
| 6-Sep | 11:20 | 707.92 | Schumasoil 200 | 2.44 | 0.28 |
| 10-Sep | 10:00 | 802.58 | Schumasoil 200 | 1.67 | 0.23 |
| 24-Sep | 10:40 | 1139.25 | Schumasoil 200 | 1.54 | 0.66 |
| 25-Sep | 10:10 | 1162.75 | Schumasoil 200 | 1.64 | 0.58 |
| 27-Sep | 10:45 | 1211.33 | Schumasoil 200 | 2.29 | 0.32 |
| 28-Sep | 10:15 | 1234.83 | Schumasoil 200 | 1.4 | 0.22 |
| 12-Jul | 11:05 | 1.00 | Schumasoil 80 | 9.5 | 2.92 |
| 14-Jul | 14:40 | 3.83 | Schumasoil 80 | 4.55 | 0.75 |
| 15-Jul | 12:10 | 25.33 | Schumasoil 80 | 5.32 | 0.38 |
| 16-Jul | 13:00 | 50.17 | Schumasoil 80 | 5.2 | 0.35 |
| 17-Jul | 11:00 | 72.17 | Schumasoil 80 | 5.32 | 0.22 |
| 21-Jul | 10:40 | 73.25 | Schumasoil 80 | 24.4 | 3 |
| 23-Jul | 11:35 | 122.17 | Schumasoil 80 | 10.1 | 1.04 |
| 23-Jul | 12:55 | 123.50 | Schumasoil 80 | 9.66 | 1.17 |
| 24-Jul | 11:40 | 146.25 | Schumasoil 80 | 8.07 | 0.78 |
| 24-Jul | 12:15 | 146.83 | Schumasoil 80 | 7.57 | 0.39 |

| Date | Time | Total Hours | Wellscreen Name | Influent Turbidity (NTU) | Effluent Turbidity (NTU) |
|---|---|---|---|---|---|
| 27-Jul | 12:10 | 169.42 | Schumasoil 80 | 71.3 | 20.7 |
| 30-Jul | 11:10 | 219.67 | Schumasoil 80 | 3030 | 144 |
| 1-Aug | 11:00 | 242.50 | Schumasoil 80 | 282 | 24.5 |
| 1-Aug | 11:30 | 243.00 | Schumasoil 80 | 251 | 31 |
| 2-Aug | 12:30 | 244.00 | Schumasoil 80 | 103 | 27 |
| 7-Aug | 10:45 | 244.83 | Schumasoil 80 | 23.6 | 9.63 |
| 7-Aug | 11:45 | 245.83 | Schumasoil 80 | 17.5 | 3.65 |
| 7-Aug | 13:00 | 247.08 | Schumasoil 80 | 21.2 | 6.09 |
| 8-Aug | 11:30 | 248.58 | Schumasoil 80 | 18.8 | 27.2 |
| 8-Aug | 12:05 | 249.17 | Schumasoil 80 | 15.9 | 10.2 |
| 10-Aug | 11:10 | 253.25 | Schumasoil 80 | 12.6 | 2.6 |
| 10-Aug | 12:10 | 254.25 | Schumasoil 80 | 10.2 | 2.52 |
| 14-Aug | 9:55 | 275.75 | Schumasoil 80 | 6.11 | 1.64 |
| 15-Aug | 11:20 | 301.17 | Schumasoil 80 | 9.16 | 1.48 |
| 15-Aug | 13:10 | 303.00 | Schumasoil 80 | 10.6 | 1.24 |
| 16-Aug | 11:30 | 325.33 | Schumasoil 80 | 8.39 | 0.99 |
| 16-Aug | 12:50 | 326.67 | Schumasoil 80 | 8.48 | 0.95 |
| 18-Aug | 15:30 | 377.33 | Schumasoil 80 | 7.07 | 0.78 |
| 20-Aug | 12:20 | 422.17 | Schumasoil 80 | 4.45 | 0.78 |
| 20-Aug | 14:20 | 424.17 | Schumasoil 80 | 4.33 | 0.69 |
| 21-Aug | 11:15 | 445.08 | Schumasoil 80 | 4.74 | 0.66 |
| 21-Aug | 12:35 | 446.42 | Schumasoil 80 | 4.41 | 0.64 |
| 27-Aug | 13:15 | 450.00 | Schumasoil 80 | 2.97 | 1.06 |
| 28-Aug | 14:20 | 475.08 | Schumasoil 80 | 3.39 | 0.66 |
| 28-Aug | 15:45 | 476.50 | Schumasoil 80 | 2.65 | 0.63 |
| 29-Aug | 10:35 | 495.33 | Schumasoil 80 | 2.51 | 0.64 |
| 30-Aug | 11:15 | 520.00 | Schumasoil 80 | 2.4 | 0.43 |
| 4-Sep | 11:50 | 640.58 | Schumasoil 80 | 2.37 | 0.51 |
| 6-Sep | 11:20 | 688.08 | Schumasoil 80 | 2.44 | 0.56 |
| 10-Sep | 10:10 | 782.92 | Schumasoil 80 | 1.67 | 0.36 |
| 24-Sep | 10:40 | 1119.42 | Schumasoil 80 | 1.54 | 0.65 |
| 25-Sep | 10:10 | 1142.92 | Schumasoil 80 | 1.64 | 0.44 |
| 27-Sep | 10:45 | 1191.50 | Schumasoil 80 | 2.29 | 0.33 |
| 28-Sep | 9:45 | 1214.50 | Schumasoil 80 | 1.52 | 0.18 |
| 12-Jul | 11:45 | 1.67 | Vee-Wire Drive Point | 7.3 | 1.38 |
| 14-Jul | 13:40 | 2.83 | Vee-Wire Drive Point | 3.65 | 1.21 |
| 15-Jul | 13:05 | 26.25 | Vee-Wire Drive Point | 4.67 | 1.03 |

| Date | Time | Total Hours | Wellscreen Name | Influent Turbidity (NTU) | Effluent Turbidity (NTU) |
|---|---|---|---|---|---|
| 16-Jul | 12:15 | 49.42 | Vee-Wire Drive Point | 4.73 | 0.83 |
| 17-Jul | 11:15 | 72.42 | Vee-Wire Drive Point | 4.98 | 0.84 |
| 21-Jul | 11:40 | 74.25 | Vee-Wire Drive Point | 23.5 | 7.63 |
| 23-Jul | 11:00 | 121.58 | Vee-Wire Drive Point | 9.58 | 2.15 |
| 23-Jul | 12:30 | 123.08 | Vee-Wire Drive Point | 10.6 | 2.07 |
| 24-Jul | 11:15 | 145.83 | Vee-Wire Drive Point | 8.1 | 1.5 |
| 24-Jul | 12:50 | 147.42 | Vee-Wire Drive Point | 8.78 | 1.59 |
| 27-Jul | 12:05 | 169.33 | Vee-Wire Drive Point | 71.3 | 19.1 |
| 29-Jul | 13:30 | 218.75 | Vee-Wire Drive Point | 136 | 26.3 |
| 30-Jul | 10:40 | 219.17 | Vee-Wire Drive Point | 2450 | 342 |
| 1-Aug | 10:35 | 242.08 | Vee-Wire Drive Point | 285 | 41.8 |
| 1-Aug | 11:15 | 242.75 | Vee-Wire Drive Point | 220 | 56.8 |
| 2-Aug | 12:25 | 243.92 | Vee-Wire Drive Point | 130 | 50.2 |
| 7-Aug | 11:15 | 245.33 | Vee-Wire Drive Point | 16.3 | 5.6 |
| 7-Aug | 12:20 | 246.42 | Vee-Wire Drive Point | 17.7 | 12.6 |
| 7-Aug | 13:30 | 247.58 | Vee-Wire Drive Point | 19.5 | 5.67 |
| 8-Aug | 13:10 | 250.25 | Vee-Wire Drive Point | 17 | 4.77 |
| 8-Aug | 13:50 | 250.92 | Vee-Wire Drive Point | 14.2 | 4.67 |
| 10-Aug | 10:20 | 252.42 | Vee-Wire Drive Point | 18.2 | 5.74 |
| 10-Aug | 12:50 | 254.92 | Vee-Wire Drive Point | 11.5 | 7.16 |
| 14-Aug | 9:25 | 275.25 | Vee-Wire Drive Point | 7.95 | 2.34 |
| 14-Aug | 10:20 | 276.17 | Vee-Wire Drive Point | 6.27 | 4.42 |
| 15-Aug | 10:40 | 300.50 | Vee-Wire Drive Point | 11.1 | 5.46 |
| 15-Aug | 12:30 | 302.33 | Vee-Wire Drive Point | 8.86 | 6.6 |
| 16-Aug | 11:00 | 324.83 | Vee-Wire Drive Point | 9.79 | 1.87 |
| 16-Aug | 12:20 | 326.17 | Vee-Wire Drive Point | 9.63 | 1.43 |
| 18-Aug | 15:00 | 376.83 | Vee-Wire Drive Point | 7.72 | 1.32 |
| 20-Aug | 11:40 | 421.50 | Vee-Wire Drive Point | 4.58 | 1.26 |
| 20-Aug | 13:40 | 423.50 | Vee-Wire Drive Point | 4.39 | 0.84 |
| 21-Aug | 10:35 | 444.42 | Vee-Wire Drive Point | 5.21 | 1.00 |
| 21-Aug | 13:15 | 447.08 | Vee-Wire Drive Point | 4.55 | 0.83 |
| 27-Aug | 12:45 | 449.50 | Vee-Wire Drive Point | 3.2 | 1.64 |
| 28-Aug | 14:05 | 474.83 | Vee-Wire Drive Point | 3.15 | 1.12 |
| 28-Aug | 15:25 | 476.17 | Vee-Wire Drive Point | 2.61 | 0.71 |
| 29-Aug | 10:05 | 494.83 | Vee-Wire Drive Point | 2.54 | 0.96 |
| 30-Aug | 11:45 | 520.50 | Vee-Wire Drive Point | 2.57 | 0.78 |
| 4-Sep | 12:15 | 641.00 | Vee-Wire Drive Point | 2.64 | 1.00 |
| 6-Sep | 11:00 | 687.75 | Vee-Wire Drive Point | 3.15 | 0.42 |
| 10-Sep | 9:40 | 782.42 | Vee-Wire Drive Point | 1.83 | 0.22 |

| Date | Time | Total Hours | Wellscreen Name | Influent Turbidity (NTU) | Effluent Turbidity (NTU) |
|---|---|---|---|---|---|
| 24-Sep | 10:20 | 1119.08 | Vee-Wire Drive Point | 1.89 | 0.36 |
| 25-Sep | 9:40 | 1142.42 | Vee-Wire Drive Point | 1.61 | 0.30 |
| 27-Sep | 10:20 | 1191.08 | Vee-Wire Drive Point | 1.43 | 0.18 |
| 28-Sep | 10:15 | 1215.00 | Vee-Wire Drive Point | 1.4 | 0.50 |

## APPENDIX C PARTICLE COUNT MEASUREMENTS

Table C.1 – Particle Count Results

| | | | | Diluted Count | | Full Strength Count | |
|---|---|---|---|---|---|---|---|
| Name | Date | Time | Size (µm) | cumulative | differential | cumulative | differential |
| Raw Water | 24/09/01 | 11:44 | 2 | 1906 | 623 | 9530 | 3115 |
| | | | 3 | 1283 | 934 | 6415 | 4670 |
| | | | 5 | 349 | 167 | 1745 | 835 |
| | | | 7 | 182 | 132 | 910 | 660 |
| | | | 10 | 50 | 38 | 250 | 190 |
| | | | 15 | 12 | 12 | 60 | 60 |
| | | 11:43 | 2 | 1917 | 627 | 9585 | 3135 |
| | | | 3 | 1290 | 930 | 6450 | 4650 |
| | | | 5 | 360 | 169 | 1800 | 845 |
| | | | 7 | 191 | 136 | 955 | 680 |
| | | | 10 | 55 | 43 | 275 | 215 |
| | | | 15 | 12 | 12 | 60 | 60 |
| | | 11:42 | 2 | 1906 | 625 | 9530 | 3125 |
| | | | 3 | 1281 | 929 | 6405 | 4645 |
| | | | 5 | 352 | 168 | 1760 | 840 |
| | | | 7 | 184 | 131 | 920 | 655 |
| | | | 10 | 53 | 41 | 265 | 205 |
| | | | 15 | 12 | 12 | 60 | 60 |
| Vee-Wire Drive Point | 24/09/01 | 11:51 | 2 | 1542 | 450 | 7710 | 2250 |
| | | | 3 | 1092 | 722 | 5460 | 3610 |
| | | | 5 | 370 | 147 | 1850 | 735 |
| | | | 7 | 223 | 149 | 1115 | 745 |
| | | | 10 | 74 | 57 | 370 | 285 |
| | | | 15 | 17 | 17 | 85 | 85 |
| | | 11:50 | 2 | 1532 | 443 | 7660 | 2215 |
| | | | 3 | 1089 | 716 | 5445 | 3580 |
| | | | 5 | 373 | 150 | 1865 | 750 |
| | | | 7 | 223 | 146 | 1115 | 730 |
| | | | 10 | 77 | 59 | 385 | 295 |
| | | | 15 | 18 | 18 | 90 | 90 |
| | | 11:49 | 2 | 1544 | 447 | 7720 | 2235 |
| | | | 3 | 1097 | 716 | 5485 | 3580 |
| | | | 5 | 381 | 153 | 1905 | 765 |
| | | | 7 | 228 | 147 | 1140 | 735 |
| | | | 10 | 81 | 59 | 405 | 295 |
| | | | 15 | 22 | 22 | 110 | 110 |

| | | | | Diluted Count | | Full Strength Count | |
|---|---|---|---|---|---|---|---|
| Name | Date | Time | Size (µm) | cumulative | differential | cumulative | differential |
| Sandblocker | 24/09/01 | 11:58 | 2 | 280 | 86 | 1400 | 430 |
| | | | 3 | 194 | 139 | 970 | 695 |
| | | | 5 | 55 | 22 | 275 | 110 |
| | | | 7 | 33 | 22 | 165 | 110 |
| | | | 10 | 11 | 9 | 55 | 45 |
| | | | 15 | 2 | 2 | 10 | 10 |
| | | 11:57 | 2 | 285 | 87 | 1425 | 435 |
| | | | 3 | 198 | 140 | 990 | 700 |
| | | | 5 | 58 | 23 | 290 | 115 |
| | | | 7 | 35 | 22 | 175 | 110 |
| | | | 10 | 13 | 10 | 65 | 50 |
| | | | 15 | 3 | 3 | 15 | 15 |
| | | 11:56 | 2 | 303 | 92 | 1515 | 460 |
| | | | 3 | 211 | 146 | 1055 | 730 |
| | | | 5 | 65 | 24 | 325 | 120 |
| | | | 7 | 41 | 26 | 205 | 130 |
| | | | 10 | 15 | 12 | 75 | 60 |
| | | | 15 | 3 | 3 | 15 | 15 |
| Schumasoil 80 | 24/09/01 | 12:05 | 2 | 688 | 130 | 3440 | 650 |
| | | | 3 | 558 | 351 | 2790 | 1755 |
| | | | 5 | 207 | 98 | 1035 | 490 |
| | | | 7 | 109 | 89 | 545 | 445 |
| | | | 10 | 20 | 14 | 100 | 70 |
| | | | 15 | 6 | 6 | 30 | 30 |
| | | 12:04 | 2 | 684 | 129 | 3420 | 645 |
| | | | 3 | 555 | 354 | 2775 | 1770 |
| | | | 5 | 201 | 94 | 1005 | 470 |
| | | | 7 | 107 | 87 | 535 | 435 |
| | | | 10 | 20 | 14 | 100 | 70 |
| | | | 15 | 6 | 6 | 30 | 30 |
| | | 12:03 | 2 | 690 | 132 | 3450 | 660 |
| | | | 3 | 558 | 357 | 2790 | 1785 |
| | | | 5 | 201 | 97 | 1005 | 485 |
| | | | 7 | 104 | 83 | 520 | 415 |
| | | | 10 | 21 | 15 | 105 | 75 |
| | | | 15 | 6 | 6 | 30 | 30 |
| Schumasoil 200 | 24/09/01 | 12:05 | 2 | 280 | 90 | 1400 | 450 |
| | | | 3 | 190 | 136 | 950 | 680 |
| | | | 5 | 54 | 24 | 270 | 120 |

| | | | | Diluted Count | | Full Strength Count | |
|---|---|---|---|---|---|---|---|
| Name | Date | Time | Size (µm) | cumulative | differential | cumulative | differential |
| | | | 7 | 30 | 21 | 150 | 105 |
| | | | 10 | 9 | 7 | 45 | 35 |
| | | | 15 | 2 | 2 | 10 | 10 |
| | | 12:04 | 2 | 288 | 92 | 1440 | 460 |
| | | | 3 | 196 | 140 | 980 | 700 |
| | | | 5 | 56 | 24 | 280 | 120 |
| | | | 7 | 32 | 22 | 160 | 110 |
| | | | 10 | 10 | 9 | 50 | 45 |
| | | | 15 | 1 | 1 | 5 | 5 |
| | | 12:03 | 2 | 293 | 95 | 1465 | 475 |
| | | | 3 | 198 | 142 | 990 | 710 |
| | | | 5 | 56 | 25 | 280 | 125 |
| | | | 7 | 31 | 22 | 155 | 110 |
| | | | 10 | 9 | 7 | 45 | 35 |
| | | | 15 | 2 | 2 | 10 | 10 |
| Raw Water | 25/09/01 | 10:54 | 2 | 1603 | 525 | 8015 | 2625 |
| | | | 3 | 1078 | 791 | 5390 | 3955 |
| | | | 5 | 287 | 142 | 1435 | 710 |
| | | | 7 | 145 | 109 | 725 | 545 |
| | | | 10 | 36 | 29 | 180 | 145 |
| | | | 15 | 7 | 7 | 35 | 35 |
| | | 10:55 | 2 | 1602 | 523 | 8010 | 2615 |
| | | | 3 | 1079 | 793 | 5395 | 3965 |
| | | | 5 | 286 | 142 | 1430 | 710 |
| | | | 7 | 144 | 107 | 720 | 535 |
| | | | 10 | 37 | 28 | 185 | 140 |
| | | | 15 | 9 | 9 | 45 | 45 |
| | | 10:56 | 2 | 1609 | 524 | 8045 | 2620 |
| | | | 3 | 1085 | 798 | 5425 | 3990 |
| | | | 5 | 287 | 146 | 1435 | 730 |
| | | | 7 | 141 | 105 | 705 | 525 |
| | | | 10 | 36 | 28 | 180 | 140 |
| | | | 15 | 8 | 8 | 40 | 40 |
| Vee-Wire Drive Point | 25/09/01 | 10:59 | 2 | 2052 | 565 | 10260 | 2825 |
| | | | 3 | 1487 | 964 | 7435 | 4820 |
| | | | 5 | 523 | 205 | 2615 | 1025 |
| | | | 7 | 318 | 203 | 1590 | 1015 |
| | | | 10 | 115 | 86 | 575 | 430 |

| | | | | Diluted Count | | Full Strength Count | |
|---|---|---|---|---|---|---|---|
| Name | Date | Time | Size (µm) | cumulative | differential | cumulative | differential |
| | | | 15 | 29 | 29 | 145 | 145 |
| | | 11:00 | 2 | 2047 | 568 | 10235 | 2840 |
| | | | 3 | 1479 | 957 | 7395 | 4785 |
| | | | 5 | 522 | 208 | 2610 | 1040 |
| | | | 7 | 314 | 201 | 1570 | 1005 |
| | | | 10 | 113 | 86 | 565 | 430 |
| | | | 15 | 27 | 27 | 135 | 135 |
| | | 11:01 | 2 | 2018 | 563 | 10090 | 2815 |
| | | | 3 | 1455 | 951 | 7275 | 4755 |
| | | | 5 | 504 | 202 | 2520 | 1010 |
| | | | 7 | 302 | 198 | 1510 | 990 |
| | | | 10 | 104 | 80 | 520 | 400 |
| | | | 15 | 24 | 24 | 120 | 120 |
| Sandblocker | 25/09/01 | 11:05 | 2 | 312 | 88 | 1560 | 440 |
| | | | 3 | 224 | 147 | 1120 | 735 |
| | | | 5 | 77 | 30 | 385 | 150 |
| | | | 7 | 47 | 30 | 235 | 150 |
| | | | 10 | 17 | 13 | 85 | 65 |
| | | | 15 | 4 | 4 | 20 | 20 |
| | | 11:06 | 2 | 288 | 84 | 1440 | 420 |
| | | | 3 | 204 | 137 | 1020 | 685 |
| | | | 5 | 67 | 27 | 335 | 135 |
| | | | 7 | 40 | 25 | 200 | 125 |
| | | | 10 | 15 | 11 | 75 | 55 |
| | | | 15 | 4 | 4 | 20 | 20 |
| | | 11:07 | 2 | 287 | 82 | 1435 | 410 |
| | | | 3 | 205 | 135 | 1025 | 675 |
| | | | 5 | 70 | 29 | 350 | 145 |
| | | | 7 | 41 | 25 | 205 | 125 |
| | | | 10 | 16 | 11 | 80 | 55 |
| | | | 15 | 5 | 5 | 25 | 25 |
| Schumasoil 80 | 25/09/01 | 11:13 | 2 | 2418 | 752 | 12090 | 3760 |
| | | | 3 | 1666 | 1168 | 8330 | 5840 |
| | | | 5 | 498 | 242 | 2490 | 1210 |
| | | | 7 | 256 | 203 | 1280 | 1015 |
| | | | 10 | 53 | 46 | 265 | 230 |
| | | | 15 | 7 | 7 | 35 | 35 |
| | | 11:14 | 2 | 2405 | 749 | 12025 | 3745 |
| | | | 3 | 1656 | 1171 | 8280 | 5855 |

| | | | | Diluted Count | | Full Strength Count | |
|---|---|---|---|---|---|---|---|
| Name | Date | Time | Size (µm) | cumulative | differential | cumulative | differential |
| | | | 5 | 485 | 239 | 2425 | 1195 |
| | | | 7 | 246 | 196 | 1230 | 980 |
| | | | 10 | 50 | 44 | 250 | 220 |
| | | | 15 | 6 | 6 | 30 | 30 |
| | | 11:15 | 2 | 2366 | 734 | 11830 | 3670 |
| | | | 3 | 1632 | 1153 | 8160 | 5765 |
| | | | 5 | 479 | 238 | 2395 | 1190 |
| | | | 7 | 241 | 192 | 1205 | 960 |
| | | | 10 | 49 | 42 | 245 | 210 |
| | | | 15 | 7 | 7 | 35 | 35 |
| Schumasoil 200 | 25/09/01 | 11:17 | 2 | 257 | 84 | 1285 | 420 |
| | | | 3 | 173 | 120 | 865 | 600 |
| | | | 5 | 53 | 24 | 265 | 120 |
| | | | 7 | 29 | 19 | 145 | 95 |
| | | | 10 | 10 | 8 | 50 | 40 |
| | | | 15 | 2 | 2 | 10 | 10 |
| | | 11:18 | 2 | 253 | 82 | 1265 | 410 |
| | | | 3 | 171 | 119 | 855 | 595 |
| | | | 5 | 52 | 21 | 260 | 105 |
| | | | 7 | 31 | 20 | 155 | 100 |
| | | | 10 | 11 | 9 | 55 | 45 |
| | | | 15 | 2 | 2 | 10 | 10 |
| | | 11:19 | 2 | 250 | 83 | 1250 | 415 |
| | | | 3 | 167 | 116 | 835 | 580 |
| | | | 5 | 51 | 22 | 255 | 110 |
| | | | 7 | 29 | 19 | 145 | 95 |
| | | | 10 | 10 | 8 | 50 | 40 |
| | | | 15 | 2 | 2 | 10 | 10 |
| Raw Water | 27/09/01 | 11:47 | 2 | 1818 | 568 | 9090 | 2840 |
| | | | 3 | 1250 | 891 | 6250 | 4455 |
| | | | 5 | 359 | 167 | 1795 | 835 |
| | | | 7 | 192 | 137 | 960 | 685 |
| | | | 10 | 55 | 44 | 275 | 220 |
| | | | 15 | 11 | 11 | 55 | 55 |
| | | 11:46 | 2 | 1823 | 565 | 9115 | 2825 |
| | | | 3 | 1258 | 892 | 6290 | 4460 |
| | | | 5 | 366 | 173 | 1830 | 865 |
| | | | 7 | 193 | 137 | 965 | 685 |
| | | | 10 | 56 | 44 | 280 | 220 |

| | | | | Diluted Count | | Full Strength Count | |
|---|---|---|---|---|---|---|---|
| Name | Date | Time | Size (µm) | cumulative | differential | cumulative | differential |
| | | | 15 | 12 | 12 | 60 | 60 |
| | | 11:45 | 2 | 1812 | 564 | 9060 | 2820 |
| | | | 3 | 1248 | 874 | 6240 | 4370 |
| | | | 5 | 374 | 169 | 1870 | 845 |
| | | | 7 | 205 | 139 | 1025 | 695 |
| | | | 10 | 66 | 47 | 330 | 235 |
| | | | 15 | 19 | 19 | 95 | 95 |
| Vee-Wire Drive Point | 27/09/01 | 11:50 | 2 | 396 | 132 | 1980 | 660 |
| | | | 3 | 264 | 193 | 1320 | 965 |
| | | | 5 | 71 | 32 | 355 | 160 |
| | | | 7 | 39 | 27 | 195 | 135 |
| | | | 10 | 12 | 10 | 60 | 50 |
| | | | 15 | 2 | 2 | 10 | 10 |
| | | 11:49 | 2 | 413 | 135 | 2065 | 675 |
| | | | 3 | 278 | 199 | 1390 | 995 |
| | | | 5 | 79 | 34 | 395 | 170 |
| | | | 7 | 45 | 30 | 225 | 150 |
| | | | 10 | 15 | 12 | 75 | 60 |
| | | | 15 | 3 | 3 | 15 | 15 |
| | | 11:48 | 2 | 474 | 154 | 2370 | 770 |
| | | | 3 | 320 | 229 | 1600 | 1145 |
| | | | 5 | 91 | 38 | 455 | 190 |
| | | | 7 | 53 | 35 | 265 | 175 |
| | | | 10 | 18 | 13 | 90 | 65 |
| | | | 15 | 5 | 5 | 25 | 25 |
| Sandblocker | 27/09/01 | 11:54 | 2 | 133 | 39 | 665 | 195 |
| | | | 3 | 94 | 64 | 470 | 320 |
| | | | 5 | 30 | 12 | 150 | 60 |
| | | | 7 | 18 | 11 | 90 | 55 |
| | | | 10 | 7 | 5 | 35 | 25 |
| | | | 15 | 2 | 2 | 10 | 10 |
| | | 11:53 | 2 | 131 | 37 | 655 | 185 |
| | | | 3 | 94 | 62 | 470 | 310 |
| | | | 5 | 32 | 13 | 160 | 65 |
| | | | 7 | 19 | 12 | 95 | 60 |
| | | | 10 | 7 | 5 | 35 | 25 |
| | | | 15 | 2 | 2 | 10 | 10 |
| | | 11:52 | 2 | 141 | 40 | 705 | 200 |

| | | | | Diluted Count | | Full Strength Count | |
|---|---|---|---|---|---|---|---|
| Name | Date | Time | Size (µm) | cumulative | differential | cumulative | differential |
| | | | 3 | 101 | 65 | 505 | 325 |
| | | | 5 | 36 | 14 | 180 | 70 |
| | | | 7 | 22 | 13 | 110 | 65 |
| | | | 10 | 9 | 7 | 45 | 35 |
| | | | 15 | 2 | 2 | 10 | 10 |
| Schumasoil 80 | 27/09/01 | 11:57 | 2 | 174 | 59 | 870 | 295 |
| | | | 3 | 115 | 88 | 575 | 440 |
| | | | 5 | 27 | 13 | 135 | 65 |
| | | | 7 | 14 | 10 | 70 | 50 |
| | | | 10 | 4 | 3 | 20 | 15 |
| | | | 15 | 1 | 1 | 5 | 5 |
| | | 11:56 | 2 | 205 | 72 | 1025 | 360 |
| | | | 3 | 133 | 107 | 665 | 535 |
| | | | 5 | 26 | 13 | 130 | 65 |
| | | | 7 | 13 | 10 | 65 | 50 |
| | | | 10 | 3 | 2 | 15 | 10 |
| | | | 15 | 1 | 1 | 5 | 5 |
| | | 11:55 | 2 | 212 | 76 | 1060 | 380 |
| | | | 3 | 136 | 107 | 680 | 535 |
| | | | 5 | 29 | 14 | 145 | 70 |
| | | | 7 | 15 | 10 | 75 | 50 |
| | | | 10 | 5 | 4 | 25 | 20 |
| | | | 15 | 1 | 1 | 5 | 5 |
| Schumasoil 200 | 27/09/01 | 12:01 | 2 | 108 | 37 | 540 | 185 |
| | | | 3 | 71 | 52 | 355 | 260 |
| | | | 5 | 19 | 9 | 95 | 45 |
| | | | 7 | 10 | 7 | 50 | 35 |
| | | | 10 | 3 | 2 | 15 | 10 |
| | | | 15 | 1 | 1 | 5 | 5 |
| | | 12:00 | 2 | 111 | 37 | 555 | 185 |
| | | | 3 | 74 | 55 | 370 | 275 |
| | | | 5 | 19 | 8 | 95 | 40 |
| | | | 7 | 11 | 7 | 55 | 35 |
| | | | 10 | 4 | 3 | 20 | 15 |
| | | | 15 | 1 | 1 | 5 | 5 |
| | | 11:59 | 2 | 122 | 39 | 610 | 195 |
| | | | 3 | 83 | 59 | 415 | 295 |
| | | | 5 | 24 | 10 | 120 | 50 |
| | | | 7 | 14 | 8 | 70 | 40 |

| | | | | Diluted Count | | Full Strength Count | |
|---|---|---|---|---|---|---|---|
| Name | Date | Time | Size (µm) | cumulative | differential | cumulative | differential |
| | | | 10 | 6 | 4 | 30 | 20 |
| | | | 15 | 2 | 2 | 10 | 10 |
| Raw Water | 28/09/01 | 11:09 | 2 | 2054 | 613 | 10270 | 3065 |
| | | | 3 | 1441 | 1011 | 7205 | 5055 |
| | | | 5 | 430 | 198 | 2150 | 990 |
| | | | 7 | 232 | 163 | 1160 | 815 |
| | | | 10 | 69 | 54 | 345 | 270 |
| | | | 15 | 15 | 15 | 75 | 75 |
| | | 11:08 | 2 | 2079 | 616 | 10395 | 3080 |
| | | | 3 | 1463 | 1022 | 7315 | 5110 |
| | | | 5 | 441 | 202 | 2205 | 1010 |
| | | | 7 | 239 | 167 | 1195 | 835 |
| | | | 10 | 72 | 57 | 360 | 285 |
| | | | 15 | 15 | 15 | 75 | 75 |
| | | 11:07 | 2 | 2060 | 608 | 10300 | 3040 |
| | | | 3 | 1452 | 1017 | 7260 | 5085 |
| | | | 5 | 435 | 198 | 2175 | 990 |
| | | | 7 | 237 | 163 | 1185 | 815 |
| | | | 10 | 74 | 57 | 370 | 285 |
| | | | 15 | 17 | 17 | 85 | 85 |
| Vee-Wire Drive Point | 28/09/01 | 11:12 | 2 | 1066 | 290 | 5330 | 1450 |
| | | | 3 | 776 | 511 | 3880 | 2555 |
| | | | 5 | 265 | 108 | 1325 | 540 |
| | | | 7 | 157 | 105 | 785 | 525 |
| | | | 10 | 52 | 41 | 260 | 205 |
| | | | 15 | 11 | 11 | 55 | 55 |
| | | 11:11 | 2 | 1073 | 294 | 5365 | 1470 |
| | | | 3 | 779 | 510 | 3895 | 2550 |
| | | | 5 | 269 | 109 | 1345 | 545 |
| | | | 7 | 160 | 101 | 800 | 505 |
| | | | 10 | 59 | 45 | 295 | 225 |
| | | | 15 | 14 | 14 | 70 | 70 |
| | | 11:10 | 2 | 1063 | 291 | 5315 | 1455 |
| | | | 3 | 772 | 509 | 3860 | 2545 |
| | | | 5 | 263 | 108 | 1315 | 540 |
| | | | 7 | 155 | 102 | 775 | 510 |
| | | | 10 | 53 | 41 | 265 | 205 |
| | | | 15 | 12 | 12 | 60 | 60 |

| | | | | Diluted Count | | Full Strength Count | |
|---|---|---|---|---|---|---|---|
| Name | Date | Time | Size (µm) | cumulative | differential | cumulative | differential |
| Sandblocker | 28/09/01 | 11:19 | 2 | 101 | 32 | 505 | 160 |
| | | | 3 | 69 | 50 | 345 | 250 |
| | | | 5 | 19 | 8 | 95 | 40 |
| | | | 7 | 11 | 6 | 55 | 30 |
| | | | 10 | 5 | 4 | 25 | 20 |
| | | | 15 | 1 | 1 | 5 | 5 |
| | | 11:18 | 2 | 103 | 32 | 515 | 160 |
| | | | 3 | 71 | 50 | 355 | 250 |
| | | | 5 | 21 | 8 | 105 | 40 |
| | | | 7 | 13 | 7 | 65 | 35 |
| | | | 10 | 6 | 4 | 30 | 20 |
| | | | 15 | 2 | 2 | 10 | 10 |
| | | 11:17 | 2 | 115 | 37 | 575 | 185 |
| | | | 3 | 78 | 55 | 390 | 275 |
| | | | 5 | 23 | 10 | 115 | 50 |
| | | | 7 | 13 | 7 | 65 | 35 |
| | | | 10 | 6 | 4 | 30 | 20 |
| | | | 15 | 2 | 2 | 10 | 10 |
| Schumasoil 80 | 28/09/01 | 11:23 | 2 | 252 | 65 | 1260 | 325 |
| | | | 3 | 187 | 125 | 935 | 625 |
| | | | 5 | 62 | 26 | 310 | 130 |
| | | | 7 | 36 | 25 | 180 | 125 |
| | | | 10 | 11 | 8 | 55 | 40 |
| | | | 15 | 3 | 3 | 15 | 15 |
| | | 11:22 | 2 | 263 | 65 | 1315 | 325 |
| | | | 3 | 198 | 130 | 990 | 650 |
| | | | 5 | 68 | 29 | 340 | 145 |
| | | | 7 | 39 | 25 | 195 | 125 |
| | | | 10 | 14 | 11 | 70 | 55 |
| | | | 15 | 3 | 3 | 15 | 15 |
| | | 11:21 | 2 | 262 | 65 | 1310 | 325 |
| | | | 3 | 197 | 130 | 985 | 650 |
| | | | 5 | 67 | 27 | 335 | 135 |
| | | | 7 | 40 | 25 | 200 | 125 |
| | | | 10 | 15 | 11 | 75 | 55 |
| | | | 15 | 4 | 4 | 20 | 20 |
| Schumasoil 200 | 28/09/01 | 11:27 | 2 | 223 | 67 | 1115 | 335 |
| | | | 3 | 156 | 11 | 780 | 55 |
| | | | 5 | 45 | 20 | 225 | 100 |

| | | | | Diluted Count | | Full Strength Count | |
|---|---|---|---|---|---|---|---|
| Name | Date | Time | Size (µm) | cumulative | differential | cumulative | differential |
| | | | 7 | 25 | 17 | 125 | 85 |
| | | | 10 | 8 | 6 | 40 | 30 |
| | | | 15 | 2 | 2 | 10 | 10 |
| | | 11:26 | 2 | 229 | 68 | 1145 | 340 |
| | | | 3 | 161 | 110 | 805 | 550 |
| | | | 5 | 51 | 21 | 255 | 105 |
| | | | 7 | 30 | 20 | 150 | 100 |
| | | | 10 | 10 | 8 | 50 | 40 |
| | | | 15 | 2 | 2 | 10 | 10 |
| | | 11:25 | 2 | 230 | 68 | 1150 | 340 |
| | | | 3 | 162 | 111 | 810 | 555 |
| | | | 5 | 51 | 22 | 255 | 110 |
| | | | 7 | 29 | 19 | 145 | 95 |
| | | | 10 | 10 | 8 | 50 | 40 |
| | | | 15 | 2 | 2 | 10 | 10 |

# APPENDIX D LABORATORY TEST PROCEDURES

## D.1 Constant Head Permeability Tests

### D.1.1 Equipment Setup

The constant head permeability tests conducted in this study were set up in the following manner:

- A reservoir with adjustable water elevation was used to provide a constant head for the soil sample.
- Two permeameter cells were used:
    - The first permeameter served only to de-air the distilled water flowing through the test equipment. The permeameter contained a small amount of coarse sand (enough to fill the cell to a depth of 5cm to 10cm). Water flowing through this sand released air as it warmed up, and air bubbles formed in the void spaces between the sand grains.
    - The second permeameter contained the sample of clean or dirty sand from the test box to be tested.

### D.1.2 Sample Preparation

The objective of measuring the permeability of the samples of sand taken from the test boxes was to determine the relationship between permeability and density. To that end, both types of sand (clean and dirty) were prepared at loose and dense states. The same preparation procedures were used for both types of sand.

Loose, Wet Pluviated Samples:

- A small amount of water was poured into the permeameter cell (to a depth of 3cm to 5cm). The oven-dried sand was poured into this standing water from the lowest height practical.
- When enough sand had been poured into the cell to bring the level of sand up to the level of water, water was again poured into the cell to create a depth of 3cm to 5cm.

- This process was continued until the permeameter was full of sand and water (the maximum depth of sand was usually restricted to 19.5cm).

Dense, Vibro-Compacted Samples:

- A small amount of water was again poured into the cell (3cm to 5cm deep) and oven-dried sand poured into the cell until it was approximately one-fifth full.

- A surcharge load (583g, or approximately 1.3 kPa) was placed on the sand, the cell was clamped to a vibratory table, and the cell and sand were vibrated for two to three minutes.

- The cell was filled with more sand and compacted again. The permeameter was filled with sand in five approximately equal layers.

### D.1.3 Test Procedure

- A glass beaker and stopwatch were used to measure the flow rate (volume divided by time) of water flowing through the cell. The volume of water was determined by weighing the glass beaker before and after sampling.

- The water level in four manometers attached at different points to the cell was recorded to determine the gradient across three zones of the sample.

- The elevation of the constant-head reservoir was changed (raised or lowered) and the measurements of flow rate and manometer water levels were repeated.

## D.2 Dry Density Measurement Procedure for Test Boxes

The test for measuring the dry density of sand in the test boxes was based on retrieving a known volume of sand and determining the masses of sand and water in the sample. The Shelby tube used to collect the sand sample had the following dimensions:

- Length: 201mm

- Diameter: 97.5mm
- Volume: 1500.7 $cm^3$

### D.2.1 Procedure

- The Shelby tube was pushed downwards into the sand in the test boxes. The sand around the tube was excavated and a steel plate slid beneath the tube to prevent sand from falling out of the tube. The distance from the top of the Shelby tube and the top of the test box was measured.
- The Shelby tube, plate and sand were placed into a plastic bag. The tube and plate were cleaned of sand, and the sample of sand labelled and sealed (a knot was tied in the bag to prevent moisture loss).
- The density sampling continued until four or five samples of sand had been collected from each of the boxes.
- In the laboratory, the bags of sand were weighed to determine the mass of wet sand ($M_w$).
- Three samples of sand from each bag were taken to determine the moisture content (w) of the bagged samples. The dry density ($\rho_d$) in $kg/m^3$ of each of the bagged samples was calculated as:

$$\rho_d = \frac{\frac{M_w}{1500.7cm^3}}{1+w}$$

- The void ratio of the bagged samples was calculated as:

$$e = \frac{2650kg/m^3}{\rho_d} - 1$$

### D.3 Maximum and Minimum Index Density Tests

The maximum and minimum index density tests were carried out as specified in ASTM D4253-00 and ASTM D4254-00. The only exception made to these standards was in the vibration used to prepare the maximum index density samples – the vibration table used allowed no explicit control over the amplitude or double amplitude of vibration. A best guess was made to judge the appropriate setting for the vibration table. Refer to the ASTM standards for a complete explanation of the testing procedure.

# APPENDIX E LABORATORY MEASURMENTS

## E.1 Hydraulic Conductivity Measurements

Permeameter Dimensions:

- Diameter: 75.3mm
- Manometer heights: 85mm ($h_1$), 139mm ($h_2$), 185mm ($h_3$), 235mm ($h_4$)

### E.1.1 Clean Sand, Wet Pluviated

Table E.1 – Sand Properties: Clean, Loose Sample

| | |
|---|---|
| Mass of Sand (g) | 1441 |
| Height of Sand in Permeameter (mm) | 195 |
| Dry Density (kg/m3) | 1660 |
| Void Ratio | 0.597 |

Table E.2 – Hydraulic Conductivity Measurements: Clean, Loose Sample

| Test No. | Water Volume (mL) | Time (s) | Manometer Water Levels (mm) | | | |
|---|---|---|---|---|---|---|
| | | | $h_1$ | $h_2$ | $h_3$ | $h_4$ |
| 1 | 269.3 | 35.2 | 262 | 293 | 325 | 368 |
| 2 | 221.7 | 30.2 | 233 | 265 | 295 | 340 |
| 3 | 258.7 | 36.6 | 215 | 245 | 275 | 324 |
| 4 | 225.1 | 37.5 | 132 | 158 | 184 | 225 |
| 5 | 246.9 | 42.1 | 126 | 151 | 177 | 219 |
| 6 | 254.7 | 43.4 | 126 | 152 | 177 | 218 |
| 7 | 222.8 | 46.3 | 57 | 78 | 98 | 132 |
| 8 | 214.3 | 47.7 | 40 | 59 | 78 | 111 |
| 9 | 245.9 | 55.4 | 36 | 54 | 73 | 106 |

Table E.3 – Hydraulic Conductivity Calculations: Clean, Loose Sample

| Test No. | Velocity (mm/s) | Gradient, i | | | | Hydraulic Conductivity, k (mm/s) | | | |
|---|---|---|---|---|---|---|---|---|---|
| | | $i_{1-2}$ | $i_{2-3}$ | $i_{3-4}$ | $i_{1-4}$ | $k_{1-2}$ | $k_{2-3}$ | $k_{3-4}$ | $k_{1-4}$ |
| 1 | 1.718 | 1.718 | 0.70 | 0.86 | 0.71 | 2.99 | 2.47 | 2.00 | 2.43 |
| 2 | 1.648 | 1.648 | 0.65 | 0.90 | 0.71 | 2.78 | 2.53 | 1.83 | 2.31 |
| 3 | 1.587 | 1.587 | 0.65 | 0.98 | 0.73 | 2.86 | 2.43 | 1.62 | 2.18 |
| 4 | 1.348 | 1.348 | 0.57 | 0.82 | 0.62 | 2.80 | 2.38 | 1.64 | 2.17 |
| 5 | 1.317 | 1.317 | 0.57 | 0.84 | 0.62 | 2.84 | 2.33 | 1.57 | 2.12 |
| 6 | 1.318 | 1.318 | 0.54 | 0.82 | 0.61 | 2.74 | 2.42 | 1.61 | 2.15 |
| 7 | 1.081 | 1.081 | 0.43 | 0.68 | 0.50 | 2.78 | 2.49 | 1.59 | 2.16 |
| 8 | 1.009 | 1.009 | 0.41 | 0.66 | 0.47 | 2.87 | 2.44 | 1.53 | 2.13 |
| 9 | 0.997 | 0.997 | 0.41 | 0.66 | 0.47 | 2.99 | 2.41 | 1.51 | 2.14 |
| Average Hydraulic Conductivity | | | | | | 2.84 | 2.42 | 1.58 | 2.15 |

## E.1.2 Clean Sand, Vibro-Compacted

Table E.4 – Sand Properties: Clean, Dense Sample

| | |
|---|---|
| Mass of Sand (g) | 1500 |
| Height of Sand in Permeameter (mm) | 192 |
| Dry Density (kg/m$^3$) | 1755 |
| Void Ratio | 0.508 |

Table E.5 – Hydraulic Conductivity Measurements: Clean, Dense Sample

| Test No. | Water Volume (mL) | Time (s) | Manometer Water Levels (mm) | | | |
|---|---|---|---|---|---|---|
| | | | $h_1$ | $h_2$ | $h_3$ | $h_4$ |
| 1 | 168 | 26.2 | 18 | 70 | 127 | 199 |
| 2 | 189 | 30.2 | 18 | 70 | 126 | 197 |
| 3 | 190 | 31.3 | 13 | 63 | 117 | 188 |
| 4 | 198 | 33.2 | 8 | 58 | 111 | 185 |
| 5 | 228 | 34.8 | 26 | 78 | 138 | 229 |
| 6 | 182 | 26.8 | 35 | 90 | 153 | 245 |
| 7 | 160 | 24.8 | 21 | 72 | 132 | 224 |
| 8 | 178 | 28.0 | 18 | 68 | 129 | 222 |
| 9 | 197 | 27.8 | 38 | 93 | 160 | 292 |
| 10 | 147 | 22.1 | 22 | 74 | 141 | 273 |
| 11 | 151 | 23.2 | 18 | 68 | 133 | 270 |
| 12 | 179 | 28.1 | 16 | 66 | 129 | 273 |

Table E.6 – Hydraulic Conductivity Calculations: Clean, Dense Sample

| Test No. | Velocity (mm/s) | Gradient, i | | | | Hydraulic Conductivity, k (mm/s) | | | |
|---|---|---|---|---|---|---|---|---|---|
| | | $i_{1-2}$ | $i_{2-3}$ | $i_{3-4}$ | $i_{1-4}$ | $k_{1-2}$ | $k_{2-3}$ | $k_{3-4}$ | $k_{1-4}$ |
| 1 | 1.438 | 0.96 | 1.24 | 1.44 | 1.21 | 1.49 | 1.16 | 1.00 | 1.19 |
| 2 | 1.408 | 0.96 | 1.22 | 1.42 | 1.19 | 1.46 | 1.16 | 0.99 | 1.18 |
| 3 | 1.361 | 0.93 | 1.17 | 1.42 | 1.17 | 1.47 | 1.16 | 0.96 | 1.17 |
| 4 | 1.340 | 0.93 | 1.15 | 1.48 | 1.18 | 1.45 | 1.16 | 0.91 | 1.14 |
| 5 | 1.473 | 0.96 | 1.30 | 1.82 | 1.35 | 1.53 | 1.13 | 0.81 | 1.09 |
| 6 | 1.527 | 1.02 | 1.37 | 1.84 | 1.40 | 1.50 | 1.11 | 0.83 | 1.09 |
| 7 | 1.449 | 0.94 | 1.30 | 1.84 | 1.35 | 1.53 | 1.11 | 0.79 | 1.07 |
| 8 | 1.427 | 0.93 | 1.33 | 1.86 | 1.36 | 1.54 | 1.08 | 0.77 | 1.05 |
| 9 | 1.589 | 1.02 | 1.46 | 2.64 | 1.69 | 1.56 | 1.09 | 0.60 | 0.94 |
| 10 | 1.492 | 0.96 | 1.46 | 2.64 | 1.67 | 1.55 | 1.02 | 0.57 | 0.89 |
| 11 | 1.462 | 0.93 | 1.41 | 2.74 | 1.68 | 1.58 | 1.03 | 0.53 | 0.87 |
| 12 | 1.429 | 0.93 | 1.37 | 2.88 | 1.71 | 1.54 | 1.04 | 0.50 | 0.83 |
| Average Hydraulic Conductivity | | | | | | 1.52 | 1.11 | 0.77 | 1.04 |

### E.1.3 Dirty Sand, Wet Pluviated

Table E.7 – Sand Properties: Dirty, Loose Sample

| | |
|---|---|
| Mass of Sand (g) | 1304 |
| Height of Sand in Permeameter (mm) | 195 |
| Dry Density (kg/m$^3$) | 1500 |
| Void Ratio | 0.764 |

Table E.8 – Hydraulic Conductivity Measurements: Dirty, Loose Sample

| Test No. | Water Volume (mL) | Time (s) | Manometer Water Levels (mm) | | | |
|---|---|---|---|---|---|---|
| | | | $h_1$ | $h_2$ | $h_3$ | $h_4$ |
| 1 | 240.3 | 42.6 | 77 | 122 | 163 | 201 |
| 2 | 234.7 | 42.5 | 70 | 115 | 156 | 195 |
| 3 | 237.2 | 44.2 | 60 | 107 | 148 | 181 |
| 4 | 250.2 | 47.6 | 58 | 101 | 140 | 179 |
| 5 | 326.5 | 62.7 | 55 | 97 | 135 | 173 |
| 6 | 316.8 | 50.4 | 119 | 172 | 220 | 270 |
| 7 | 247.4 | 41.7 | 96 | 147 | 192 | 240 |
| 8 | 217.5 | 37.0 | 93 | 145 | 189 | 237 |
| 9 | 212.7 | 37.3 | 80 | 130 | 170 | 217 |
| 10 | 207.9 | 37.9 | 68 | 114 | 156 | 199 |
| 11 | 273.4 | 40.7 | 137 | 195 | 247 | 299 |
| 12 | 198.8 | 31.3 | 115 | 168 | 221 | 274 |
| 13 | 214.1 | 34.1 | 110 | 165 | 217 | 267 |
| 14 | 248.4 | 40.0 | 105 | 160 | 208 | 260 |

Table E.9 – Hydraulic Conductivity Calculations: Dirty, Loose Sample

| Test No. | Velocity (mm/s) | Gradient, i | | | | Hydraulic Conductivity, k (mm/s) | | | |
|---|---|---|---|---|---|---|---|---|---|
| | | $i_{1-2}$ | $i_{2-3}$ | $i_{3-4}$ | $i_{1-4}$ | $k_{1-2}$ | $k_{2-3}$ | $k_{3-4}$ | $k_{1-4}$ |
| 1 | 1.268 | 0.83 | 0.89 | 0.76 | 0.83 | 1.52 | 1.42 | 1.67 | 1.53 |
| 2 | 1.240 | 0.83 | 0.89 | 0.78 | 0.83 | 1.49 | 1.39 | 1.59 | 1.49 |
| 3 | 1.205 | 0.87 | 0.89 | 0.66 | 0.81 | 1.38 | 1.35 | 1.83 | 1.49 |
| 4 | 1.181 | 0.80 | 0.85 | 0.78 | 0.81 | 1.48 | 1.39 | 1.51 | 1.46 |
| 5 | 1.168 | 0.78 | 0.83 | 0.76 | 0.79 | 1.50 | 1.41 | 1.54 | 1.49 |
| 6 | 1.413 | 0.98 | 1.04 | 1.00 | 1.01 | 1.44 | 1.35 | 1.41 | 1.40 |
| 7 | 1.331 | 0.94 | 0.98 | 0.96 | 0.96 | 1.41 | 1.36 | 1.39 | 1.39 |
| 8 | 1.321 | 0.96 | 0.96 | 0.96 | 0.96 | 1.37 | 1.38 | 1.38 | 1.38 |
| 9 | 1.282 | 0.93 | 0.87 | 0.94 | 0.91 | 1.38 | 1.47 | 1.36 | 1.40 |
| 10 | 1.233 | 0.85 | 0.91 | 0.86 | 0.87 | 1.45 | 1.35 | 1.43 | 1.41 |
| 11 | 1.508 | 1.07 | 1.13 | 1.04 | 1.08 | 1.40 | 1.33 | 1.45 | 1.40 |
| 12 | 1.428 | 0.98 | 1.15 | 1.06 | 1.06 | 1.46 | 1.24 | 1.35 | 1.35 |
| 13 | 1.412 | 1.02 | 1.13 | 1.00 | 1.05 | 1.39 | 1.25 | 1.41 | 1.35 |
| 14 | 1.393 | 1.02 | 1.04 | 1.04 | 1.03 | 1.37 | 1.34 | 1.34 | 1.35 |
| Average Hydraulic Conductivity | | | | | | 1.43 | 1.36 | 1.48 | 1.42 |

### E.1.4 Dirty Sand, Vibro-Compacted (A)

Table E.10 – Sand Properties: Dirty, Dense Sample (A)

| | |
|---|---|
| Mass of Sand (g) | 1500 |
| Height of Sand in Permeameter (mm) | 183 |
| Dry Density (kg/m$^3$) | 1845 |
| Void Ratio | 0.437 |

Table E.11 – Hydraulic Conductivity Measurements: Dirty, Dense Sample (A)

| Test No. | Water Volume (mL) | Time (s) | Manometer Water Levels (mm) | | | |
|---|---|---|---|---|---|---|
| | | | $h_1$ | $h_2$ | $h_3$ | $h_4$ |
| 1 | 84 | 31.1 | 35 | 93 | 187 | 414 |
| 2 | 81 | 30.8 | 33 | 91 | 186 | 413 |
| 3 | 87 | 33.6 | 31 | 89 | 182 | 413 |
| 4 | 69 | 27.1 | 29 | 87 | 179 | 413 |
| 5 | 92 | 31.8 | 60 | 126 | 233 | 512 |
| 6 | 73 | 25.8 | 57 | 122 | 228 | 513 |
| 7 | 83 | 29.5 | 54 | 117 | 225 | 514 |
| 8 | 87 | 30.5 | 29 | 95 | 204 | 510 |
| 9 | 78 | 31.1 | 88 | 147 | 250 | 600 |
| 10 | 84 | 34.2 | 81 | 140 | 244 | 603 |
| 11 | 71 | 29.7 | 74 | 133 | 236 | 605 |
| 12 | 71 | 29.9 | 72 | 130 | 233 | 606 |
| 13 | 81 | 30.1 | 114 | 180 | 299 | 737 |
| 14 | 83 | 31.2 | 104 | 170 | 288 | 736 |
| 15 | 81 | 32.1 | 90 | 154 | 275 | 740 |
| 16 | 88 | 35.3 | 84 | 146 | 267 | 741 |

Table E.12 – Hydraulic Conductivity Calculations: Dirty, Dense Sample (A)

| Test No. | Velocity (mm/s) | Gradient, i | | | | Hydraulic Conductivity, k (mm/s) | | | |
|---|---|---|---|---|---|---|---|---|---|
| | | $i_{1-2}$ | $i_{2-3}$ | $i_{3-4}$ | $i_{1-4}$ | $k_{1-2}$ | $k_{2-3}$ | $k_{3-4}$ | $k_{1-4}$ |
| 1 | 0.606 | 1.07 | 2.04 | 4.54 | 2.53 | 0.56 | 0.30 | 0.13 | 0.24 |
| 2 | 0.591 | 1.07 | 2.07 | 4.54 | 2.53 | 0.55 | 0.29 | 0.13 | 0.23 |
| 3 | 0.582 | 1.07 | 2.02 | 4.62 | 2.55 | 0.54 | 0.29 | 0.13 | 0.23 |
| 4 | 0.573 | 1.07 | 2.00 | 4.68 | 2.56 | 0.53 | 0.29 | 0.12 | 0.22 |
| 5 | 0.651 | 1.22 | 2.33 | 5.58 | 3.01 | 0.53 | 0.28 | 0.12 | 0.22 |
| 6 | 0.635 | 1.20 | 2.30 | 5.70 | 3.04 | 0.53 | 0.28 | 0.11 | 0.21 |
| 7 | 0.632 | 1.17 | 2.35 | 5.78 | 3.07 | 0.54 | 0.27 | 0.11 | 0.21 |
| 8 | 0.642 | 1.22 | 2.37 | 6.12 | 3.21 | 0.52 | 0.27 | 0.10 | 0.20 |
| 9 | 0.564 | 1.09 | 2.24 | 7.00 | 3.41 | 0.52 | 0.25 | 0.08 | 0.17 |
| 10 | 0.552 | 1.09 | 2.26 | 7.18 | 3.48 | 0.50 | 0.24 | 0.08 | 0.16 |
| 11 | 0.538 | 1.09 | 2.24 | 7.38 | 3.54 | 0.49 | 0.24 | 0.07 | 0.15 |
| 12 | 0.533 | 1.07 | 2.24 | 7.46 | 3.56 | 0.50 | 0.24 | 0.07 | 0.15 |
| 13 | 0.605 | 1.22 | 2.59 | 8.76 | 4.15 | 0.50 | 0.23 | 0.07 | 0.15 |
| 14 | 0.598 | 1.22 | 2.57 | 8.96 | 4.21 | 0.49 | 0.23 | 0.07 | 0.14 |
| 15 | 0.567 | 1.19 | 2.63 | 9.30 | 4.33 | 0.48 | 0.22 | 0.06 | 0.13 |
| 16 | 0.560 | 1.15 | 2.63 | 9.48 | 4.38 | 0.49 | 0.21 | 0.06 | 0.13 |
| Average Hydraulic Conductivity | | | | | | 0.52 | 0.26 | 0.09 | 0.18 |

### E.1.5 Dirty Sand, Vibro-Compacted (B)

Table E.13 – Sand Properties: Dirty, Dense Sample (B)

| | |
|---|---|
| Mass of Sand (g) | 1500 |
| Height of Sand in Permeameter (mm) | 184 |
| Dry Density (kg/m$^3$) | 1830 |
| Void Ratio | 0.448 |

Table E.14 – Hydraulic Conductivity Measurements: Dirty, Dense Sample (B)

| Test No. | Water Volume (mL) | Time (s) | Manometer Water Levels (mm) | | | |
|---|---|---|---|---|---|---|
| | | | $h_1$ | $h_2$ | $h_3$ | $h_4$ |
| 1 | 89 | 28.6 | -55 | 101 | 324 | 530 |
| 2 | 82 | 26.4 | -55 | 97 | 317 | 527 |
| 3 | 97 | 31.8 | -60 | 94 | 315 | 528 |
| 4 | 86 | 28.9 | -61 | 93 | 314 | 532 |
| 5 | 78 | 26.3 | -60 | 92 | 311 | 534 |
| 6 | 79 | 24.4 | -55 | 112 | 356 | 607 |
| 7 | 82 | 25.7 | -55 | 109 | 350 | 605 |
| 8 | 82 | 26.4 | -60 | 105 | 344 | 603 |
| 9 | 79 | 26.5 | -62 | 100 | 337 | 607 |
| 10 | 87 | 30.2 | -60 | 97 | 330 | 606 |
| 11 | 80 | 25.0 | -55 | 125 | 392 | 709 |
| 12 | 96 | 31.1 | -60 | 121 | 387 | 715 |
| 13 | 76 | 25.1 | -60 | 118 | 379 | 717 |
| 14 | 77 | 27.5 | -65 | 108 | 359 | 719 |
| 15 | 88 | 24.4 | -45 | 238 | 568 | 788 |
| 16 | 84 | 23.7 | -46 | 237 | 567 | 792 |
| 17 | 81 | 23.6 | -50 | 235 | 566 | 794 |
| 18 | 81 | 24.4 | -50 | 233 | 563 | 797 |

Table E.15 – Hydraulic Conductivity Calculations: Dirty, Dense Sample (B)

| Test No. | Velocity (mm/s) | Gradient, i | | | | Hydraulic Conductivity, k (mm/s) | | | |
|---|---|---|---|---|---|---|---|---|---|
| | | $i_{1-2}$ | $i_{2-3}$ | $i_{3-4}$ | $i_{1-4}$ | $k_{1-2}$ | $k_{2-3}$ | $k_{3-4}$ | $k_{1-4}$ |
| 1 | 0.698 | 2.89 | 4.85 | 4.12 | 3.90 | 0.24 | 0.14 | 0.17 | 0.18 |
| 2 | 0.699 | 2.81 | 4.78 | 4.20 | 3.88 | 0.25 | 0.15 | 0.17 | 0.18 |
| 3 | 0.686 | 2.85 | 4.80 | 4.26 | 3.92 | 0.24 | 0.14 | 0.16 | 0.17 |
| 4 | 0.669 | 2.85 | 4.80 | 4.36 | 3.95 | 0.23 | 0.14 | 0.15 | 0.17 |
| 5 | 0.667 | 2.81 | 4.76 | 4.46 | 3.96 | 0.24 | 0.14 | 0.15 | 0.17 |
| 6 | 0.727 | 3.09 | 5.30 | 5.02 | 4.41 | 0.24 | 0.14 | 0.14 | 0.16 |
| 7 | 0.718 | 3.04 | 5.24 | 5.10 | 4.40 | 0.24 | 0.14 | 0.14 | 0.16 |
| 8 | 0.699 | 3.06 | 5.20 | 5.18 | 4.42 | 0.23 | 0.13 | 0.13 | 0.16 |
| 9 | 0.669 | 3.00 | 5.15 | 5.40 | 4.46 | 0.22 | 0.13 | 0.12 | 0.15 |
| 10 | 0.646 | 2.91 | 5.07 | 5.52 | 4.44 | 0.22 | 0.13 | 0.12 | 0.15 |
| 11 | 0.718 | 3.33 | 5.80 | 6.34 | 5.09 | 0.22 | 0.12 | 0.11 | 0.14 |
| 12 | 0.694 | 3.35 | 5.78 | 6.56 | 5.17 | 0.21 | 0.12 | 0.11 | 0.13 |
| 13 | 0.679 | 3.30 | 5.67 | 6.76 | 5.18 | 0.21 | 0.12 | 0.10 | 0.13 |
| 14 | 0.629 | 3.20 | 5.46 | 7.20 | 5.23 | 0.20 | 0.12 | 0.09 | 0.12 |
| 15 | 0.811 | 5.24 | 7.17 | 4.40 | 5.55 | 0.15 | 0.11 | 0.18 | 0.15 |
| 16 | 0.795 | 5.24 | 7.17 | 4.50 | 5.59 | 0.15 | 0.11 | 0.18 | 0.14 |
| 17 | 0.770 | 5.28 | 7.20 | 4.56 | 5.63 | 0.15 | 0.11 | 0.17 | 0.14 |
| 18 | 0.746 | 5.24 | 7.17 | 4.68 | 5.65 | 0.14 | 0.10 | 0.16 | 0.13 |
| Average Hydraulic Conductivity | | | | | | 0.21 | 0.13 | 0.14 | 0.15 |

## E.2 Dry Density Measurements

Table E.16 – Density measurements from test boxes

| Bag No. | Box | Start Elevation (mm) | End Elevation (mm) | Mass Wet (kg) | Volume ($m^3$) | Moisture Content (%) | Dry Density ($kg/m^3$) | Void Ratio |
|---|---|---|---|---|---|---|---|---|
| 1-1 | South | 800.1 | 596.9 | 2.46 | 0.0015 | 3.3 | 1588 | 0.668 |
| 1-2 | South | 673.1 | 469.9 | 2.40 | 0.0015 | 3.0 | 1555 | 0.704 |
| 1-3 | South | 558.8 | 355.6 | 2.35 | 0.0015 | 3.0 | 1521 | 0.742 |
| 1-4 | South | 431.8 | 228.6 | 2.45 | 0.0015 | 3.7 | 1574 | 0.684 |
| 1-5 | South | 254.0 | 50.8 | 2.82 | 0.0015 | 14.9 | 1633 | 0.622 |
| 2-1 | North | 762.0 | 558.8 | 2.65 | 0.0015 | 3.4 | 1706 | 0.553 |
| 2-2 | North | 609.6 | 406.4 | 2.47 | 0.0015 | 2.2 | 1609 | 0.647 |
| 2-3 | North | 482.6 | 279.4 | 2.45 | 0.0015 | 2.6 | 1590 | 0.667 |
| 2-4 | North | 355.6 | 152.4 | 2.58 | 0.0015 | 8.5 | 1586 | 0.671 |

Table E.17 – Moisture content measurements

| Bag No. | Dish No. | Mass Wet (g) | Mass Dry (g) | Tare (g) | Water Content (%) |
|---|---|---|---|---|---|
| 1-1 | A | 45.73 | 44.36 | 0.95 | 3.16 |
| 1-1 | B | 44.29 | 42.80 | 0.95 | 3.56 |
| 1-1 | C | 42.84 | 41.51 | 0.95 | 3.28 |
| 1-2 | A | 44.82 | 43.63 | 0.95 | 2.79 |
| 1-2 | B | 48.37 | 46.99 | 0.95 | 3.00 |
| 1-2 | C | 48.28 | 46.82 | 0.95 | 3.18 |
| 1-3 | A | 43.23 | 42.06 | 0.95 | 2.85 |
| 1-3 | B | 41.80 | 40.64 | 0.95 | 2.92 |
| 1-3 | C | 48.47 | 47.00 | 0.95 | 3.19 |
| 1-4 | A | 44.34 | 42.72 | 0.95 | 3.88 |
| 1-4 | B | 43.84 | 42.28 | 0.95 | 3.77 |
| 1-4 | C | 45.44 | 44.01 | 0.95 | 3.32 |
| 1-5 | A | 62.97 | 54.93 | 0.95 | 14.89 |
| 1-5 | B | 61.96 | 54.53 | 0.95 | 13.87 |
| 1-5 | C | 66.04 | 57.02 | 0.95 | 16.09 |
| 2-1 | A | 49.29 | 47.75 | 0.95 | 3.29 |
| 2-1 | B | 45.17 | 43.70 | 0.95 | 3.44 |
| 2-1 | C | 41.94 | 40.55 | 0.95 | 3.51 |
| 2-2 | A | 49.18 | 48.17 | 0.95 | 2.14 |
| 2-2 | B | 48.49 | 47.46 | 0.95 | 2.21 |
| 2-2 | C | 43.75 | 42.79 | 0.95 | 2.29 |
| 2-3 | A | 43.48 | 42.40 | 0.95 | 2.61 |
| 2-3 | B | 41.66 | 40.62 | 0.95 | 2.62 |
| 2-3 | C | 47.75 | 46.52 | 0.95 | 2.70 |
| 2-4 | A | 48.51 | 44.67 | 0.95 | 8.78 |
| 2-4 | B | 43.41 | 40.19 | 0.95 | 8.21 |
| 2-4 | C | 49.42 | 45.64 | 0.95 | 8.46 |

## E.3 Maximum and Minimum Index Density Measurements

Table E.18 – Maximum and Minimum Index Density Test Results

| | Mass of Sand (kg) | Volume of Sand (cm3) | Dry Density (kg/m3) | Void Ratio |
|---|---|---|---|---|
| Clean, Loose Sand | 1.523 | 936 | 1627 | 0.629 |
| Clean, Dense Sand | 2.871 | 1161 | 1782 | 0.487 |
| Dirty, Loose Sand | 1.400 | 936 | 1495 | 0.772 |
| Dirty, Dense Sand | 1.500 | 789 | 1900 | 0.395 |

# APPENDIX F NUMERICAL MODELLING PROCEDURES

## F.1 Iterative Determination of Material Properties and Boundary Conditions

In the test box and riverbed models, several variables had to be determined iteratively. These variables affect the results of the numerical models, and could only be calculated correctly using the numerical model results. The procedures outlined below were used to determine the correct values to assign to the these variables.

### F.1.1 Test Box Model

- After setting up the model geometry and assigning hydraulic conductivities to the clean and dirty sand layers, initial guesses were made of the values of three parameters – wellscreen_k (the equivalent hydraulic conductivity of the wellscreen), pipe_k (the equivalent hydraulic conductivity of the connecting pipe), and exit_head (the total head boundary condition applied to the aperture of the connecting pipe).

- The model was solved using the initial estimates of these three parameters. The average (mean) velocity in the wellscreen and the velocity in the connecting pipe were determined from the model results.

- The velocity in the wellscreen was used to calculate the value of wellscreen_k using: $k = \frac{2g\text{Ø}}{\text{V}}\left[1.8\log_{10}\left(\frac{6.9\nu}{\text{V}\text{Ø}} + \left(\frac{\varepsilon}{3.7\text{Ø}}\right)^{1.11}\right)\right]^2$, where g is gravitational acceleration (9.81 $m/s^2$), Ø is the pipe diameter (m), V is velocity (m/s), $\nu$ is kinematic viscosity ($m^2/s$), and $\varepsilon$ is pipe roughness (m).

- The velocity in the connecting pipe (V) was used to determine the value of pipe_k using the same equation, and to determine the value of total head at the pipe aperture (the sum of the elevation head, pressure head and velocity head) using the following equation:

$$exit_head = h_e + h_p + h_v = 0.11m + 0 + \frac{\text{V}^2}{2g} \qquad [1]$$

- The values of wellscreen_k, pipe_k and exit_head were adjusted for the next solution of the numerical model. The model was solved, and the new values of these three parameters were determined from the numerical model's calculation of average velocity in the wellscreen and connecting pipe.

- Iteration continued until the values of wellscreen_k, pipe_k and exit_head changed by less than 1% from one iteration to the next.

- The correct values of hydraulic conductivity and average velocity are reached when they are consistent – i.e., when the hydraulic conductivity and average velocity result in each other being calculated by the numerical model and the equation above.

### F.1.2 Riverbed Model

Two techniques were used to simulate pipe hydraulics using porous media in the numerical models of the riverbed: the uniform conductivity method, and a more rigorous solution method. The difference between these two techniques is described in Chapter 3. Below is an explanation of the iterative procedures used to determine the correct hydraulic conductivities in each solution technique.

#### F.1.2.1. Uniform Conductivity Method

- The same technique used to determine the values of wellscreen_k, pipe_k and exit_head in the test box model was used to select an appropriate value for well_k in the riverbed model. Iterations again continued until well_k changed by less than 1% from one iteration to the next.

#### F.1.2.2. Rigorous Solution Method

- The rigorous solution method used a function approximating velocity along the wellscreen to calculate the equivalent hydraulic conductivity of the wellscreen at every point along its length.

- Before any modelling, it was necessary to choose a type of function to approximate velocity along the length of the wellscreen – either linear, as: $V(z) = az + b$, or exponential, as: $V(z) = \exp(az + b) - \exp(b) + c$. This determination was made based on the results of the uniform conductivity solution of the same case – if the profile of axial velocity appeared to be approximately linear, a linear function was used, otherwise the velocity in the wellscreen was approximated by an exponential function.

- The wellscreen's velocity approximation was a function of two or three constants: a and b (and c for exponential functions). Initially, these constants were set so that velocity at the well toe (z = 0) was zero, and the velocity at the well heel (z = L) was equal to the well heel velocity computed from the uniform conductivity solution. The numerical model was then solved.

- The constants a, b and c were adjusted by trial and error so that the approximate velocity function matched the computed velocity distribution in the wellscreen reasonably well (to save time, exact matches were never required). In particular, the approximated velocity and computed velocity at the well heel (z = L) were matched exactly. The model was solved again with the new values of a, b and c.

- Iteration continued until the approximated velocity at the well heel changed by less than 1% from one iteration to the next.

- See Figure I.6 for an example of the hydraulic conductivity profile along the wellscreen.

## F.2 Determination of Accuracy Settings

The parameters ERRLIM and NGRID were used to control the accuracy of the numerical models used in this study (see Appendix H for an explanation of how these two parameters are treated by FlexPDE). In general, smaller values of ERRLIM and larger values of NGRID were used to produce more accurate solutions.

The values of ERRLIM and NGRID were adjusted so that the model results appeared to be free of obvious errors. Errors were most noticeable in the model output of contours of total head. When the model accuracy was set too low, the computed contours indicated that some areas of the model domain had values of total head greater than 12m – the largest head that should have been computed. Other errors were observed by examining the profile of axial velocity along the axis of the wellscreen – jagged lines were taken as indicative of an inaccurate solution. If any of these errors were observed, the ERRLIM and NGRID parameters were adjusted to achieve greater accuracy and the model was solved again.

# APPENDIX G TEXT INPUT TO FLEXPDE

Below is a sample of the input files that were used to model the flow of water in the test equipment. The variables that were adjusted are listed in **bold** type. Exclamation marks ( ! ) or braces ( { ), ( } ) are used to indicate comments.

```
TITLE'Test Box Model'
{Project:  EL_Smith, Problem:  3D box Steady State}
{3D model of plywood test box. One wellscreen modelled. Z-direction along axis
            of wellscreen. Steady State}

COORDINATES
 Cartesian3

SELECT
 ERRLIM      = 1e-5          {control over accuracy of solution}
 NGRID       = 30            {control over grid discretization in direction
            parallel to wellscreen}
 NRMATRIX    = 10            {control over number of Newton-Raphson
            iterations}

VARIABLES
 h(range=0.7)                {total head}

DEFINITIONS

{Other}
 uww=9.807      {kN/m^3}     {unit weight of water}
 u=uww*(h-z)    {kPa}        {pressure head}
 s=0                         {storage}
 kx                          {hydraulic conductivity in x-direction}
 ky                          {hydraulic conductivity in y-direction}
 kz                          {hydraulic conductivity in z-direction}

Gradx= -dx(h)*kx
Grady= -dy(h)*ky
Gradz= -dz(h)*kz

vx = Gradx
vy = Grady
vz = Gradz

{Box Dimensions}

box_long     = 2.43         {length of box}
box_wide     = 1.2          {width of box}
box_deep     = 0.8          {depth of sand in box}

{Wellscreen and Pipe Dimensions and Location}

in_rad       = 0.016        {inside radius of wellscreen and
            connecting pipe}
out_rad      = 0.03         {outside radius of connecting pipe}
scr_cen_x    = 0.4          {x-coordinate of wellscreen center - distance
            from side of box to wellscreen axis}
```

```
scr_cen_y       = 0.11          {y-coordinate of wellscreen center - distance
                from bottom of box to wellscreen axis}
well_long       = 0.91          {length of wellscreen}
pipe_long       = 0.76          {length of connecting pipe}

{Material Properties}

sand_k          = 1.58e-3
                {hydraulic conductivity of clean sand}
dirty_sand_k    = 5.86e-4
                {hydraulic conductivity of dirty sand layer at top of box}
wellscreen_k    = 15.2
                {hydraulic conductivity to give head loss equivalent to roughness
                of wellscreen}
pipe_k          = 27.0
                {hydraulic conductivity to give head loss equivalent to roughness
                of connecting pipe}

exit_head       = 0.215
                {total head condition at the aperture of the connecting pipe}

transfer("box_head3.trn",h0)
                {take previous solution and call it h0 to use as initial conditions}

EQUATIONS
 div(vector(kx*dx(h),ky*dy(h),kz*dz(h))) + s = 0

INITIAL VALUES
h=h0                                    {use h0 as initial conditions}

EXTRUSION
{Four surfaces to define extrusion. 1) start of box, 2) start of wellscreen, 3) end of
                wellscreen and start of pipe, 4) end of pipe and box.}

Surface "surface 1"  z = 0
Surface "surface 2"  z = box_long - pipe_long - well_long
Surface "surface 3"  z = box_long - pipe_long
Surface "surface 4"  z = box_long

BOUNDARIES

{Sand Used in Box}
Region 1        'clean sand'
Kx = sand_k
Ky = sand_k
Kz = sand_k

start(0,0)

{zero flux (impermeable) boundary on box walls}
Layer 1
natural(h)=0
Layer 2
natural(h)=0
Layer 3
natural(h)=0
```

```
 Line to (box_wide,0)
 Line to (box_wide,box_deep)

{constant head boundary at top of box}
Layer 1
value(h)= (1.2-0.27)
Layer 2
value(h)= (1.2-0.27)
Layer 3
value(h)= (1.2-0.27)
 Line to (0,box_deep)

{zero flux (impermeable) boundary on box walls}
Layer 1
natural(h)=0
Layer 2
natural(h)=0
Layer 3
natural(h)=0
 Line to (0,0)

{Wall of Pipe Connecting Wellscreen to Exterior of Box - Prevents Radial Inflow}
Region 2          'pipe walls'
Kx = sand_k
Ky = sand_k
Kz = sand_k
Layer 3 Void

{circle around center coordinates of wellscreen - outside radius}
start(scr_cen_x-out_rad,scr_cen_y)
 arc(center=scr_cen_x,scr_cen_y) angle=360 to finish

{Wellscreen and Interior of Connecting Pipe}
Region 3          'wellscreen'
Layer 1
Kx = sand_k
Ky = sand_k
Kz = sand_k
Layer 2
Kx = wellscreen_k
Ky = wellscreen_k
Kz = wellscreen_k
Layer 3
Kx = pipe_k
Ky = pipe_k
Kz = pipe_k
Surface 4 value(h)=exit_head

{circle around center coordinates of wellscreen - inside radius}
start(scr_cen_x-in_rad,scr_cen_y)
 arc(center=scr_cen_x,scr_cen_y) angle=360 to finish

{Layer of Dirty Sand at Top of Test Box - Schmutzedecke}
Region 4          'dirty sand'
Kx = dirty_sand_k
Ky = dirty_sand_k
```

```
Kz = dirty_sand_k

start(0,box_deep)
  Line to (box_wide,box_deep)
  Line to (box_wide,box_deep-0.075)
  Line to (0,box_deep-0.075)
  Line to finish

PLOTS
Grid(x,y,z)
Grid(x,y) on z=2.43 as "Mesh"
Grid(z,y) on x=0.4 as "Mesh"

Contour(h) on y=0.1 as "Horizontal plane through screen"
Contour(h) on x=0.4 as "Vertical plane through screen"
Contour(h) on z=1.22 as "Vertical plane across screen"

elevation(vz) from (scr_cen_x,scr_cen_y,0.76) to (scr_cen_x,scr_cen_y,1.67)
elevation(h) from (scr_cen_x,scr_cen_y,0.76) to (scr_cen_x,scr_cen_y,2.43)

Summary as"Wellscreen Effluent"
   report(  val(sqrt(vx^2+vy^2+vz^2)*pi*in_rad^2,scr_cen_x,scr_cen_y,1.67)  ) as
                  "velocity times area "

transfer(h) file="box_head3.trn"

END
```

---

Below is a sample of the input files that were used to model groundwater flow to a horizontal well placed in riverbed sediments. The text shown below is taken from the rigorous solution of a horizontal well 250m long, 300mm in diameter and 5m below the river in an aquifer with a horizontal hydraulic conductivity of $10^{-3}$ m/s. In the uniform conductivity solution method, **well_k** was assigned a constant value based on the results of the previous iteration. The variables that were adjusted to examine the sensitivity of the numerical model are listed in **bold** type. Exclamation marks ( ! ) or braces ( { ), ( } ) are used to indicate comments.

```
TITLE 'river half-width model'

COORDINATES
                Cartesian3

SELECT
 errlim = 1e-5
 ngrid  = 40
 nrmatrix = 10

VARIABLES
 h(range=7)
```

```
DEFINITIONS
 uww=9.807        {kN/m^3}
 u=uww*(h-z)      {kPa}
 s=0
 kx
 ky
 kz

Gradx= -dx(h)*kx
Grady= -dy(h)*ky
Gradz= -dz(h)*kz
FlowGrady = dy(h)*ky
FlowGradz = dz(h)*kz

vx = Gradx
vy = Grady
vz = Gradz

{Geometry}
well_rad        = 0.150
well_diam       = 2*well_rad
well_cen_y      = 5
well_length     = 250

exit_head       = well_cen_y

{Calculation of friction factor in wellbore}
a               = 5.7e-3
b               = 0.25
c               = 0.2
velocity        = exp(a * (z+0.1) + b) - exp(b) + c
Re              = velocity*well_diam/1e-6
f1              = ( 1.8 * LOG10( 6.9 / Re + ( 1e-3 / ( 3.7 * well_diam ))^1.11
                ))^(-2)
f2              = max(( 1 - 10 * well_diam * dz(velocity) / ( velocity )), 0.25 )
f3              = f1 * f2

{material properties}
aq_k            = 1e-3
                {hydraulic conductivity of aquifer}
well_k          = ( 2 * 9.81 * well_diam )/( f3 * velocity )
                {equivalent hydraulic conductivity of wellscreen}

transfer("head_250-300-3.trn",h0)

EQUATIONS
 div(vector(kx*dx(h),ky*dy(h),kz*dz(h))) + s = 0

INITIAL VALUES
h=h0

EXTRUSION
Surface "surface 1" z = -100
 Layer "Layer 1"
Surface "surface 2" z = 0
```

```
 Layer "Layer 2"
Surface "surface 3" z = well_length
 Layer "Layer 3"
Surface "surface 4" z = well_length + 100

BOUNDARIES
  REGION 1  'aquifer'
kx = aq_k
ky = aq_k/10
kz = aq_k
surface 1 value(h)=12
surface 4 value(h)=12

start(0,0)
natural(h)=0
Line to (65,0)
Line to (65,12)
Line to (25,12)

value(h)=12
Line to (25,10)
Line to (0,10)

natural(h)=0
Line to (0,0)
Line to finish

  REGION 2  'well'
kx = aq_k
ky = aq_k/10
kz = aq_k
Layer 2
kx = well_k
ky = well_k
kz = well_k
surface 3 value(h)=exit_head

start(0,well_cen_y-well_rad)
  Arc(center=0,well_cen_y) angle=180
  Line to finish

FEATURE 'top'
  START(0,well_cen_y+well_rad+0.1)
  Arc(center=0,well_cen_y) angle=-90

FEATURE 'bot'
  START(0+well_rad+0.1,well_cen_y)
  Arc(center=0,well_cen_y) angle=-90

PLOTS
grid (x,y) on z = 0
contour(h) on z = well_length/2
contour(h) on y = well_cen_y zoom(0,-100,65,450)
contour(h) on x = 0 zoom(0,-100,10,450)
```

```
elevation(vz) from (0,well_cen_y,0) to (0,well_cen_y,well_length) points =
              (well_length+1) print file="vel_250-300-3.dat"
elevation(h) from (0,well_cen_y,0) to (0,well_cen_y,well_length)
elevation(f2) from (0,well_cen_y,0) to (0,well_cen_y,well_length)
elevation(kz) from (0,well_cen_y,0) to (0,well_cen_y,well_length)

summary as "Well Effluent"

 report(val(sqrt(vx^2+vy^2+vz^2)*pi*well_rad^2,0,well_cen_y,well_length-0.1))
              as "velocity times area "

transfer(h) file="head_250-300-3.trn"

END
```

# APPENDIX H NUMERICAL MODEL INPUT PARAMETERS AND RESULTS

Table H.1 – Input parameters and model results – test box model, uniform conductivity solution method

| No. | Input Parameters | | | | | | | Model Results | |
|---|---|---|---|---|---|---|---|---|---|
| | Clean Sand Hydraulic Conductivity (m/s) | Dirty Sand Hydraulic Conductivity (m/s) | Wellscreen Hydraulic Conductivity (m/s) | Connecting Pipe Hydraulic Conductivity (m/s) | Total Head at Wellscreen Aperture (m) | NGRID | ERRLIM | Flow Rate (L/s) | RMS Error |
| 1 | $1.58 \times 10^{-3}$ | $5.86 \times 10^{-4}$ | 15 | 27 | 0.215 | 30 | $1 \times 10^{-5}$ | 1.155 | $4.367 \times 10^{-6}$ |
| 2 | $5.96 \times 10^{-4}$ | $2.21 \times 10^{-4}$ | 30 | 57 | 0.133 | 40 | $1 \times 10^{-5}$ | 0.527 | $3.982 \times 10^{-6}$ |

Table H.2 – Input parameters and model results – riverbed model, uniform conductivity solution method

| No. | Input Parameters | | | | | | | Model Results | | |
|---|---|---|---|---|---|---|---|---|---|---|
| | well_length (m) * | well_rad (m) * | aq_k (m/s) * | well_cen_y (m) * | NGRID * | ERRLIM * | well_k (m/s) * | Flow Rate ($m^3/s$) | Average Velocity (m/s) | RMS Error |
| 1 | 50 | 0.150 | $10^{-3}$ | 5 | 50 | $8 \times 10^{-5}$ | 185 | 0.155 | 1.157 | $6.461 \times 10^{-6}$ |
| 2 | 100 | 0.150 | $10^{-3}$ | 5 | 40 | $1 \times 10^{-4}$ | 118 | 0.261 | 1.833 | $8.346 \times 10^{-6}$ |
| 3 | 175 | 0.150 | $10^{-3}$ | 5 | 40 | $1 \times 10^{-4}$ | 103 | 0.335 | 2.108 | $7.794 \times 10^{-6}$ |
| 4 | 250 | 0.150 | $10^{-3}$ | 5 | 40 | $1 \times 10^{-4}$ | 105 | 0.371 | 2.063 | $7.000 \times 10^{-6}$ |
| 5 | 500 | 0.150 | $10^{-3}$ | 5 | 40 | $1 \times 10^{-4}$ | 129 | 0.428 | 1.678 | $5.632 \times 10^{-6}$ |
| 6 | 50 | 0.100 | $10^{-3}$ | 5 | 55 | $1 \times 10^{-4}$ | 63 | 0.127 | 2.038 | $5.660 \times 10^{-6}$ |
| 7 | 100 | 0.100 | $10^{-3}$ | 5 | 55 | $1 \times 10^{-4}$ | 56 | 0.167 | 2.291 | $5.342 \times 10^{-6}$ |
| 8 | 175 | 0.100 | $10^{-3}$ | 5 | 55 | $1 \times 10^{-4}$ | 62 | 0.190 | 2.062 | $4.749 \times 10^{-6}$ |
| 9 | 250 | 0.100 | $10^{-3}$ | 5 | 55 | $1 \times 10^{-4}$ | 70 | 0.204 | 1.815 | $4.378 \times 10^{-6}$ |
| 10 | 500 | 0.100 | $10^{-3}$ | 5 | 55 | $1 \times 10^{-4}$ | 96 | 0.239 | 1.334 | $3.746 \times 10^{-6}$ |
| 11 | 50 | 0.050 | $10^{-3}$ | 5 | 70 | $1 \times 10^{-4}$ | 21 | 0.053 | 2.406 | $3.099 \times 10^{-6}$ |
| 12 | 100 | 0.050 | $10^{-3}$ | 5 | 60 | $1 \times 10^{-4}$ | 28 | 0.061 | 1.844 | $2.924 \times 10^{-6}$ |
| 13 | 175 | 0.050 | $10^{-3}$ | 5 | 60 | $1 \times 10^{-4}$ | 36 | 0.070 | 1.430 | $2.727 \times 10^{-6}$ |
| 14 | 250 | 0.050 | $10^{-3}$ | 5 | 70 | $1 \times 10^{-4}$ | 43 | 0.076 | 1.194 | $2.318 \times 10^{-6}$ |
| 15 | 500 | 0.050 | $10^{-3}$ | 5 | 70 | $1 \times 10^{-4}$ | 60 | 0.090 | 0.844 | $1.983 \times 10^{-6}$ |
| 16 | 50 | 0.150 | $10^{-4}$ | 5 | 40 | $1 \times 10^{-4}$ | 1575 | 0.017 | 0.126 | $8.014 \times 10^{-6}$ |
| 17 | 100 | 0.150 | $10^{-4}$ | 5 | 40 | $1 \times 10^{-4}$ | 915 | 0.031 | 0.225 | $9.325 \times 10^{-6}$ |
| 18 | 175 | 0.150 | $10^{-4}$ | 5 | 40 | $1 \times 10^{-4}$ | 570 | 0.051 | 0.370 | $9.745 \times 10^{-6}$ |
| 19 | 250 | 0.150 | $10^{-4}$ | 5 | 40 | $1 \times 10^{-4}$ | 420 | 0.071 | 0.505 | $1.025 \times 10^{-5}$ |
| 20 | 500 | 0.150 | $10^{-4}$ | 5 | 40 | $1 \times 10^{-4}$ | 257 | 0.122 | 0.832 | $1.089 \times 10^{-5}$ |

| No. | Input Parameters | | | | | | | Model Results | | |
|---|---|---|---|---|---|---|---|---|---|---|
| | well_length (m) * | well_rad (m) * | aq_k (m/s) * | well_cen_y (m) * | NGRID * | ERRLIM * | well_k (m/s) * | Flow Rate ($m^3/s$) | Average Velocity (m/s) | RMS Error |
| 21 | 50 | 0.100 | $10^{-4}$ | 5 | 50 | $1x10^{-4}$ | 480 | 0.015 | 0.255 | $6.958x10^{-6}$ |
| 22 | 100 | 0.100 | $10^{-4}$ | 5 | 40 | $1x10^{-4}$ | 270 | 0.028 | 0.459 | $7.766x10^{-6}$ |
| 23 | 175 | 0.100 | $10^{-4}$ | 5 | 40 | $1x10^{-4}$ | 177 | 0.044 | 0.712 | $9.182x10^{-6}$ |
| 24 | 250 | 0.100 | $10^{-4}$ | 5 | 40 | $1x10^{-4}$ | 107 | 0.055 | 0.831 | $8.790x10^{-6}$ |
| 25 | 500 | 0.100 | $10^{-4}$ | 5 | 45 | $1x10^{-4}$ | 123 | 0.076 | 1.013 | $7.361x10^{-6}$ |
| 26 | 50 | 0.050 | $10^{-4}$ | 5 | 60 | $1x10^{-4}$ | 61 | 0.012 | 0.812 | $4.812x10^{-6}$ |
| 27 | 100 | 0.050 | $10^{-4}$ | 5 | 40 | $1x10^{-4}$ | 45 | 0.019 | 1.139 | $5.744x10^{-6}$ |
| 28 | 175 | 0.050 | $10^{-4}$ | 5 | 60 | $1x10^{-4}$ | 44 | 0.023 | 1.164 | $4.547x10^{-6}$ |
| 29 | 250 | 0.050 | $10^{-4}$ | 5 | 60 | $1x10^{-4}$ | 47 | 0.024 | 1.079 | $4.307x10^{-6}$ |
| 30 | 500 | 0.050 | $10^{-4}$ | 5 | 60 | $1x10^{-4}$ | 61 | 0.028 | 0.829 | $3.421x10^{-6}$ |
| 31 | 50 | 0.150 | $10^{-5}$ | 5 | 50 | $1x10^{-4}$ | 10700 | $1.7x10^{-3}$ | 0.013 | $7.670x10^{-6}$ |
| 32 | 100 | 0.150 | $10^{-5}$ | 5 | 40 | $1x10^{-4}$ | 6800 | $3.1x10^{-3}$ | 0.023 | $8.850x10^{-6}$ |
| 33 | 175 | 0.150 | $10^{-5}$ | 5 | 40 | $1x10^{-4}$ | 4500 | $5.2x10^{-3}$ | 0.038 | $9.813x10^{-6}$ |
| 34 | 250 | 0.150 | $10^{-5}$ | 5 | 40 | $1x10^{-4}$ | 3450 | $7.3x10^{-3}$ | 0.052 | $1.037x10^{-5}$ |
| 35 | 500 | 0.150 | $10^{-5}$ | 5 | 40 | $8x10^{-5}$ | 1850 | 0.014 | 0.104 | $1.047x10^{-5}$ |
| 36 | 50 | 0.100 | $10^{-5}$ | 5 | 50 | $1x10^{-4}$ | 3575 | $1.5x10^{-3}$ | 0.026 | $6.972x10^{-6}$ |
| 37 | 100 | 0.100 | $10^{-5}$ | 5 | 50 | $1x10^{-4}$ | 2230 | $2.8x10^{-3}$ | 0.047 | $8.319x10^{-6}$ |
| 38 | 175 | 0.100 | $10^{-5}$ | 5 | 40 | $1x10^{-4}$ | 1430 | $4.7x10^{-3}$ | 0.078 | $9.656x10^{-6}$ |
| 39 | 250 | 0.100 | $10^{-5}$ | 5 | 50 | $1x10^{-4}$ | 1070 | $6.7x10^{-3}$ | 0.108 | $1.021x10^{-5}$ |
| 40 | 500 | 0.100 | $10^{-5}$ | 5 | 40 | $1x10^{-4}$ | 602 | 0.013 | 0.201 | $1.141x10^{-5}$ |
| 41 | 50 | 0.050 | $10^{-5}$ | 5 | 60 | $1x10^{-4}$ | 509 | $1.3x10^{-3}$ | 0.088 | $5.088x10^{-6}$ |
| 42 | 100 | 0.050 | $10^{-5}$ | 5 | 50 | $1x10^{-4}$ | 290 | $2.5x10^{-3}$ | 0.163 | $6.596x10^{-6}$ |
| 43 | 175 | 0.050 | $10^{-5}$ | 5 | 50 | $1x10^{-4}$ | 186 | $4.1x10^{-3}$ | 0.264 | $7.512x10^{-6}$ |
| 44 | 250 | 0.050 | $10^{-5}$ | 5 | 50 | $1x10^{-4}$ | 143 | $5.5x10^{-3}$ | 0.346 | $7.878x10^{-6}$ |
| 45 | 500 | 0.050 | $10^{-5}$ | 5 | 40 | $7x10^{-5}$ | 99 | $8.7x10^{-3}$ | 0.508 | $6.441x10^{-6}$ |
| 46 | 50 | 0.150 | $10^{-6}$ | 5 | 40 | $1x10^{-4}$ | 45000 | $1.5x10^{-4}$ | $1.3x10^{-4}$ | $8.017x10^{-6}$ |
| 47 | 100 | 0.150 | $10^{-6}$ | 5 | 40 | $1x10^{-4}$ | 32700 | $3.0x10^{-4}$ | $2.3x10^{-4}$ | $8.850x10^{-6}$ |
| 48 | 175 | 0.150 | $10^{-6}$ | 5 | 40 | $1x10^{-4}$ | 24200 | $5.1x10^{-4}$ | $3.8x10^{-4}$ | $9.814x10^{-6}$ |
| 49 | 500 | 0.150 | $10^{-6}$ | 5 | 50 | $8x10^{-5}$ | 10000 | $1.4x10^{-3}$ | 0.012 | $1.012x10^{-5}$ |
| 50 | 50 | 0.100 | $10^{-6}$ | 5 | 45 | $1x10^{-4}$ | 16500 | $1.4x10^{-4}$ | $2.7x10^{-4}$ | $7.244x10^{-5}$ |
| 51 | 100 | 0.100 | $10^{-6}$ | 5 | 50 | $1x10^{-4}$ | 12100 | $2.7x10^{-4}$ | $4.5x10^{-4}$ | $8.320x10^{-5}$ |
| 52 | 175 | 0.100 | $10^{-6}$ | 5 | 50 | $1x10^{-4}$ | 8500 | $4.6x10^{-4}$ | $7.9x10^{-4}$ | $9.489x10^{-5}$ |
| 53 | 500 | 0.100 | $10^{-6}$ | 5 | 50 | $1x10^{-4}$ | 2400 | $1.3x10^{-3}$ | 0.043 | $1.140x10^{-5}$ |
| 54 | 50 | 0.050 | $10^{-6}$ | 5 | 60 | $1x10^{-4}$ | 2975 | $1.2x10^{-4}$ | $8.8x10^{-4}$ | $5.078x10^{-6}$ |

| No. | Input Parameters | | | | | | | Model Results | | |
|---|---|---|---|---|---|---|---|---|---|---|
| | well_length (m) * | well_rad (m) * | aq_k (m/s) * | well_cen_y (m) * | NGRID * | ERRLIM * | well_k (m/s) * | Flow Rate ($m^3/s$) | Average Velocity (m/s) | RMS Error |
| 55 | 100 | 0.050 | $10^{-6}$ | 5 | 60 | $1x10^{-4}$ | 1984 | $2.3x10^{-4}$ | 0.016 | $6.343x10^{-6}$ |
| 56 | 175 | 0.050 | $10^{-6}$ | 5 | 60 | $1x10^{-4}$ | 1360 | $4.0x10^{-4}$ | 0.027 | $7.464x10^{-6}$ |
| 57 | 500 | 0.050 | $10^{-6}$ | 5 | 50 | $8x10^{-5}$ | 520 | $1.1x10^{-3}$ | 0.086 | $8.227x10^{-6}$ |
| 58 | 250 | 0.150 | $10^{-3}$ | 7.5 | 70 | $8x10^{-5}$ | 131 | 0.292 | 1.643 | $6.043x10^{-6}$ |
| 59 | 250 | 0.150 | $10^{-3}$ | 5 | 60 | $1x10^{-4}$ | 105 | 0.371 | 2.063 | $6.222x10^{-6}$ |
| 60 | 250 | 0.150 | $10^{-3}$ | 2.5 | 40 | $1x10^{-4}$ | 90 | 0.427 | 2.400 | $6.308x10^{-6}$ |
| 61 | 250 | 0.150 | $10^{-3}$ | 0.5 | 40 | $1x10^{-4}$ | 85 | 0.434 | 2.526 | $5.508x10^{-6}$ |

* Note: well_length = wellscreen length; well_rad = wellscreen radius; aq_k = aquifer horizontal permeability; well_cen_y = elevation of well above aquifer base = (10m - depth); NGRID = mesh density control (larger NGRID – finer mesh. Default is 15); ERRLIM = solution accuracy control (smaller ERRLIM – more accurate solution. Default is 0.001); well_k = uniform permeability assigned to entire wellscreen

From the Help file included with FlexPDE 3.01b2:

NGRID: "Specifies the number of mesh rows in each dimension. SELECT NGRID=<number> controls the maximum cell size. The mesh will be generated with approximately NGRID cells in the larger dimension (X or Y), and corresponding size in the smaller dimension, subject to smaller size requirements from other criteria. In 3D problems, cell layers will be created with thickness compatible with the 2D NGRID dimension, subject to smaller size requirements from other criteria. Where thick layers adjoin thin layers, there will be a gradual approach to the thin-layer dimension in the cells of the thick layer."

ERRLIM: "FlexPDE applies a consistency check to integrals of the PDE's over the mesh cells. From this it estimates the relative uncertainty in the solution variables and compares this to an accuracy tolerance. If any mesh cell exceeds the tolerance, that cell is split, and the solution is

recomputed. The error tolerance is called ERRLIM, and can be set in the SELECT section of the script. The default value of ERRLIM is 0.001, which means that FlexPDE will refine the mesh until the estimated error in any variable (relative to the variable range) is less than 0.1% over every cell of the mesh. [Note: This does not mean that FlexPDE can guarantee that the solutions is accurate to 0.1% over the domain. Individual cell errors may cancel or accumulate in ways that are hard to predict.]"

Table H.3 – Input parameters and model results – riverbed model, rigorous solution method

| No. | well_length (m) | well_rad (m) | aq_k (m/s) | well_cen_y (m) | NGRID | ERRLIM | V(z) Approximation | Flow Rate ($m^3/s$) | RMS Error |
|---|---|---|---|---|---|---|---|---|---|
| 1 | 50 | 0.150 | $10^{-3}$ | 5 | 50 | $1x10^{-5}$ | 0.0423(z)+0.2 | 0.151 | $3.988x10^{-6}$ |
| 2 | 50 | 0.150 | $10^{-4}$ | 5 | 60 | $1x10^{-5}$ | 0.00425(z)+0.015 | 0.016 | $3.578x10^{-6}$ |
| 3 | 250 | 0.150 | $10^{-3}$ | 5 | 40 | $1x10^{-5}$ | EXP(0.0057(z)+0.25)-EXP(0.25)+0.2 | 0.305 | $4.453x10^{-6}$ |
| 4 | 250 | 0.150 | $10^{-4}$ | 5 | 40 | $1x10^{-5}$ | 0.00371(z)+0.05 | 0.069 | $3.728x10^{-6}$ |
| 5 | 250 | 0.150 | $10^{-5}$ | 5 | 40 | $1x10^{-5}$ | 0.00039(z)+0.002 | 0.007 | $1.316x10^{-6}$ |
| 6 | 250 | 0.100 | $10^{-3}$ | 5 | 40 | $1x10^{-5}$ | EXP(0.0101(z)-1)-EXP(-1)+0.1 | 0.139 | $3.000x10^{-6}$ |
| 7 | 250 | 0.100 | $10^{-4}$ | 5 | 40 | $1x10^{-5}$ | 0.00655(z)+0.05 | 0.053 | $6.699x10^{-6}$ |
| 8 | 500 | 0.150 | $10^{-3}$ | 5 | 60 | $1x10^{-5}$ | EXP(0.0069(z)-2)-EXP(-2)+0.25 | 0.311 | $3.274x10^{-6}$ |

# APPENDIX I NUMERICAL MODEL GRAPHICAL OUTPUT

The figures presented below are taken from the models using the rigorous solution to pipe hydraulics. They are intended to be representative of the type of output generated by FlexPDE. In every figure, X, Y, Z and h are measured in metres, while kz and vz are in metres per second.

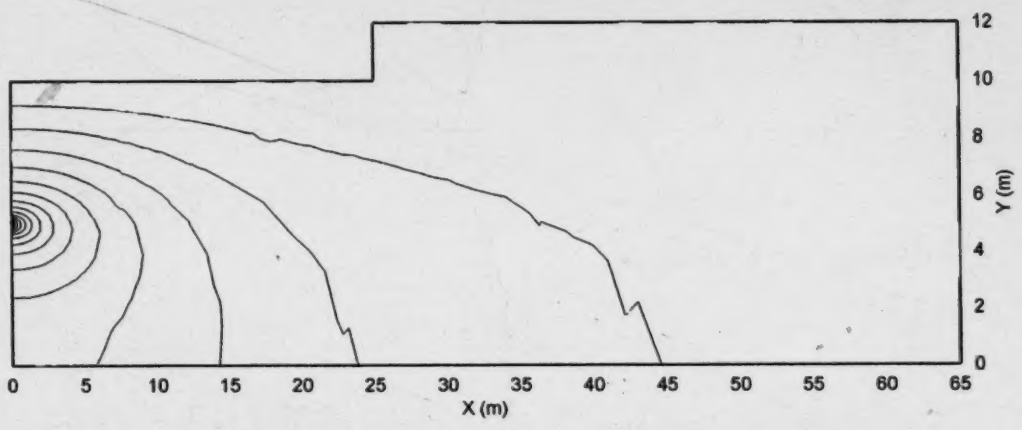


Figure I.1 – Example model output: contours of total head at z = 25m; L = 50m, Ø = 300mm, $k_h = 10^{-3}$ m/s

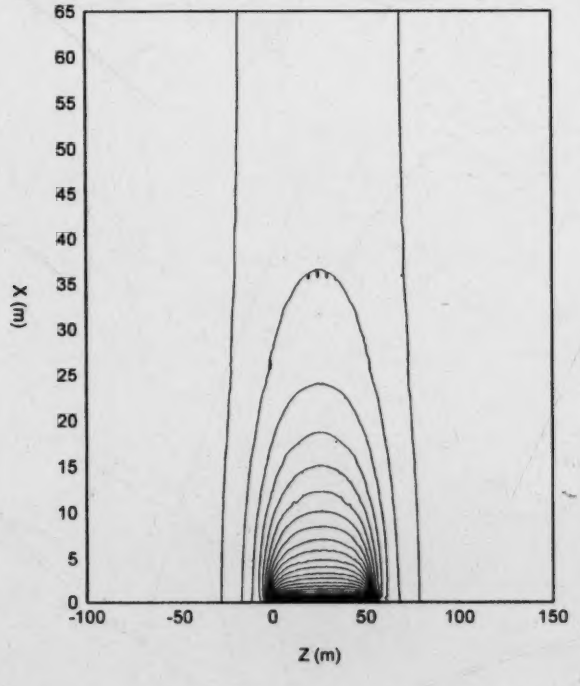


Figure I.2 – Example model output: contours of total head at y = 5m; L = 50m, Ø = 300mm, $k_h = 10^{-3}$ m/s

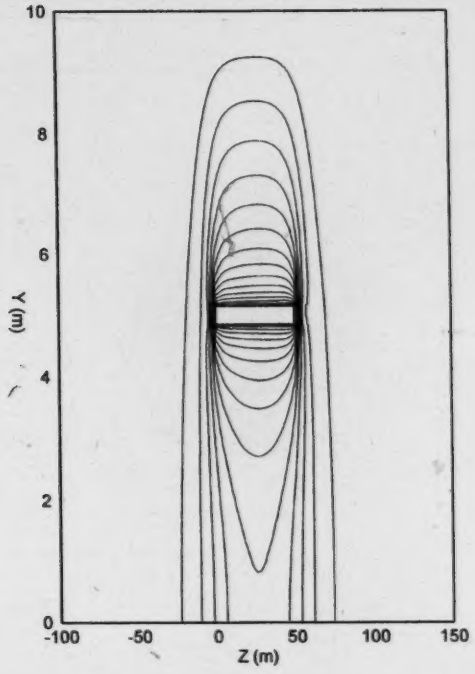


Figure I.3 – Example model output: contours of total head at x = 0m; L = 50m, Ø = 300mm, $k_h = 10^{-3}$ m/s

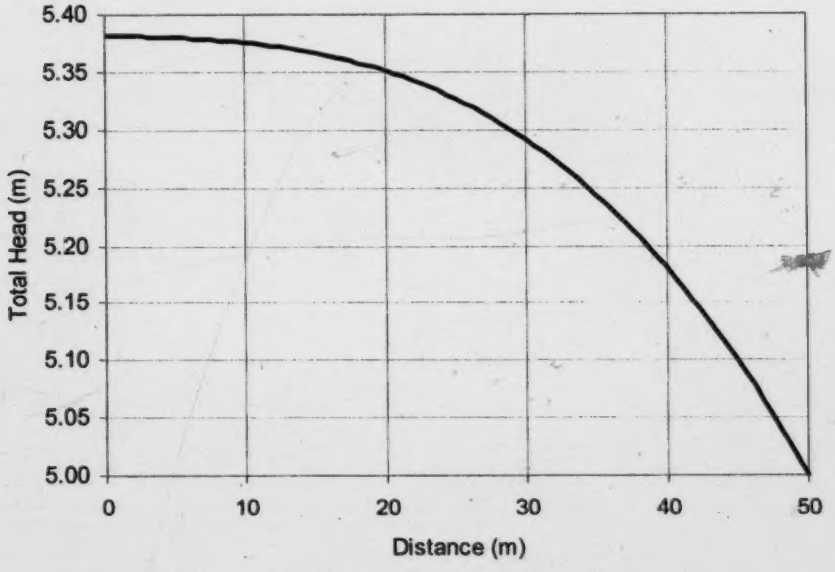


Figure I.4 – Example model output: profile of total head along axis of wellscreen; L = 50m, Ø = 300mm, $k_h = 10^{-3}$ m/s

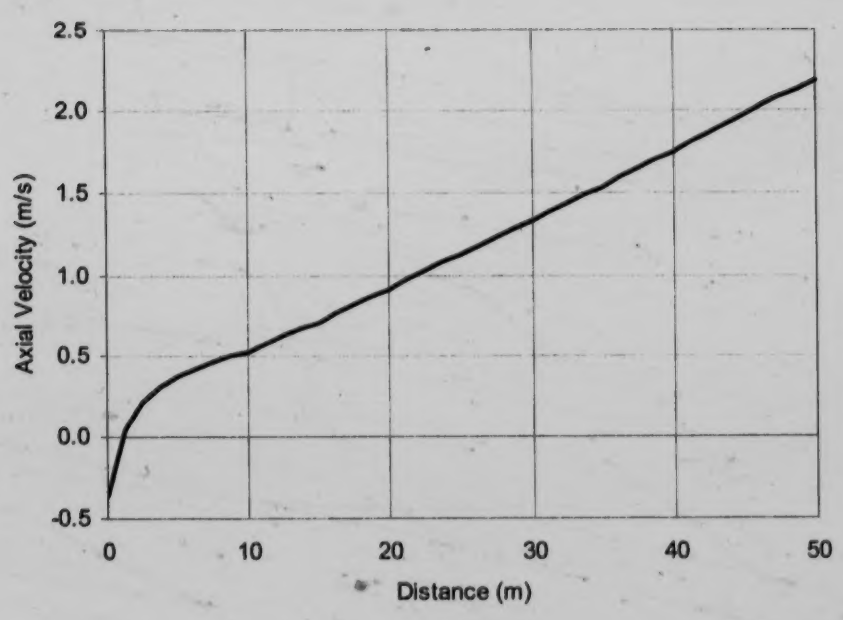


Figure I.5 – Example model output: profile of axial velocity along axis of wellscreen; L = 50m, Ø = 300mm, $k_h = 10^{-3}$ m/s

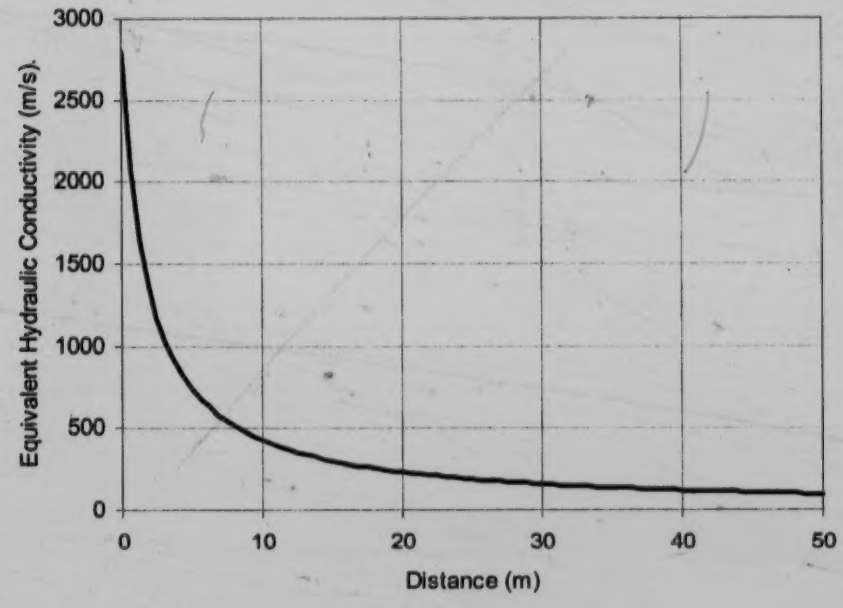


Figure I.6 – Example model output: profile of hydraulic conductivity along axis of wellscreen; L = 50m, Ø = 300mm, $k_h = 10^{-3}$ m/s

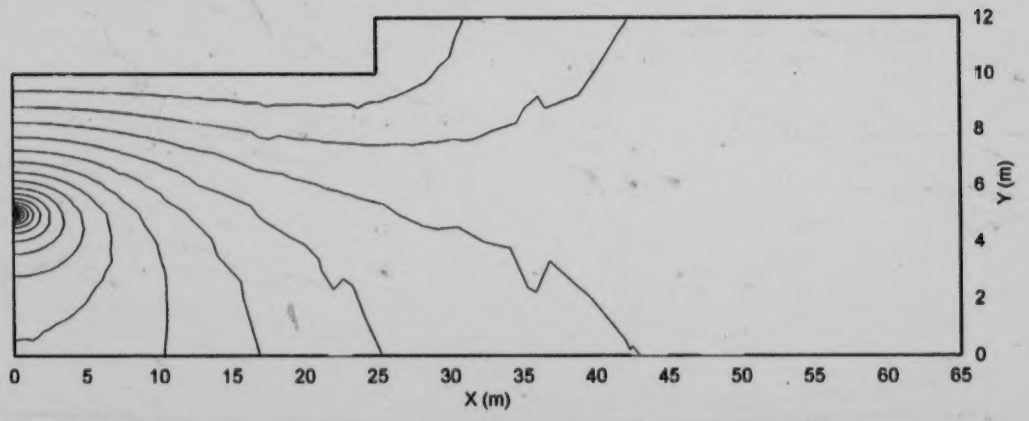


Figure I.7 – Example model output: contours of total head at z = 250m; L = 250m, Ø = 200mm, $k_h = 10^{-3}$ m/s

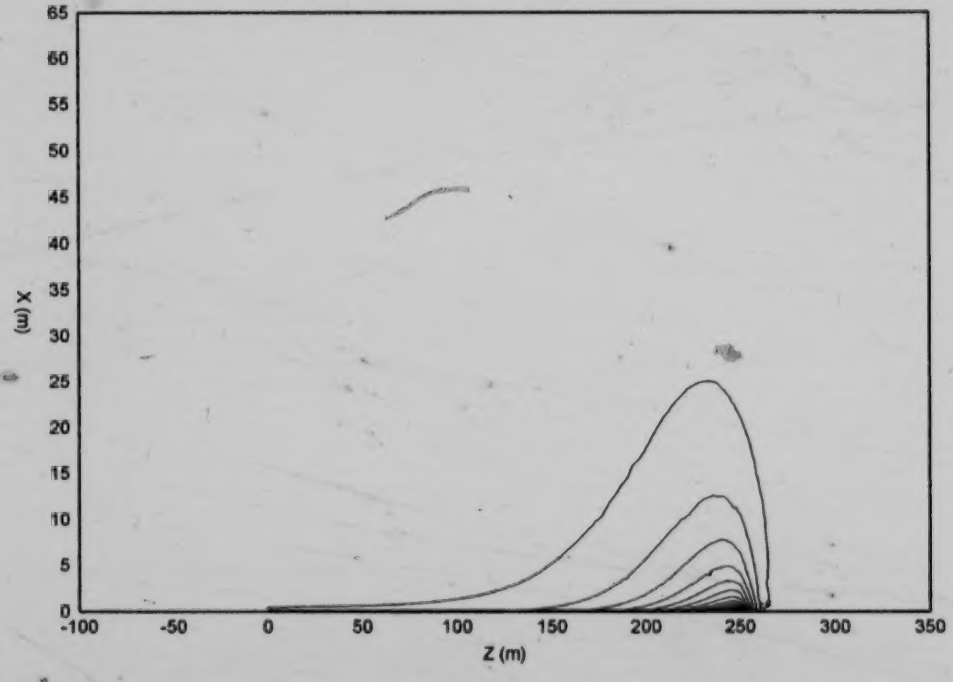


Figure I.8 – Example model output: contours of total head at y = 5m; L = 250m, Ø = 200mm, $k_h = 10^{-3}$ m/s

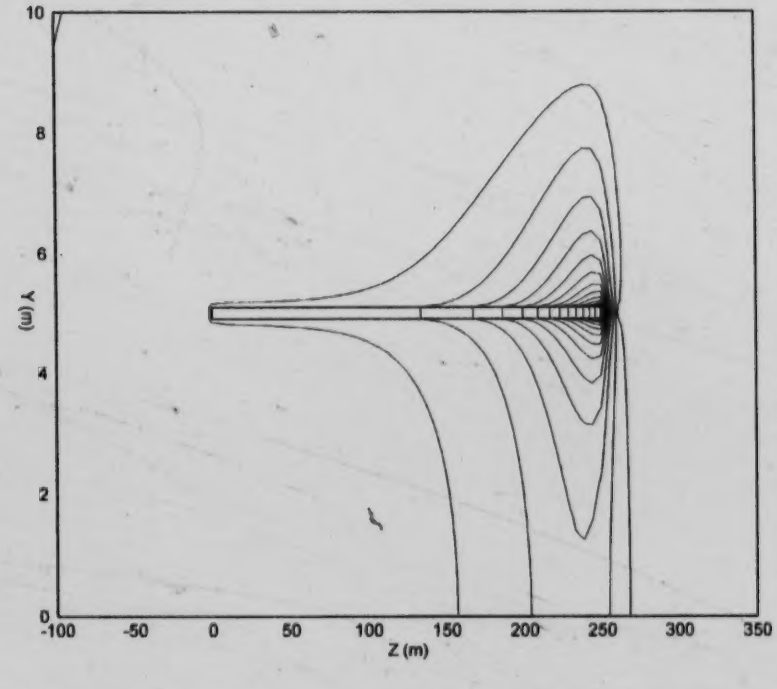


Figure I.9 – Example model output: contours of total head at x = 0m; L = 250m, Ø = 200mm, $k_h = 10^{-3}$ m/s

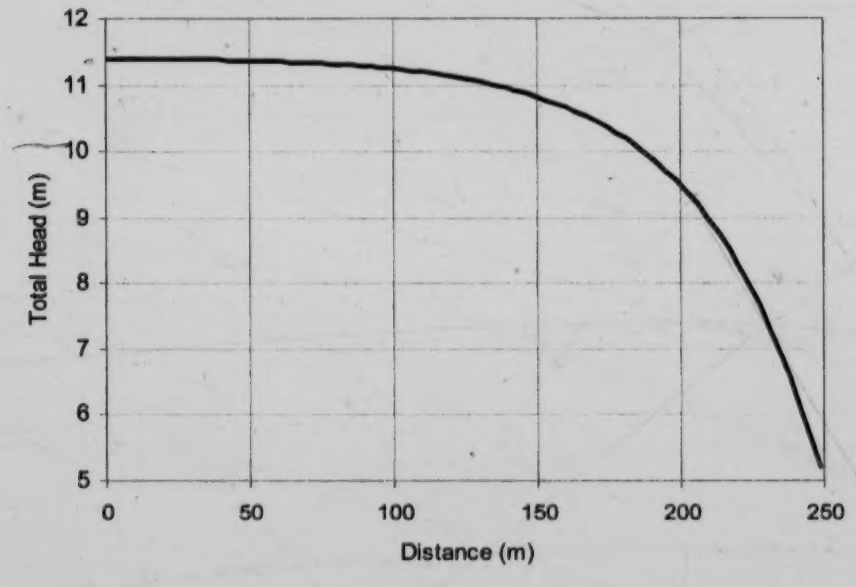


Figure I.10 – Example model output: profile of total head along axis of wellscreen; L = 250m, Ø = 200mm, $k_h = 10^{-3}$ m/s

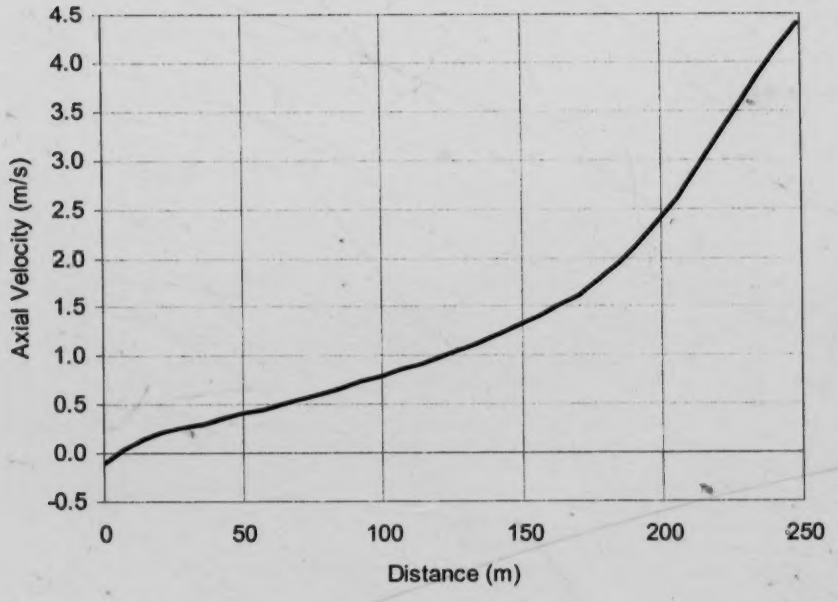


Figure I.11 – Example model output: profile of axial velocity along axis of wellscreen; L = 250m, Ø = 200mm, $k_h = 10^{-3}$ m/s

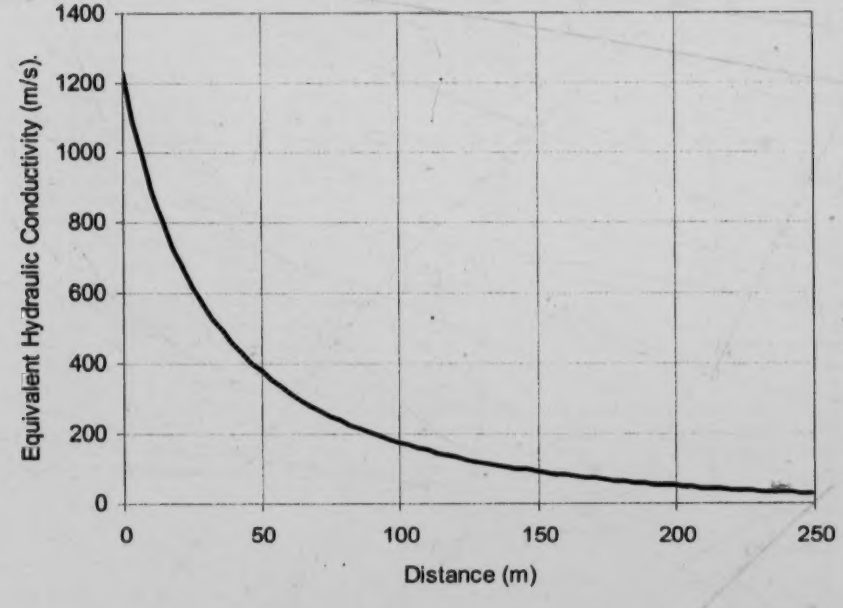


Figure I.12 – Example model output: profile of hydraulic conductivity along axis of wellscreen; L = 250m, Ø = 200mm, $k_h = 10^{-3}$ m/s

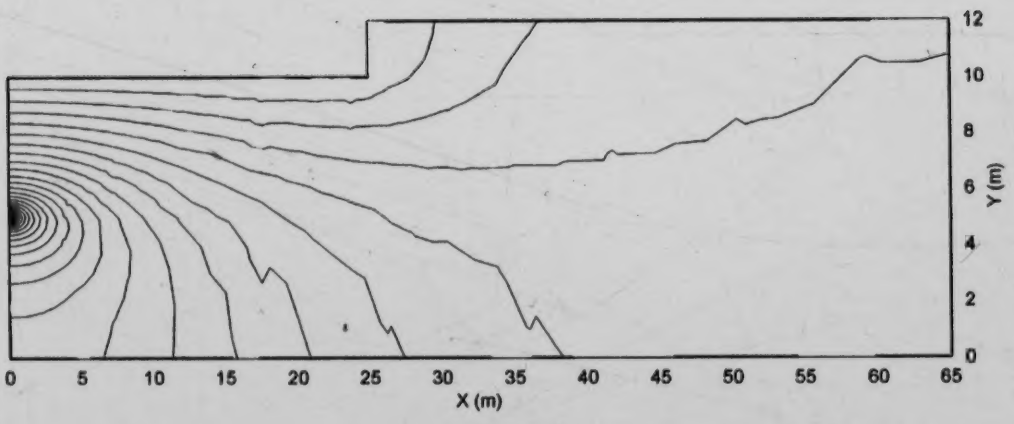


Figure I.13 – Example model output: contours of total head at z = 125m; L = 250m, Ø = 300mm, $k_h = 10^{-3}$ m/s

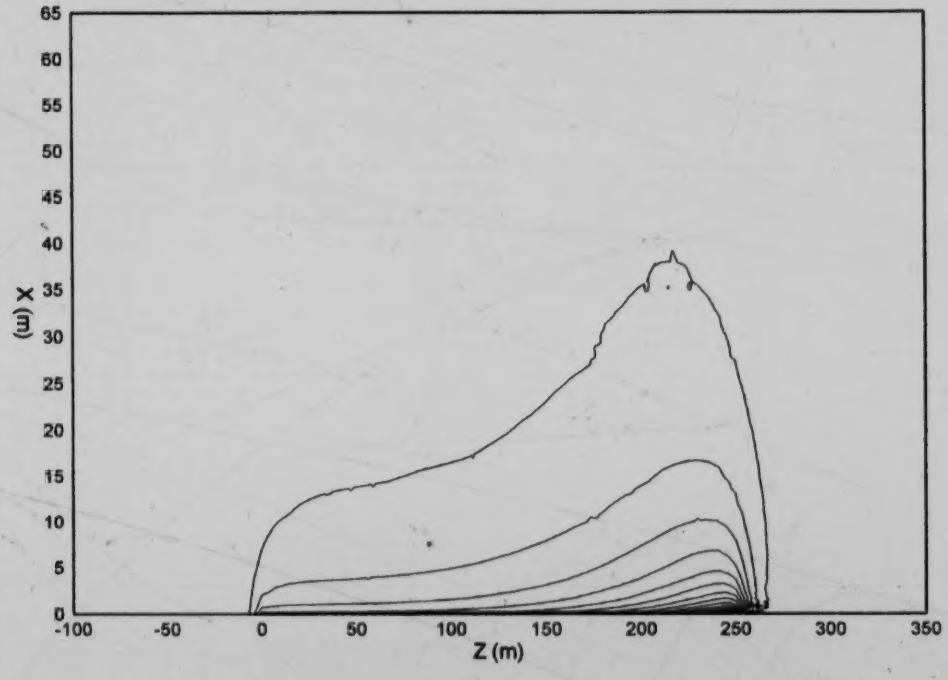


Figure I.14 – Example model output: contours of total head at y = 5m; L = 250m, Ø = 300mm, $k_h = 10^{-3}$ m/s

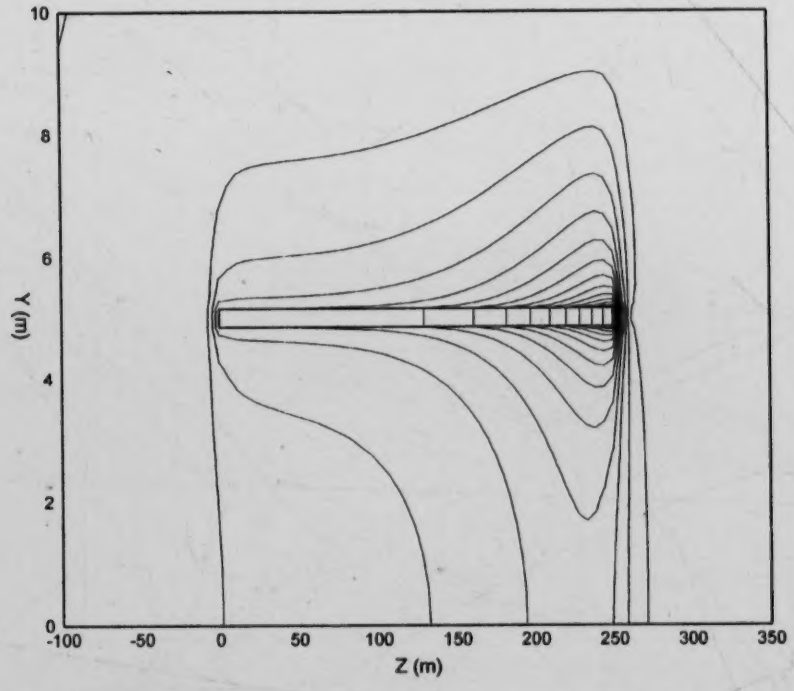


Figure I.15 – Example model output: contours of total head at x = 0m; L = 250m, Ø = 300mm, $k_h = 10^{-3}$ m/s

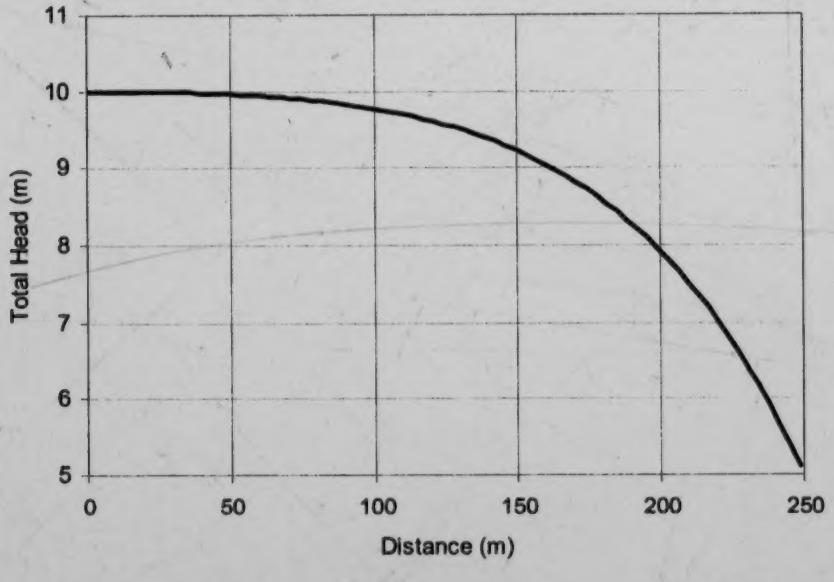


Figure I.16 – Example model output: profile of total head along axis of wellscreen; L = 250m, Ø = 300mm, $k_h = 10^{-3}$ m/s

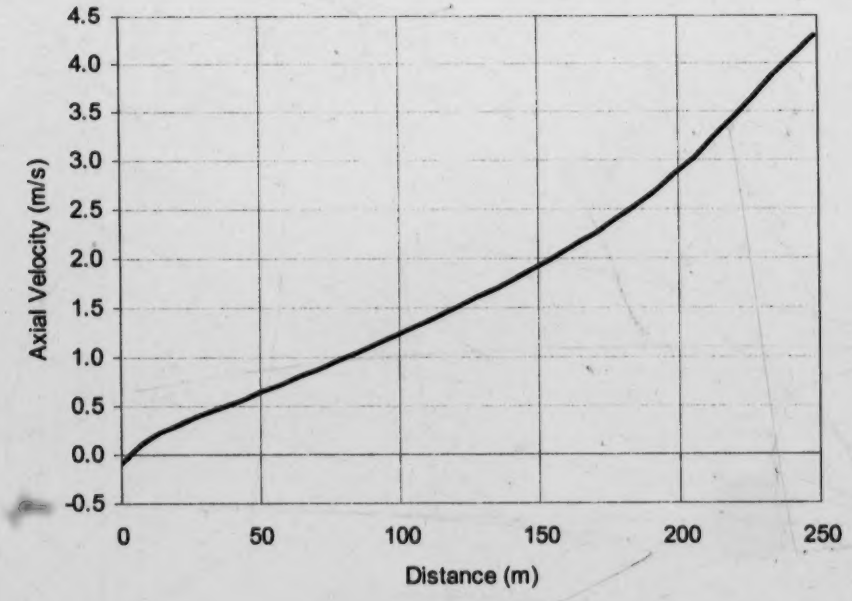


Figure I.17 – Example model output: profile of axial velocity along axis of wellscreen; L = 250m, Ø = 300mm, $k_h = 10^{-3}$ m/s

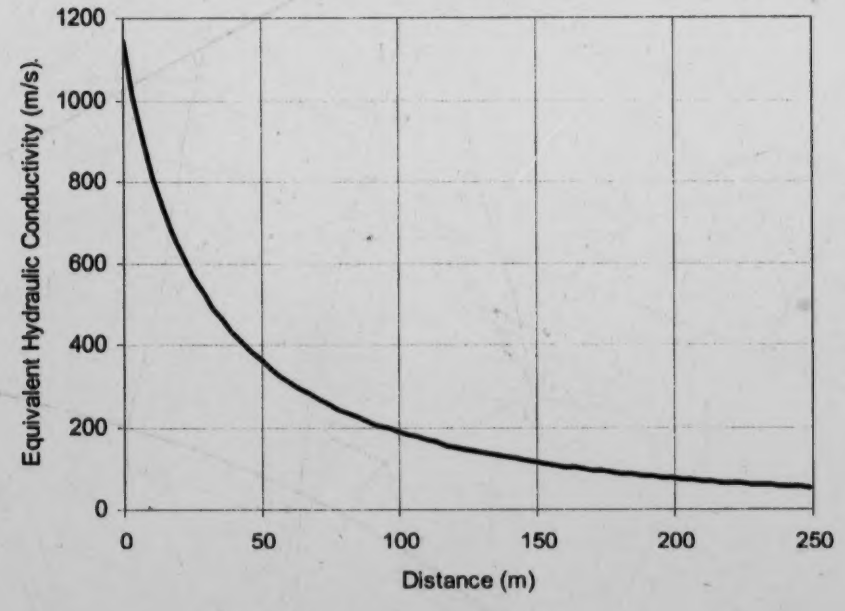


Figure I.18 – Example model output: profile of hydraulic conductivity along axis of wellscreen; L = 250m, Ø = 300mm, $k_h = 10^{-3}$ m/s

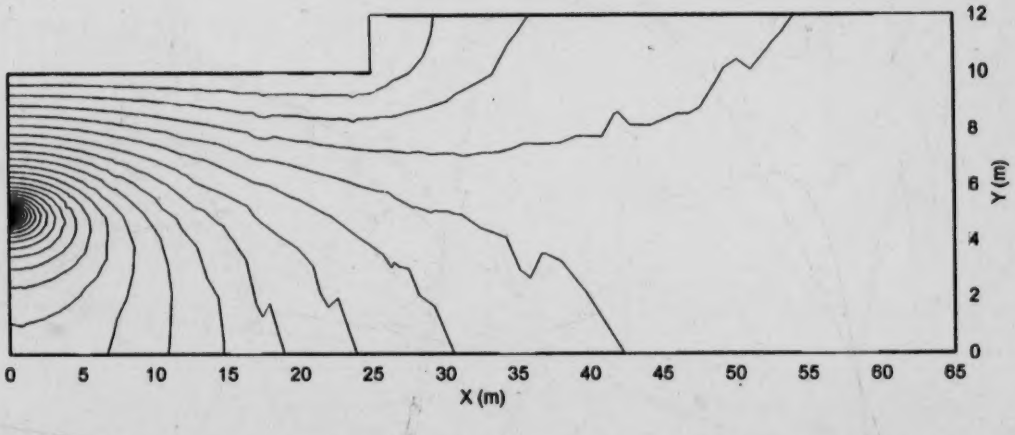


Figure I.19 – Example model output: contours of total head at z = 125m; L = 250m, Ø = 300mm, $k_h = 10^{-5}$ m/s

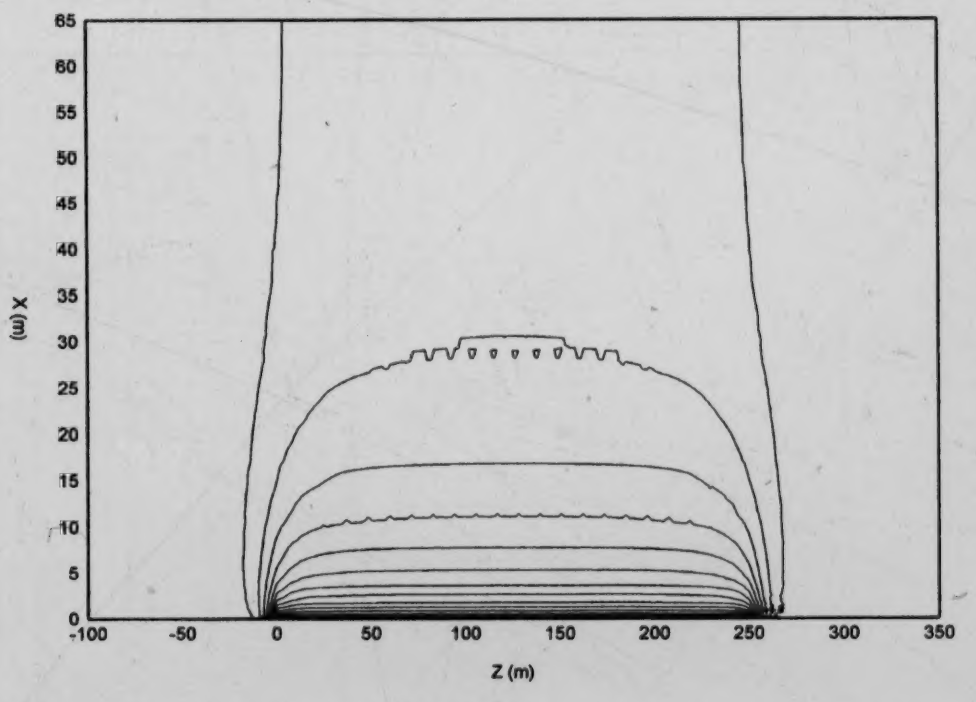


Figure I.20 – Example model output: contours of total head at y = 5m; L = 250m, Ø = 300mm, $k_h = 10^{-5}$ m/s

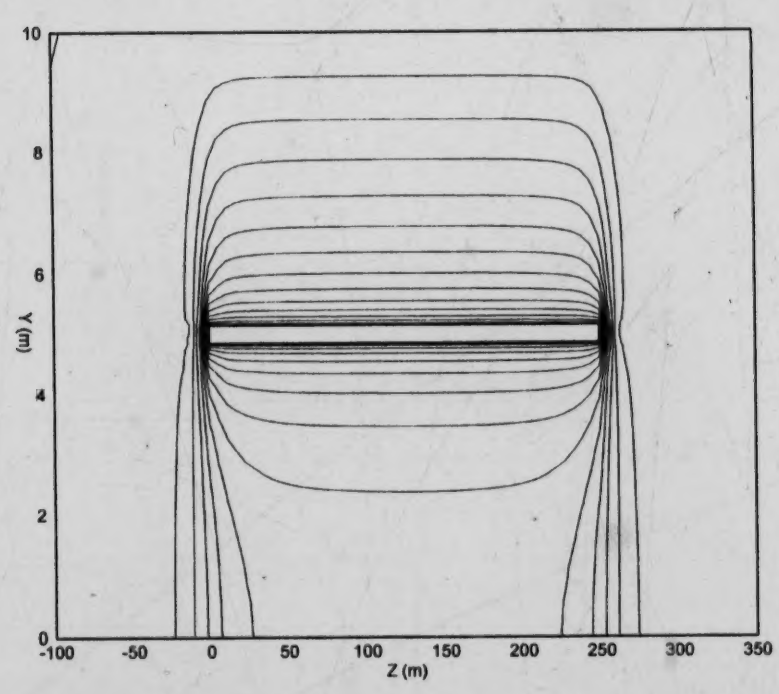


Figure I.21 – Example model output: contours of total head at x = 0m; L = 250m, Ø = 300mm, $k_h = 10^{-5}$ m/s

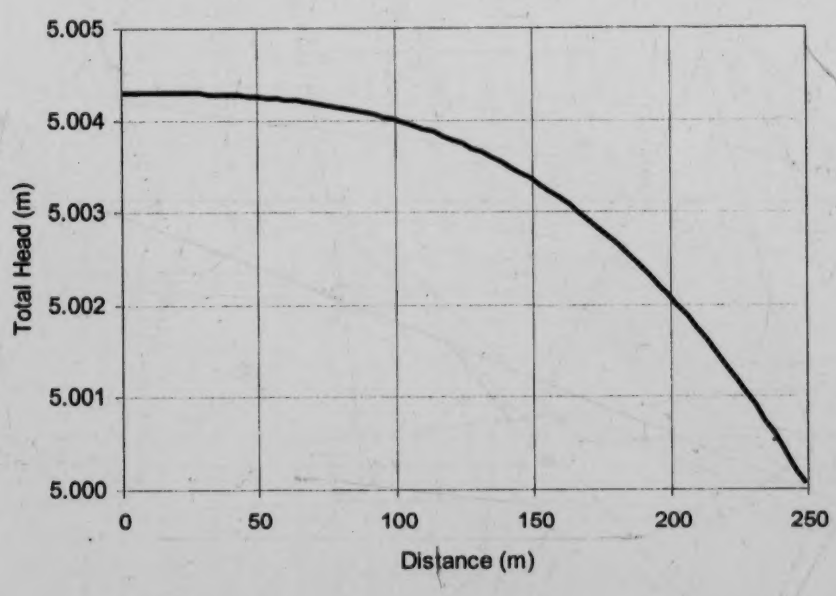


Figure I.22 – Example model output: profile of total head along axis of wellscreen; L = 250m, Ø = 300mm, $k_h = 10^{-5}$ m/s

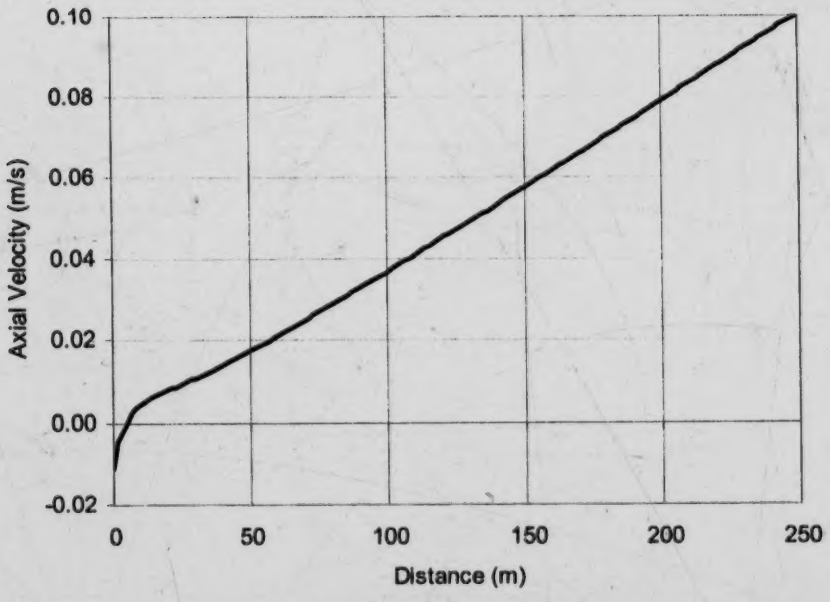


Figure I.23 – Example model output: profile of axial velocity along axis of wellscreen; L = 250m, Ø = 300mm, $k_h = 10^{-5}$ m/s

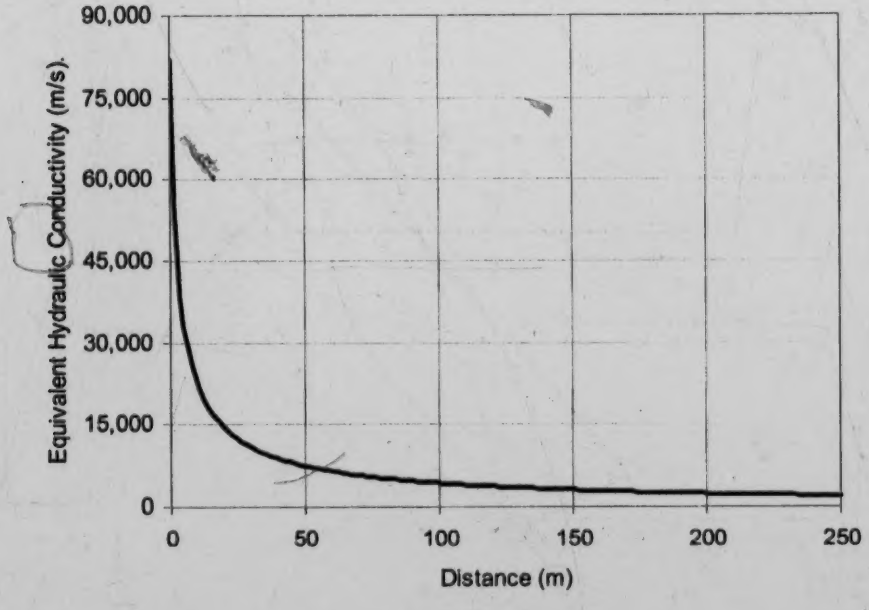


Figure I.24 – Example model output: profile of hydraulic conductivity along axis of wellscreen; L = 250m, Ø = 300mm, $k_h = 10^{-5}$ m/s

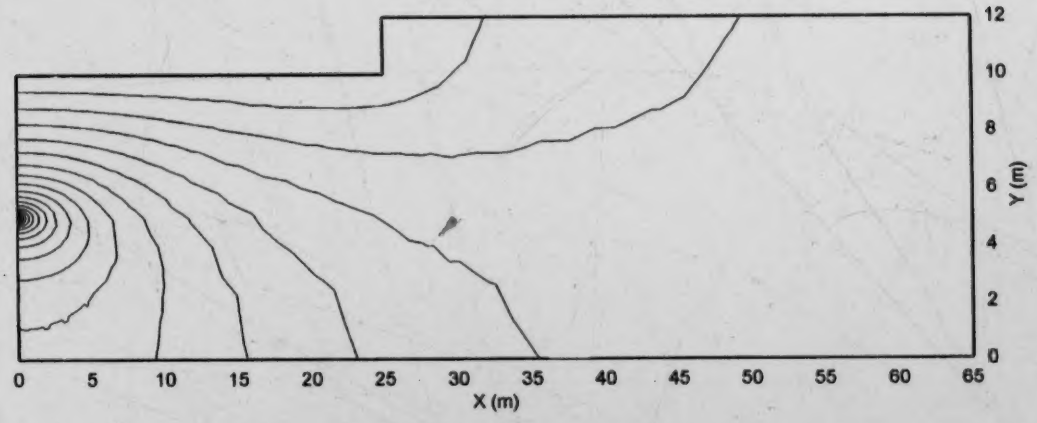


Figure I.25 – Example model output: contours of total head at z = 250m; L = 500m, Ø = 300mm, $k_h = 10^{-3}$ m/s

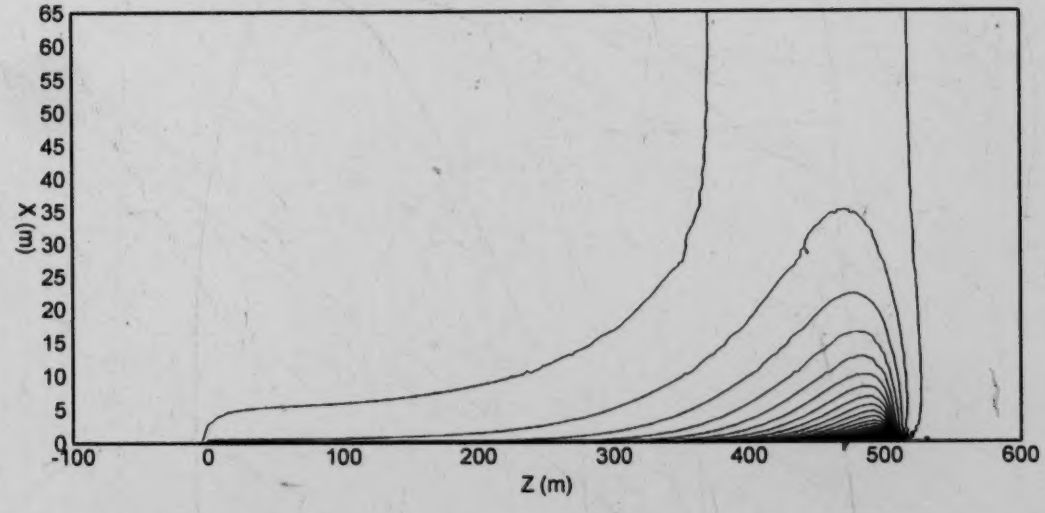


Figure I.26 – Example model output: contours of total head at y = 5m; L = 500m, Ø = 300mm, $k_h = 10^{-3}$ m/s

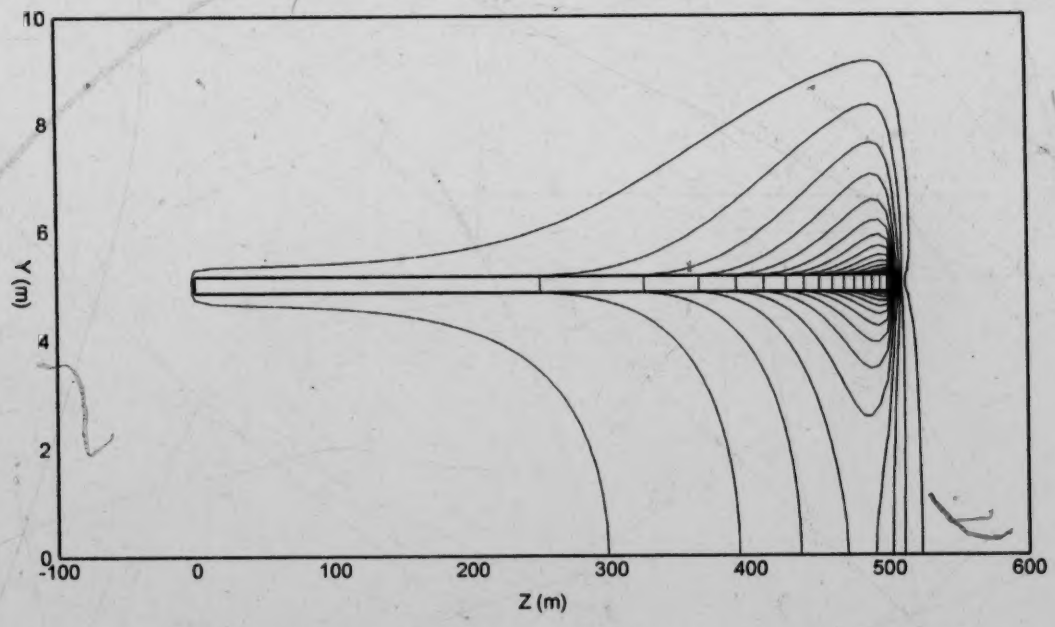


Figure I.27 – Example model output: contours of total head at x = 0m; L = 500m, Ø = 300mm, $k_h = 10^{-3}$ m/s

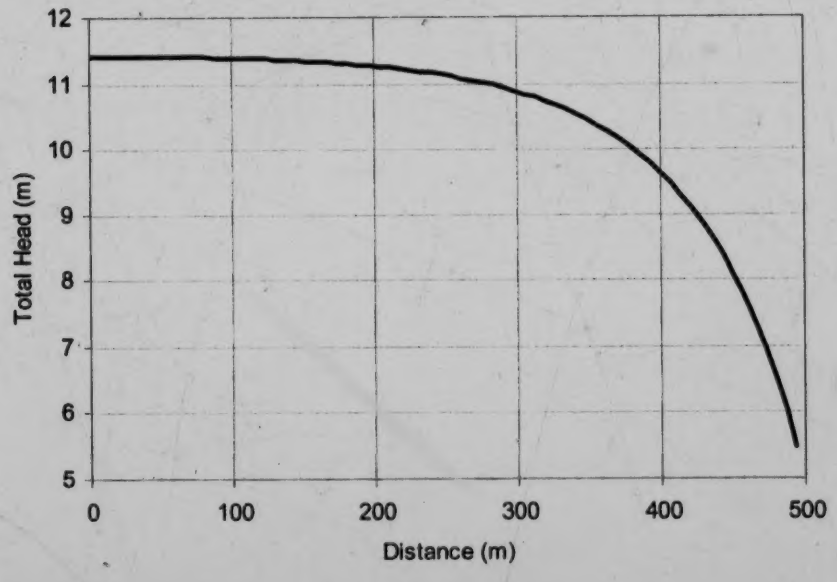


Figure I.28 – Example model output: profile of total head along axis of wellscreen; L = 500m, Ø = 300mm, $k_h = 10^{-3}$ m/s

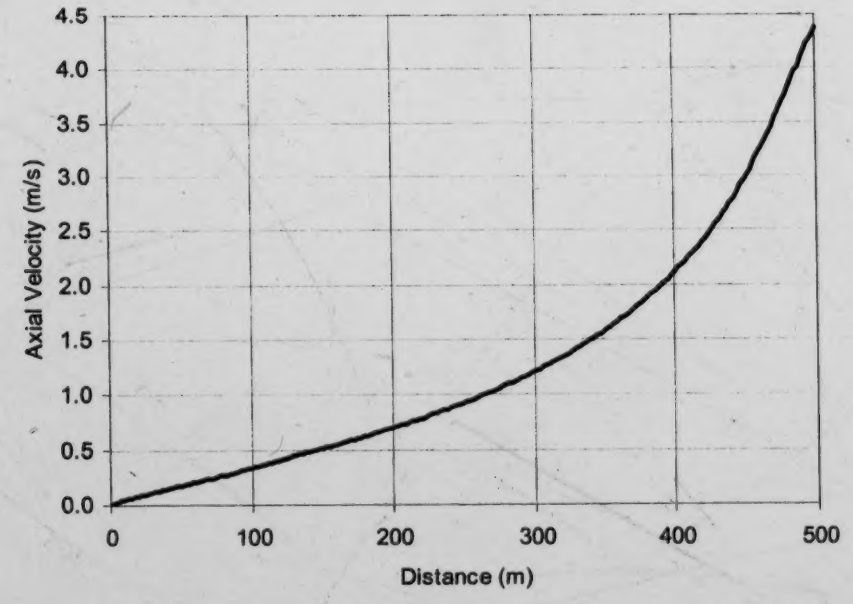


Figure I.29 – Example model output: profile of axial velocity along axis of wellscreen; L = 500m, Ø = 300mm, $k_h = 10^{-3}$ m/s

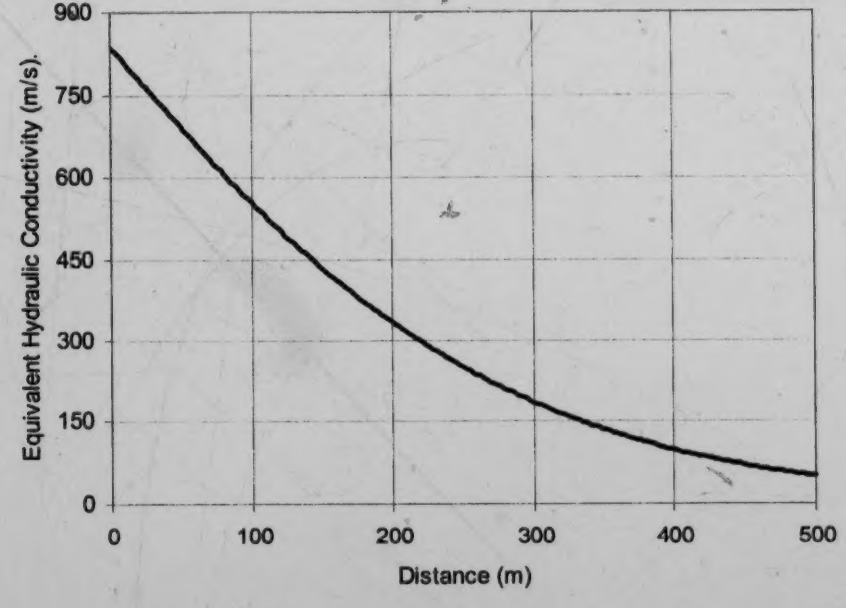


Figure I.30 – Example model output: profile of hydraulic conductivity along axis of wellscreen; L = 500m, Ø = 300mm, $k_h = 10^{-3}$ m/s

## APPENDIX J PHOTOGRAPHS

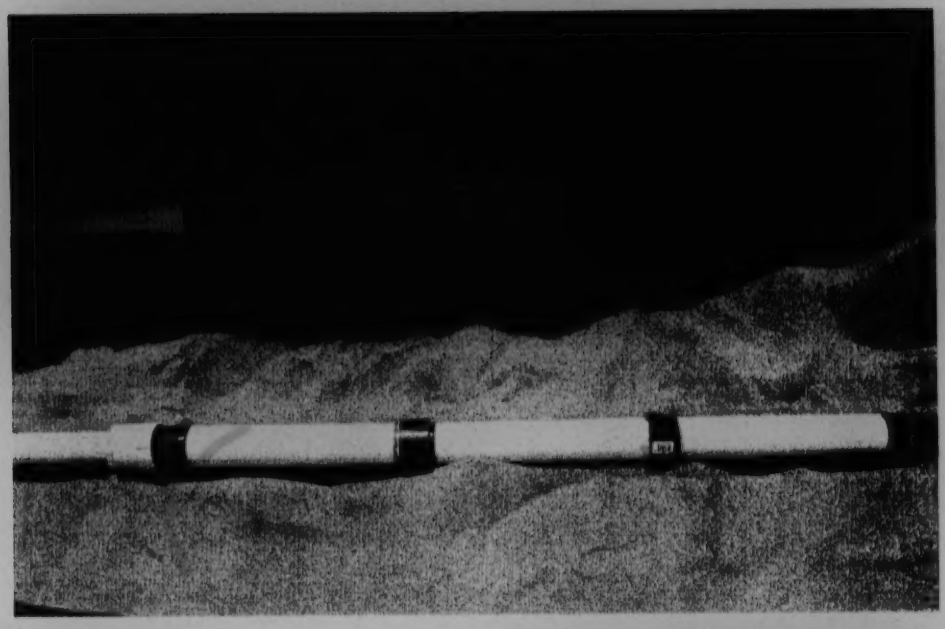

Figure J.1 – Sandblocker and Schumasoil 200 wellscreens during placement (July 2001)

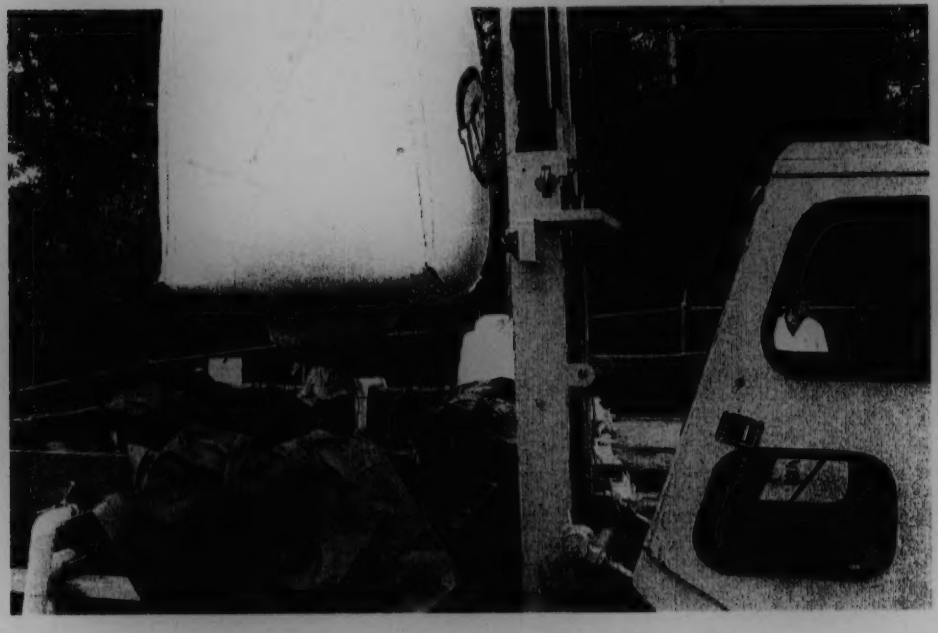

Figure J.2 – Forklift used to handle sand bags; filling south test box (July 2001)

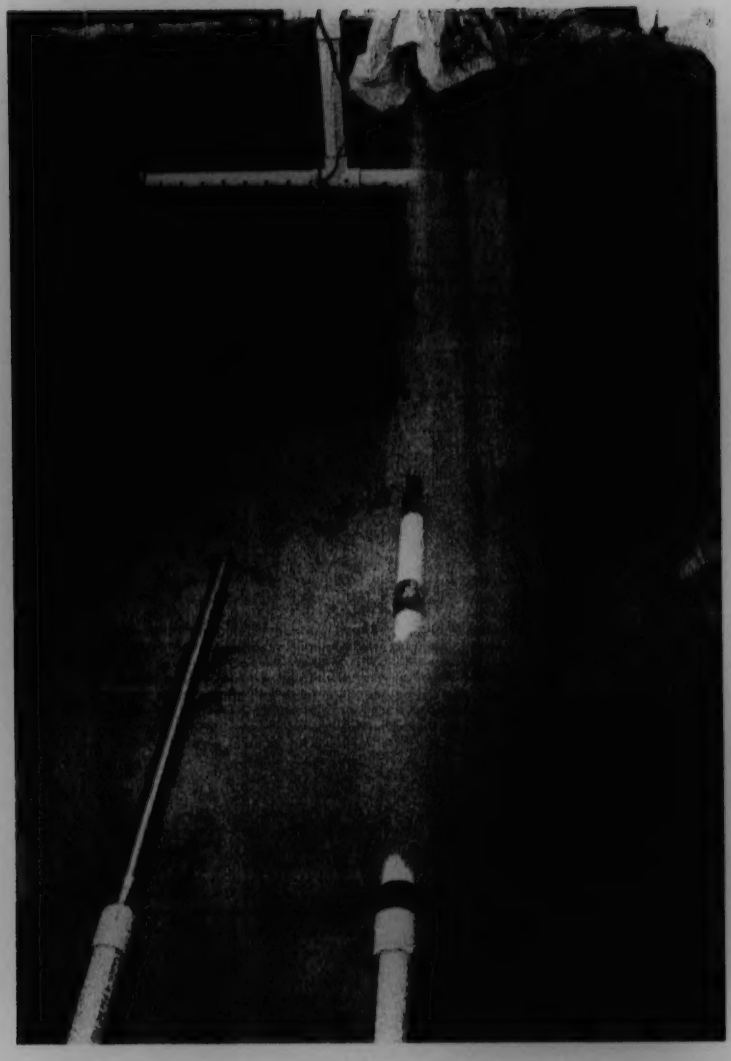

Figure J.3 – Filling the south test box with clean sand – Vee-Wire Drive Point and Schumasoil 80 wellscreens shown (July 2001)

Figure J.4 – Test boxes full of clean sand (July 2001)

Figure J.5 – Start of water circulation – north test box (July 2001)

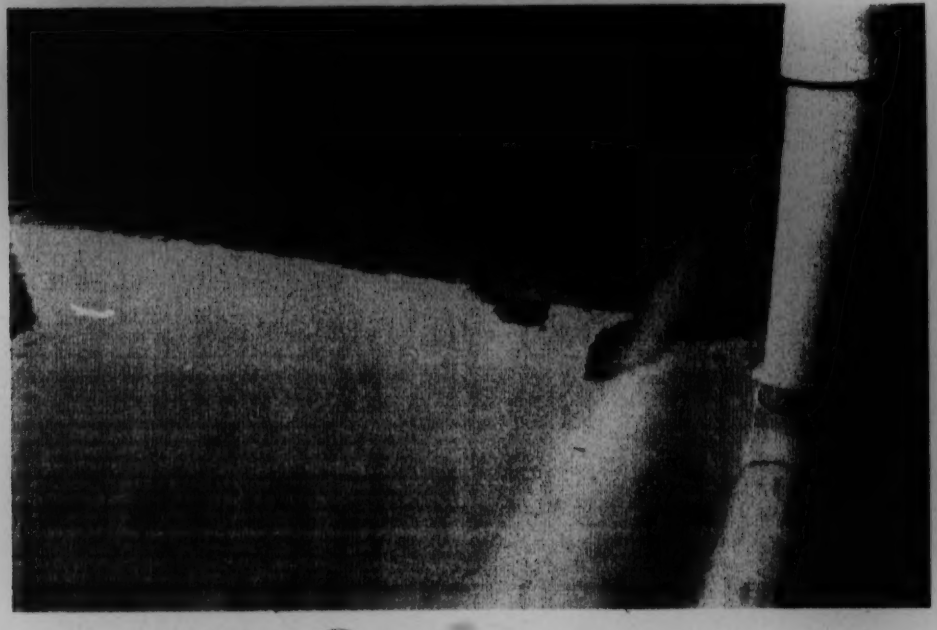

Figure J.6 – South test box filled with water; turbidity approximately 20 NTU (July 2001)

Figure J.7 – V-notch weir box; water flowing from north test box, south test box closed (July 2001)

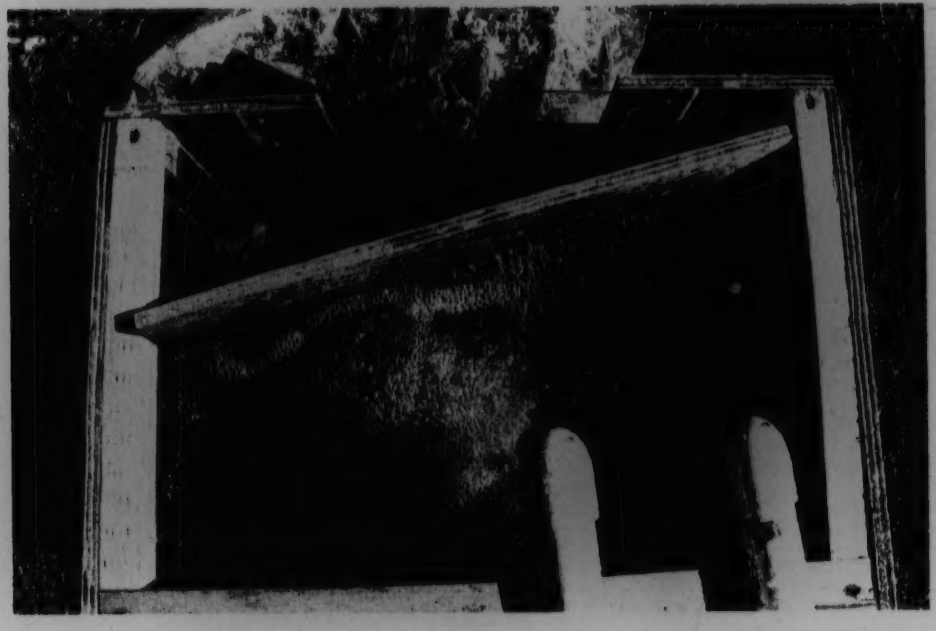

Figure J.8 – V-notch weir box; baffle used to reduce surface disturbance at v-notch (July 2001)

Figure J.9 – V-notch weir flowing full; ruler for measuring water level at right edge of plastic face (July 2001)

Figure J.10 – Overall arrangement of test equipment at E.L. Smith Water Treatment Plant (September 2001)

Figure J.11 – Shelby tube and steel plate for measuring density (October 2001)

Figure J.12 – Close-up of broken joint in Schumasoil 80 wellscreen (October 2001)

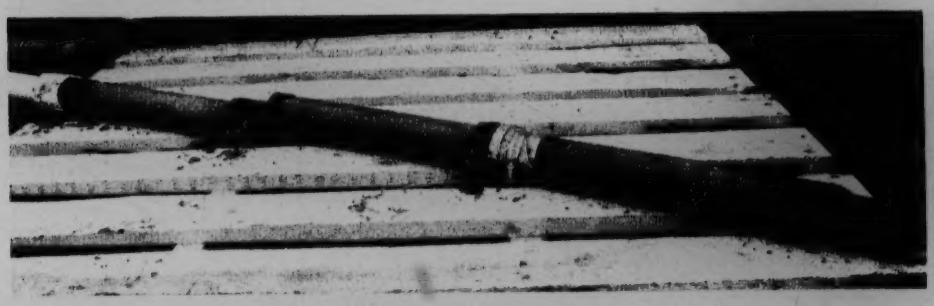

Figure J.13 – Schumasoil 80 wellscreen upon decommissioning; note broken joint (left-third), repair to damage from installation (right-third) (October 2001)

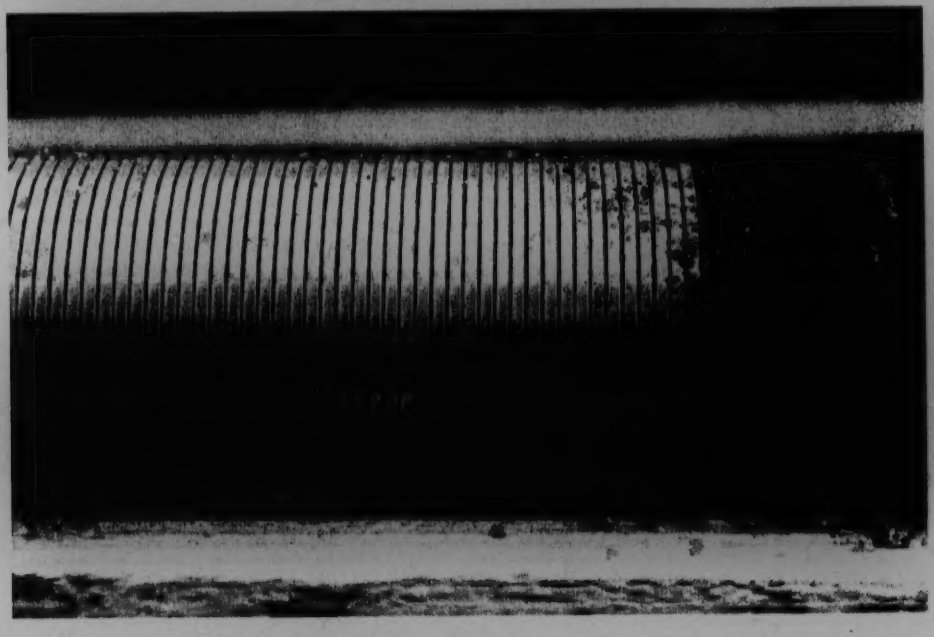

Figure J.14 – Close-up of Vee-Wire Drive Point wellscreen; note relatively clean condition, little material in openings (October 2001)

Figure J.15 – Vee-Wire Drive Point wellscreen upon decommissioning (October 2001)